Smart Grid Enabling Low Carbon Future Power Systems Towards Prosumers Era

Weiqi Hua

A Thesis presented for the degree of
Doctor of Philosophy

Department of Engineering
University of Durham
United Kingdom

October 2020

This thesis is dedicated to my parents

For their endless love, support, and encouragement

Smart Grid Enabling Low Carbon Future Power Systems Towards Prosumers Era

Weiqi Hua

Abstract

In efforts to meet the targets of carbon emissions reduction in power systems, policy makers formulate measures for facilitating the integration of renewable energy sources and demand side carbon mitigation. Smart grid provides an opportunity for bidirectional communication among policy makers, generators and consumers. With the help of smart meters, increasing number of consumers is able to produce, store, and consume energy, giving them the new role of prosumers. This thesis aims to address how smart grid enables prosumers to be appropriately integrated into energy markets for decarbonising power systems.

This thesis firstly proposes a Stackelberg game-theoretic model for dynamic negotiation of policy measures and determining optimal power profiles of generators and consumers in day-ahead market. Simulation results show that the proposed model is capable of saving electricity bills, reducing carbon emissions, and increasing the penetration of renewable energy sources. Secondly, a data-driven prosumer-centric energy scheduling tool is developed by using learning approaches to reduce computational complexity from model-based optimisation. This scheduling tool exploits convolutional neural networks to extract prosumption patterns, and uses scenarios to analyse possible variations of uncertainties caused by the intermittency of renewable energy sources and flexible demand. Case studies confirm that the proposed scheduling tool can accurately predict optimal scheduling decisions under various system scales and uncertain scenarios. Thirdly, a blockchain-based peer-to-peer trading framework is designed to trade energy and carbon allowance. The bidding/selling prices of individual prosumers can directly incentivise the reshaping of prosumption behaviours. Case studies demonstrate the execution of smart contract on the Ethereum blockchain and testify that the proposed trading framework outperforms the centralised trading and aggregator-based trading in terms of regional energy balance and reducing carbon emissions caused by long-distance transmissions.

Declaration

The work in this thesis is based on research carried out at the Department of Engineering, Durham University, United Kingdom. No part of this thesis has been submitted elsewhere for any other degree or qualification and it is all my own work unless referenced to the contrary in the text.

Parts of this work have been published in the form of following refereed papers. The authors' individual contributions to each paper are evaluated using the relevant CRediT roles.

- Chapter 3
  - **Weiqi Hua**, Dan Li, Hongjian Sun and Peter Matthews, *"Stackelberg Game-theoretic Model for Low Carbon Energy Market Scheduling,"* IET Smart Grid, Volume 3, 2020, pp. 31-41(10).

    CRediT authorship contribution statement:

    Weiqi Hua: conceptualisation of game theory framework, methodology of game theory and intelligent algorithms, software based algorithms development, investigation of the U.K. energy market and power systems, formal analysis of simulation results, data curation, writing original draft, manuscript visualization.

    Dan li: co-development of algorithm for carbon emissions tracing, validation of problem formulation, discussion of game theory model selection.

    Hongjian Sun: supervision, project administration, review and editing, funding acquisition, validation of simulation results.

    Peter Matthews: supervision, review and editing, discussion of energy market design, validation of simulation results.

– **Weiqi Hua**, Dan Li, Hongjian Sun, Peter Matthews and Fanlin Meng, *"Stochastic Environmental and Economic Dispatch of Power Systems with Virtual Power Plant in Energy and Reserve Markets, "* International Journal of Smart Grid and Clean Energy, 2018, 7(4): 231-239.

CRediT authorship contribution statement:

Weiqi Hua: conceptualisation of environmental and economic dispatch, methodology of optimisation and intelligent algorithms, software based algorithms development, investigation of the U.K. energy market and power systems, formal analysis of simulation results, data curation, writing original draft, manuscript visualization.

Dan li: validation of problem formulation, co-development of multiobjective immune algorithm.

Hongjian Sun: supervision, project administration, review and editing, funding acquisition, validation of simulation results.

Peter Matthews: supervision, review and editing, discussion of energy market design, validation of simulation results.

Fanlin Meng: discussion of the roles of energy market participants, discussion of algorithm selection.

– **Weiqi Hua**, Dan Li, Hongjian Sun and Peter Matthews, *"Unit Commitment in Achieving Low Carbon Smart Grid Environment with Virtual Power Plant,"* International Smart Cities Conference (ISC2), Wuxi, China, 2017, pp. 159-164.

CRediT authorship contribution statement:

Weiqi Hua: conceptualisation of virtual power plant, methodology of optimisation and intelligent algorithms, software based algorithms development, investigation of the virtual power plant, formal analysis of simulation results, data curation, writing original draft, manuscript visualization.

Dan li: validation of problem formulation, co-development of multiobjective immune algorithm for solving unit commitment problem.

October 8, 2020

Hongjian Sun: supervision, project administration, review and editing, funding acquisition, validation of simulation results.

Peter Matthews: supervision, review and editing, discussion of energy market design, validation of simulation results.

– **Weiqi Hua**, Hongjian Sun, Hao Xiao and Wei Pei, *'Stackelberg Game-Theoretic Strategies for Virtual Power Plant and Associated Market Scheduling Under Smart Grid Communication Environment,"* IEEE International Conference on Communications, Control, and Computing Technologies for Smart Grids (SmartGridComm), Aalborg, Denmark, 2018, pp. 1-6.

CRediT authorship contribution statement:

Weiqi Hua: conceptualisation of virtual power plant and game theory, methodology of scheduling, investigation of the locational pricing scheme, formal analysis of simulation results, data curation, writing original draft, manuscript visualization.

Hongjian Sun: supervision, project administration, review and editing, funding acquisition, validation of simulation results.

Hao Xiao: developing particle swarm algorithm, discussion of the locational pricing scheme.

Wei Pei: supervision, validation of simulation results.

– Dan Li, **Weiqi Hua**, Hongjian Sun and Wei-Yu Chiu, *"Multiobjective Optimization for Carbon Market Scheduling Based on Behavior Learning,"* Energy Procedia, Volume 142, 2017, pp. 2089-2094.

CRediT authorship contribution statement:

Dan li: design problem formulation, development of multiobjective immune algorithm, formal analysis of simulation results, writing original draft, manuscript visualization.

Weiqi Hua: methodology of optimisation and intelligent algorithms, review and editing, data curation.

Hongjian Sun: supervision, project administration, review and editing,

funding acquisition, validation of simulation results.

Wei-Yu Chiu: supervision, review and editing, discussion of solving multiobjective optimisation problems, providing original artificial immune algorithms, validation of simulation results.

- Chapter 4

  – **Weiqi Hua**, Jing Jiang, Hongjian Sun and Andrea M. Tonello, *"Data-Driven Prosumer-Centric Low Carbon Energy Scheduling Using Convolutional Neural Networks,"* IEEE Transactions on Smart Grid, Submitted on 31-Mar-2020.

  CRediT authorship contribution statement:

  Weiqi Hua: conceptualisation of machine learning, methodology of convolutional neural networks, investigation of the learning approaches, formal analysis of simulation results, data curation, writing original draft, manuscript visualization.

  Jing Jiang: supervision, review and editing, validation of simulation results.

  Hongjian Sun: supervision, project administration, review and editing, funding acquisition, validation of simulation results.

  Andrea M. Tonello: supervision, review and editing, validation of simulation results.

  – **Weiqi Hua**, Minglei You and Hongjian Sun, *"Real-Time Price Elasticity Reinforcement Learning for Low Carbon Energy Hub Scheduling Based on Conditional Random Field,"* IEEE/CIC International Conference on Communications Workshops in China (ICCC Workshops), Changchun, China, 2019, pp. 204-209.

  CRediT authorship contribution statement:

  Weiqi Hua: review and editing, investigation of machine learning for energy hub scheduling, formal analysis of simulation results, writing original draft, manuscript visualization.

Minglei You: conceptualisation of energy hub, developing hardware of RTDS and PCB, design interface between software and hardware.

Hongjian Sun: supervision, project administration, review and editing, funding acquisition, validation of simulation results.

– Minglei You, **Weiqi Hua**, Mahmoud Shahbazi and Hongjian Sun, *"Energy Hub Scheduling Method with Voltage Stability Considerations,"* IEEE/CIC International Conference on Communications in China (ICCC Workshops), Beijing, China, 2018, pp. 196-200.

CRediT authorship contribution statement:

Minglei You: conceptualisation of energy hub, methodology of scheduling and improving voltage stability, developing hardware of RTDS and PCB, design interface between software and hardware, formal analysis of simulation results, writing original draft, manuscript visualization.

Weiqi Hua: review and editing, discussion of costs evaluation, validation of simulation results.

Hongjian Sun: supervision, project administration, review and editing, funding acquisition, validation of simulation results.

Mahmoud Shahbazi: supervision, review and editing, validation of simulation results.

- Chapter 5

– **Weiqi Hua**, Jing Jiang, Hongjian Sun and Jianzhong Wu, *"A Blockchain Based Peer-to-Peer Trading Framework Integrating Energy and Carbon Markets,"* Applied Energy, Accepted on 15-Jul-2020.

CRediT authorship contribution statement:

Weiqi Hua: conceptualisation of peer-to-peer trading, methodology of smart contract and optimisation, investigation of the blockchain technologies, formal analysis of simulation results, data curation, writing original draft, manuscript visualization.

Jing Jiang: supervision, review and editing, validation of simulation results.

October 8, 2020

Hongjian Sun: supervision, project administration, review and editing, funding acquisition, validation of simulation results.

Jianzhong Wu: supervision, review and editing, validation of simulation results.

– **Weiqi Hua**, Jing Jiang, Hongjian Sun, Fei Teng and Goran Strbac, *"Blockchain Enabling Decentralised Low Carbon Negotiation and Power Systems Scheduling,"* IEEE Transactions on Smart Grid, Submitted on 17-Aug-2020.

CRediT authorship contribution statement:

Weiqi Hua: conceptualisation of low carbon negotiation and energy scheduling, methodology of smart contract and optimisation, investigation of the negotiation platform, formal analysis of simulation results, data curation, writing original draft, manuscript visualization.

Jing Jiang: supervision, review and editing, validation of simulation results.

Hongjian Sun: supervision, project administration, review and editing, funding acquisition, validation of simulation results.

Fei Teng: supervision, review and editing.

Goran Strbac: supervision, review and editing.

– **Weiqi Hua** and Hongjian Sun, *"A Blockchain-Based Peer-to-Peer Trading Scheme Coupling Energy and Carbon Markets,"* International Conference on Smart Energy Systems and Technologies (SEST), Porto, Portugal, 2019, pp. 1-6.

CRediT authorship contribution statement:

Weiqi Hua: conceptualisation of peer-to-peer trading, methodology of blockchain network, investigation of the blockchain technologies, formal analysis of simulation results, data curation, writing original draft, manuscript visualization.

Hongjian Sun: supervision, project administration, review and editing, funding acquisition, validation of simulation results.

October 8, 2020

– Hongjian Sun, **Weiqi Hua** and Minglei You, *" Blockchain and Artificial Intelligence Technologies for Smart Energy Systems–Applications in Energy Internet and Energy System Integration,"* CRC Press, Book Proposal Approved and Will Be Delivered by Jan-2021.

CRediT authorship contribution statement:

Hongjian Sun: supervision, review and editing, preparing book proposal.

Weiqi Hua: writing Chapter 1 - 6, discussing the content of book.

Minglei You: writing Chapter 1, and 7 - 8, discussing the content of book.

October 8, 2020

Acknowledgements

I would like to express my sincere gratitude to my supervisor Dr. Hongjian Sun. As the supervisor of both my master and PhD studies, Dr. Hongjian has continuously provided me with huge opportunities, supportive encouragements, tremendous suggestions. The rigorous academic attitude and positive life attitude from Dr. Hongjian are treasures for my entire life and future career.

I would like to thank the invaluable assistance and guidance from Dr. Peter Matthews, Dr. Jing Jiang from Northumbria University, Dr. Wei-yu Chiu from National Tsing Hua University, Prof. Jianzhong Wu from Cardiff University, Prof. Andrea M. Tonello from Alpen-Adria-Universität Klagenfurt, Dr. Fanlin Meng from University of Essex, Dr. Fei Teng and Prof. Goran Strbac from Imperial College London. I have learned a great deal from their expertises. I wish to show my gratitude to Dr. Velissarios Gezerlis and Dr. Tilemachos Doukoglou for their hospitality during my secondment at the OTE in Greece, and to Dr. Wei Pei and Dr. Hao Xiao for their enthusiastically hosting during my secondment at Chinese Academy of Sciences in China. I would like to thank the Hyundai Motor Company and Durham University Research Doctoral Studentship for funding my PhD research. I am also grateful for the Chinese Students Awards funded by the Great Britain-China Centre.

My sincere thanks also for my colleagues: John Heron, Monica Hernandez-Cedillo, Martha Correa-Delval, Huw Thomas, Minglei You, Diana Martinez-Trejo, Eduardo Gonzalez-Osuna, Donatella Zappala, Jacki Bell, Marcos Eduardo Cruz Victorio, and Cuong Dao. Working with them makes my PhD study more memorable and enjoyable.

I deeply appreciate all my friends in Durham: Xiangdong Wang, Dan Li, Qitao Liu, Xin Zhang, Yingjia Huang, Ning Jia, Qian Wang, Rui Fang, Baihui Cui, Xi

Zhang, MingMing Shao, Mingjuan Wang, Jiuyan Sun, Xiujuan Zhao, Yanjun Tan, Yuelin Ma, Yingjie Su, Yushu Sun, Zhenxing Zhao, and Chuxia Huang. It is my precious fortune to spend every moment of happiness and sadness with you.

I would like to pay my special appreciate to my parents and my girl friend, Ying Chen. I would not achieve this without your endless love, support, and encouragement.

Last but not the least, I would like to pay tribute to global doctors, nurses, and key workers who have worked tirelessly and selflessly to help get through the coronavirus pandemic.

October 8, 2020

Contents

List of Figures

List of Tables

Nomenclature

$\alpha^{\max}$	Maximum level of monetary compensation rate (£/kg).
$\alpha^{\min}$	Minimum level of monetary compensation rate (£/kg).
α_t	Monetary compensation rate at scheduling time t (£/kg).
$\bar{\rho}_i$	Average annual carbon emissions intensity of source i (kg/kWh).
β	Binary value indicating if the seller type is prosumer or microgrid tarder.
$\Delta\hat{\mathbf{P}}^*_x$	Matrix of training output of scenario x.
$\Delta\mathbf{p}_x$	Vector of decision variables of scenario x.
$\Delta p_{\text{main},t,x}$	Amount of modifying the power exchange from the main grid of a prosumer's scenario x at scheduling time t (kW).
$\Delta p_{i,t,x}$	Amount of modifying the generation by generator i of a prosumer's scenario x at scheduling time t (kW).
$\Delta p_{k,t,x}$	Amount of modifying the consumption by load k of a prosumer's scenario x at scheduling time t (kW).
$\Delta p_{s,t,x}$	Power charging/discharging rate of a prosumer's energy storage device of scenario x at scheduling time t (kW).
$\Delta p_s^{\max}$	Maximum charging/discharging rate (kW).
$\Delta r^{\max}$	Maximum level of abatement for the total carbon emissions rate (kg/h).
$\Delta r^{\min}$	Minimum level of abatement for the total carbon emissions rate (kg/h).

$\Delta r_{k,t}$	Amount of abatement for the carbon emissions rate of load k at scheduling time t (kg/h).
Δr_t	Amount of abatement for the total carbon emissions rate at scheduling time t (kg/h).
Δt	Scheduling interval (0.5 h).
δ_i	Operating costs coefficient of generator i (£/kWh).
δ_s	Cost coefficient of energy storage devices (£/kWh).
γ	Monetary compensation for carbon reduction of a prosumer (£).
$\gamma^{\max}$	Maximum monetary compensation for carbon reduction of a prosumer (£).
γ_k	Function of monetary compensation for carbon reduction of load k (£).
$\gamma_k^{\max}$	Maximum monetary compensation for carbon reduction of load k (£).
ι	Nominal number of iteration.
$\iota^{\max}$	Maximum number of iteration.
ι_{FDIA}	Nominal number of iteration of FDIA.
$\iota_{\text{FDIA}}^{\max}$	Maximum number of iteration of FDIA.
ι_{IA}	Nominal umber of iteration of immune algorithm.
$\iota_{\text{IA}}^{\max}$	Maximum umber of iteration of immune algorithm.
ι_{LMIA}	Nominal number of iteration of LMIA.
$\iota_{\text{LMIA}}^{\max}$	Maximum number of iteration of LMIA.
$\lfloor \cdot \rfloor$	Floor function.
$\overline{\mathbf{p}}$	Vector of upper bounds of decision variables.
$\overline{\mathbf{p}}_{\text{follower}}$	Vector of upper bounds of decision variables of all followers.

$\overline{\mathbf{p}}_{\text{leader}}$	Vector of upper bounds of decision variables of leader.
$\mathbf{\Phi}_{\text{map}}$	Array of the feature map.
$\mathbf{\Phi}_x$	Array of elasticity image of scenario x.
$\underline{\mathbf{p}}$	Vector of lower bounds of decision variables.
$\underline{\mathbf{p}}_{\text{follower}}$	Vector of lower bounds of decision variables of all followers.
$\underline{\mathbf{p}}_{\text{leader}}$	Vector of lower bounds of decision variables of leader.
$\mathbf{b}$	Bias Vector.
$\mathbf{f}_x$	Vector of objective functions of scenario x.
$\mathbf{f}_{\text{follower}}$	Vector of objective functions of all followers.
$\mathbf{f}_{\text{leader}}$	Vector of objective functions of leader.
$\mathbf{f}_{\text{rep}}$	Vector of representative objective functions form the Pareto frontier.
$\mathbf{i}$	Unit row vector.
$\mathbf{P}_{\text{B}}$	Matrix of the distribution of power inflows to each of buses.
$\mathbf{P}'_{\text{B}}$	Matrix of the distribution of power outflows from each of buses.
$\mathbf{P}_{\text{CEFC}}$	Matrix of the distribution of power loads.
$\mathbf{P}_{\text{CEFG}}$	Matrix of power outputs of generators.
$\mathbf{P}_{\text{CEFT}}$	Matrix of the distribution of the total power inflows from both other buses and generators.
$\mathbf{p}_{\text{follower}}$	Vector of decision variables of all followers.
$\mathbf{p}_{\text{leader}}$	Vector of decision variables of leader.
$\mathbf{P}_x$	Matrix of training input of scenario x.
$\mathbf{p}_x$	Vector of decision variables of scenario x.

$\mathbf{R}_{\mathrm{CEFC}}$	Matrix of carbon emissions rates of consumption.
$\mathbf{r}_{\mathrm{CEFG}}$	Vector of carbon emissions rates of generators.
$\mathbf{R}_{\mathrm{CEFL}}$	Matrix of carbon emissions rates of transmission losses.
$\mathbf{R}_{\mathrm{CEFT}}$	Matrix of carbon emissions rates of transmission.
$\mathbf{W}$	Weight array.
$\mathcal{A}$	Set of antigen population.
$\mathcal{A}^{\max}$	Set of maximum antigen population.
$\mathcal{A}^{\max}_{\mathrm{leader}}$	Set of maximum antigen population of leader.
$\mathcal{A}_{\mathrm{follower}}$	Set of antigen population of followers.
$\mathcal{A}^{\max}_{\mathrm{follower}}$	Set of maximum antigen population of followers.
$\mathcal{A}_{\mathrm{leader}}$	Set of antigen population of leader.
$\mathcal{A}_c$	Set of clonal antigen population.
$\mathcal{B}_{\mathrm{carbon},t}$	Set of bidding prices submitted by all the carbon allowance buyers for the offer of selling carbon allowance at scheduling time t.
$\mathcal{B}_{\mathrm{energy},t}$	Set of bidding prices submitted by all energy buyers for the offer of selling energy at scheduling time t.
$\mathcal{B}_t$	Set of bidding prices submitted by all the buyers for the offer of selling energy or carbon allowance at scheduling time t.
$\mathcal{I}$	Index set of generators.
$\mathcal{K}$	Index set of loads.
$\mathcal{L}$	Index set of transmission lines.
$\mathcal{M}$	Index set of historical metering data.
$\mathcal{N}$	Index set of prosumers in the same microgrid.

$\mathcal{O}_u$	Offer of seller u.
$\mathcal{P}$	Set of Pareto optimal.
$\mathcal{P}_{\text{leader}}$	Set of Pareto optimal of leader.
$\mathcal{T}$	Index set of scheduling time.
$\mathcal{T}_{\text{buyer}}$	Index set of scheduling time when a prosumer is an energy buyer.
$\mathcal{T}_{\text{seller}}$	Index set of scheduling time when a prosumer is an energy seller.
$\mathcal{U}$	Index set of sellers.
$\mathcal{U}_v^*$	Set of optimal offers combination that can meet buyer v' s demand with minimal required bidding prices.
$\mathcal{V}$	Index set of buyers.
$\mathcal{X}$	Index set of scenarios.
$\overline{f}$	Maximal value of objective function.
$\pi_{\text{carbon},t}$	Carbon price at scheduling time t (£/kg).
$\pi_{\text{carbon}}^{\max}$	Maximum level of carbon price (£/kg).
$\pi_{\text{carbon}}^{\min}$	Minimum level of carbon price (£/kg).
$\pi_{\text{ws},t}$	Wholesale electricity price at scheduling time t (£/kWh).
$\pi_{t,x}$	Retail electricity price of scenario x at scheduling time t (£/kWh).
π_t	Retail electricity price at scheduling time t (£/kWh).
$\rho_{\text{CCGT},t}$	Carbon emissions intensity of CCGT at scheduling time t (kg/kWh).
$\rho_{\text{coal},t}$	Carbon emissions intensity of coal at scheduling time t (kg/kWh).
ρ_{main}	Average carbon emissions intensity of all generation sources from the main grid (kg/kWh).

ρ_i	Carbon emissions intensity of a prosumer's own generator i (kg/kWh).
ρ_{CEFG}	Vector of carbon emissions intensities of generation.
ρ_{CEFT}	Vector of carbon emissions intensities of transmission and consumption.
τ_{now}	Current time.
τ_u	Time of auction ended specified by seller u.
$\cos\theta_{\text{CCGT},t}$	Power factor of CCGT at scheduling time t.
$\cos\theta_{\text{coal},t}$	Power factor of coal at scheduling time t.
diag	Operation to create diagonal matrix.
id_u	Encrypted address of seller u.
Pr	Occurrence probability.
$\tilde{f}$	Estimated kernel density function.
$\underline{f}$	Minimal value of objective function.
ε	Binary value indicating if the trading type is energy or carbon allowance.
ϱ	Ratio of the carbon emissions from consumption side to total carbon emissions.
ς	Bandwidth smoothing parameter.
ϑ	Random variable in $[0, 1]$.
ϑ_{Pr}	Binary variable in $\{0, 1\}$.
$\xi_{p_{i,x}}$	Function of price elasticity of generation.
$\xi_{p_{k,x}}$	Function of price elasticity of consumption.
ξ_{r_x}	Function of price elasticity of carbon emissions.
Ξ	Vector of price elasticities between any two scheduling time.

$b_{u,t}^{\text{highest}}$ Currently highest bidding price for the energy or carbon allowance to be provided by the seller u at scheduling time t (£/kWh or £/kg).

$b_{u,t}^{\min}$ Minimal accepted bidding price specified by seller u for the energy or carbon allowance to be provided at scheduling time t (£/kWh or £/kg).

$b_{\text{balance},u}$ Account balance of seller u (£).

$b_{\text{balance},v}$ Account balance of buyer v (£).

b_{balance} Account balance of a buyer (£).

$b_{\text{carbon},t}$ Bidding price of a prosumer at scheduling time t for buying carbon allowance (£/kg).

$b_{\text{carbon},t}^{\text{highest}}$ The highest bidding price for the carbon allowance selling at scheduling time t over all carbon allowance buyers (£/kg).

$b_{\text{energy},t}$ Bidding price of a prosumer at scheduling time t for buying energy (£/kWh).

$b_{\text{energy},t}^{\text{highest}}$ Currently highest bidding price for the energy selling at scheduling time t over all energy buyers (£/kWh).

$b_{u,t}^{\text{highest}*}$ Final highest bidding price for the energy or carbon allowance to be provided by the seller u at scheduling time t (£/kWh).

c Generating costs of power generation of a prosumer excluding carbon cost (£).

$c_{\text{carbon,n}}$ Carbon cost (or revenue) of power generation of prosumer n (£).

c_{carbon} Function of carbon cost/revenue of an energy seller (£).

c_i Generating costs of generator i excluding carbon cost (£).

d_v Demand of energy or carbon allowance for buyer v (kg or kWh).

e Amount of carbon emissions during the time interval Δt (kg).

f_{bid}	Bidding function.
f_{CEF}	Function of matrix calculation of carbon emissions flow.
f_{cumul}	Cumulative density function.
f_{init}	Initialisation function.
f_{kernel}	Kernel function.
f_{match}	Matching function.
f_{nn}	Neural networks relationship function.
f_{pay}	Pay-to-seller function.
f_{ReLU}	Activation function.
f_{withdraw}	Withdrawal function.
f_a	Function of inequality constraints.
f_B	Objective function of electricity bills of a MT (£).
f_b	Objective function of electricity bills of a prosumer (£).
f_c	Objective function of total carbon emissions (kg).
f_i	Objective function of profits of generator i (£).
f_k	Objective function of electricity bills of consumer k (£).
f_n	Objective function of carbon pricing neutrality (£).
f_P	Objective function of profits of a MT (£).
f_p	Objective function of profits of a prosumer (£).
f_u	Objective function of costs of using electricity by a prosumer (£).
i	Index of energy generators.
k	Index of energy loads.

l	Index of transmission lines.
$l_{x,x'}$	Distance between $p_{t,x}$ and $p'_{t,x}$ (kW).
m	Index of historical metering data.
m_u	Microgrid index of seller u.
m_v	Microgrid index of buyer v.
n	Index of prosumers in the same microgrid.
$p_{\text{main},t,x}$	Power exchange of a prosumer with the main grid of scenario x at scheduling time t (kW).
$p_{\text{main}}^{\max}$	Maximum level of power exchange of a prosumer with the main grid (kW).
$p_{\text{main}}^{\min}$	Minimum level of power exchange of a prosumer with the main grid (kW).
$p_{i,t}$	Power generation of generator i at scheduling time t (kW).
$p_i^{\max}$	Maximum power generation capacity of generator i (kW).
$p_i^{\min}$	Minimum power generation level of generator i (kW).
$p_{k,t}$	Power consumption of load k at scheduling time t (kW).
$p_k^{\max}$	Maximum power consumption level of load k (kW).
$p_k^{\min}$	Minimum power consumption level of load k (kW).
$p_{n,t}$	Residual power of prosumer n at scheduling time t (kW).
$p_{s,t,x}$	Stored power of a prosumer's energy storage device of scenario x at scheduling time t (kW).
$p_s^{\max}$	Maximum storage capacity (kW).
$p_{t,m}$	Data sample m of uncertain variable p_t (kW).

$p_{t,x}$	Scenario x of uncertain variable p_t (kW).
p_t	Uncertain variable representing power gwnwration and consumption (kW).
$r_{\text{allow},t}$	Carbon allowance of a prosumer at scheduling time t (kg/h).
$r_{\text{net},t}$	Carbon emissions rate caused by using a prosumer's own generation for supplying other prosumers' demand at scheduling time t (kg/h).
r_c	Clonal rate.
$r_{i,t}$	Carbon emissions rate caused by power generation of generator i at scheduling time t (kg/h).
$r_{k,t}$	Carbon emissions rate caused by power consumption behaviour of load k at scheduling time t (kg/h).
$r'_{k,t}$	Carbon emissions rate caused by power consumption behaviour of load k at scheduling time t before policy maker's incentive (kg/h).
$r_{l,t}$	Carbon emissions rate caused by power transmission loss of line l at scheduling time t (kg/h).
$r_{t,x}$	Carbon emissions rate of a prosumer's scenario x at scheduling time t (kg/h).
s_u	Amount of energy or carbon allowance to be supplied by seller u (kg or kWh).
t	Index of scheduling time.
u	Index of sellers.
v	Index of buyers.
x	Index of scenarios.
CCGT	Combined cycle gas turbine

CEF	Carbon emissions flow
CEFC	Carbon emissions flow from consumption
CEFG	Carbon emissions flow from generation
CEFL	Carbon emissions flow from transmission loss
CEFT	Carbon emissions flow from transmission
CNN	Convolutional neural network
DNN	Deep neural network
DRES	Distributed renewable energy source
FAIA	Followers aggregated immune algorithm
FDIA	Followers distributed immune algorithm
LCoE	Levelised cost of electricity generation
LCoS	Levelised cost of storage
LMIA	Leaders Multiobjective immune algorithm
LSTM	Long short term memory
MOP	Multiobjective problem
MT	Microgrid Trader
RNN	Recurrent neural network

Chapter 1

Introduction

1.1 Background

The world's population is expected to increase from 7.7 billion currently to 9.7 billion over the next 30 years [1], with the energy demand rising by nearly 50 % [2]. When providing essential energy to humans, the combustion of fossil fuels including coal, gas, and oil will convert solid carbon elements into gaseous carbon emissions. The large-scale release of anthropogenic carbon emissions would break the balance of natural carbon cycle and lead to irreversible effects of climate change [3]. In efforts to address this environmental challenge globally, the Intergovernmental Panel on Climate Change aims to keep global warming below 2 °C and halve the greenhouse gases by 2050 compared to the 1990 level [4]. The Kyoto Protocol [5] in 1997 is the first step towards the global low carbon targets, under which countries are expected to meet their targets through domestic policies and regulations for facilitating renewable energy, improving energy efficiency, reducing landfills emissions, and restricting industrial emissions.

The power systems represent around 40 % of global carbon emissions from the combustion of fossil fuels [6]. The carbon emissions intensity which quantifies the amount of carbon emissions produced by per unit of energy generation [7] has proportionally increased with the growth of energy demand. To facilitate a transition towards low carbon power systems, the U.K. government announced the Carbon Plan [8] in 2011 for increasing the penetration of renewable energy sources, incen-

tivising demand side carbon mitigation, and enhancing energy efficiency. This policy measure has successfully reduced the average carbon emissions intensity in the U.K. power systems from 0.545 kg/kWh in 2012 to 0.200 kg/kWh in 2019 given the increasing energy demand, and the expected carbon emissions intensity by 2030 is 0.050 kg/kWh [9].

The smart grid is an enabling technology of future low carbon power systems. The concept of smart grid refers to a range of operating and controlling measures in power systems including demand side management, renewable energy sources, energy storage, electric vehicles, smart meters, and home energy manage systems [10]. From the communication perspective [11], the smart grid enables the bidirectional communication between power systems and individual generators and consumers, which facilitates the optimal operation of generators and the active engagement of consumers. From the controlling perspective [12], the interoperability of smart grid enables market participants to cooperatively achieve the overall benefits of power systems, such as saving electricity bills for consumers, improving operating profits for generators, mitigating carbon emissions, and enhancing security of supply.

The supports of low carbon policies and advances of smart grid technologies enable consumers to actively produce, consume and store energy through renewable energy sources, storage devices, electric vehicles, and smart meters. The power systems are transitioning towards a prosumers era [13]. The new figure of prosumers represents a small-sized or medium-sized agents [14], such as residential, commercial, and industrial consumers, who produce energy for self-consumption and feed surplus energy into distribution networks. Prosumers can also strategically exchange energy with the main grid or other prosumers for meeting their demand or increasing their revenues. An intelligent power systems and flexible energy markets structure are crucial for the integration of emerging role of prosumers. How to incorporate these advanced communication, control, and computational technologies of smart grid with the regulatory supports for realising reliable, efficient, and low carbon future power systems towards prosumers era presents a challenge to be addressed in this thesis.

1.2 Research Motivations and Challenges

The motivation behind this thesis is to establish how smart grid enables prosumers to be appropriately integrated into energy markets for decarbonising future power systems. In doing this, consideration should be given to the following three aspects:

- From regulatory perspective, how to determine appropriate policy measures to facilitate the penetration of renewable energy sources and encourage passive consumers to participate in carbon mitigation.
- From individual prosumer's perspective, how to strategically schedule their own generation and consumption for improving self-benefits, e.g. bill saving and profit improving, in an environmentally friendly manner.
- From community's perspective, how to design a mechanism enabling an ensemble of prosumers corporately achieve regional benefits, e.g. energy balance, and targets of carbon emissions reduction.

Fulfilling these three aspects is the subject of active research. Nonetheless, there still remains a number of challenges. This thesis is an attempt to address the following challenges:

- The long-term low carbon policy for overall anthropogenic carbon emissions cannot target on power systems. A power systems specific low carbon policy design that can dynamically adjust incentive measures after receiving the responses from generators and consumers needs to be considered.
- The idiosyncratic prosumption patterns cause the issues of scalability and computational complexity for model-based energy scheduling.
- How individual prosumers' intrinsic features affect their decisions of generation, consumption, and incurred carbon emissions in responding to electricity prices needs to be investigated.
- It is challenging to accurately predict prosumption behaviours in particular given uncertainties caused by the intermittency of renewable energy sources and flexible demand.

- The centralised pricing scheme reflects the supply-demand relationship of overall energy markets and is uniform for all customers. This scheme is independent of energy exchange among prosumers and thus not every prosumer can be efficiently incentivised to reduce carbon emissions and participate in energy trading.

- Separately designing energy or carbon markets is not efficient, because the purchasing of carbon allowance is a part of energy costs. A decentralised trading framework needs to be designed enabling prosumers to trade energy and carbon allowance together.

- When individual prosumers proceed peer-to-peer trading, it is hard to ensure the settlement and delivery without a standardised negotiation and enforcing mechanism.

- The individual prosumers' carbon emissions caused by generation for self-consumption, consumption from self-generation, and generation (or consumption) for (or from) energy exchange with other prosumers cannot be traced using existing approaches and then incentivised properly. This is more challenging when prosumers trade energy or carbon allowance, because they need to know how much carbon allowance needs to be purchased as carbon cost.

1.3 Contributions

Through addressing the aforementioned challenges, this thesis offers the following contributions:

- A novel energy scheduling model is proposed enabling the dynamic negotiation of policy measures and power profiles between policy maker and generators/consumers to achieve low carbon power systems. The process of negotiation and reaching an agreement of optimal policy design and scheduling decisions is modelled as a Stackelberg game-theoretic problem which is solved by the developed algorithm based on artificial immune system. Case studies

demonstrate that the proposed model outperforms the models of multiobjective optimisation and aggregated scheduling in terms of electricity bills saving and carbon emissions reduction. This model can also incentivise both the increase of renewable energy sources and demand side carbon emissions reduction.

- A data-driven prosumer-centric energy scheduling tool is designed by using learning approaches to improve the scalability and computational efficiency from the model-based approaches. This scheduling tool exploits the convolutional neural networks (CNNs) and developed prosumption patterns processing approach to analyse local features, temporal transient features, and the correlation of dynamic price elasticities. A real-time scenarios selection approach is designed to improve prediction accuracy under uncertainties. Case studies verify that the proposed scheduling tool can accurately predict the optimal scheduling decisions and demonstrate the connection between intrinsic features of dynamic price elasticities and prosumers' scheduling strategies.

- A blockchain-based peer-to-peer trading framework is developed enabling prosumers to jointly trade energy and carbon allowance at both prosumer level and microgrid level. The biding/selling prices of individual prosumers can directly incentivise the reshaping of prosumption behaviours for energy balance and carbon reduction. A carbon emissions tracing approach targeting on individual prosumers' behaviours is designed to ensure a fair allocation of low carbon incentives. The proposed energy scheduling algorithms interface with the self-enforcing nature of smart contract to automate the standardised auction procedure. Case studies testify the proposed trading framework and demonstrate the execution of smart contract on the Ethereum blockchain.

1.4 Thesis Outline

The remainder of this thesis is organised as follows:

Chapter 2

In this chapter, a review of smart grid technologies and potential energy markets design towards prosumers era is performed. The current low carbon policies and carbon tracing approaches are introduced, followed by an illustration of the state-of-the-art models and approaches for energy scheduling and blockchain technologies.

Chapter 3

In this chapter, the proposed Stackelberg game-theoretic model for day-ahead energy scheduling and low carbon negotiation between the policy maker and consumers/generators is proposed. The developed algorithms based on the artificial immune systems are also introduced. Case studies based on the U.K. power systems are provided to demonstrate the effectiveness of the proposed model in terms of saving electricity bills, increasing the penetration of renewable energy sources, and reducing carbon emissions.

Chapter 4

In this chapter, the proposed data-driven prosumer-centric energy scheduling tool is introduced. The implementation of this scheduling tool includes the training phase and deploying phase, by which the training phase describes how to use scenarios, prosumption patterns, and optimal scheduling decisions for training the neural networks, and the deploying phase presents the real-time data driven energy scheduling and scenarios update algorithm. Case studies are performed under various IEEE test systems and uncertain scenarios.

Chapter 5

In this chapter, the proposed blockchain-based peer-to-peer trading framework is presented. Corresponding to each layer, the details of problem formulation and the smart contract based auction mechanism are described. The case studies based on the IEEE 37-bus distribution network are presented to examine the performance of energy balance and carbon mitigation. The execution of smart contract based on the Ethereum blockchain is also demonstrated.

Chapter 6

This chapter concludes the primary findings and results from this thesis, and indicates the potential extensions in the future work.

Chapter 2

Literature Review

2.1 Introduction

The literature review presented in this chapter is inspired by the issue of how smart grid enables prosumers to be appropriately integrated into energy markets for decarbonising power systems. The objective of this literature review is to discuss in details about a variety of smart grid technologies, potential markets design for prosumers, approaches of carbon emissions assessment, associated regulatory supports, approaches of power systems scheduling, and enabling technologies for peer-to-peer trading, for the purpose of finding out research challenges and providing a better insight in these areas.

The rest of this chapter is organised as follows: Section 2.2 discusses various smart grid technologies and the role of these technologies in integrating prosumers into energy markets. The potential market design towards prosumers era is introduced. Section 2.3 reviews the low carbon policies implemented by various countries and documented by literature, followed by a discussion of carbon emissions tracing approaches as a foundation to inform policy design. The state-of-the-art approaches for energy scheduling to achieve both environmental and economic benefits of power systems are illustrated in Section 2.4. The origin and development of blockchain technologies are discussed in Section 2.5, by which how blockchain and smart contract facilitate the peer-to-peer trading is specifically focused.

2.2 Smart Grid

Smart grid is an intelligent electricity network which cost effectively integrates communication, information and control infrastructure with all connected users, enabling bidirectional flows of energy and information [15]. The users include all generators, consumers, and prosumers. The objective of smart grid is to achieve sustainable, secure, and economic power supply and active participation of consumers. A conceptual graph of smart grid is presented in Fig. 2.1. The advances of smart grid are summarised as follows:

- Smart grid implements digital processing and communication into the electricity network to enable real-time bidirectional information flows, which allows the systems uncertainties to be precisely predicted [16, 17].
- The optimal energy dispatch and accurate forecast of smart grid provide a solution to the intermittency of renewable energy sources. Hence, smart grid enhances the penetration of renewable energy sources so as to mitigate carbon emissions from power systems.
- Smart grid ensures the continuity of power flows and thus guarantees the power systems stability and security of supply.
- The automation of distribution network enhances the energy balance through demand side management and regional energy trading.

In this section, the smart grid components and associated potential energy markets design with the integration of prosumers are introduced.

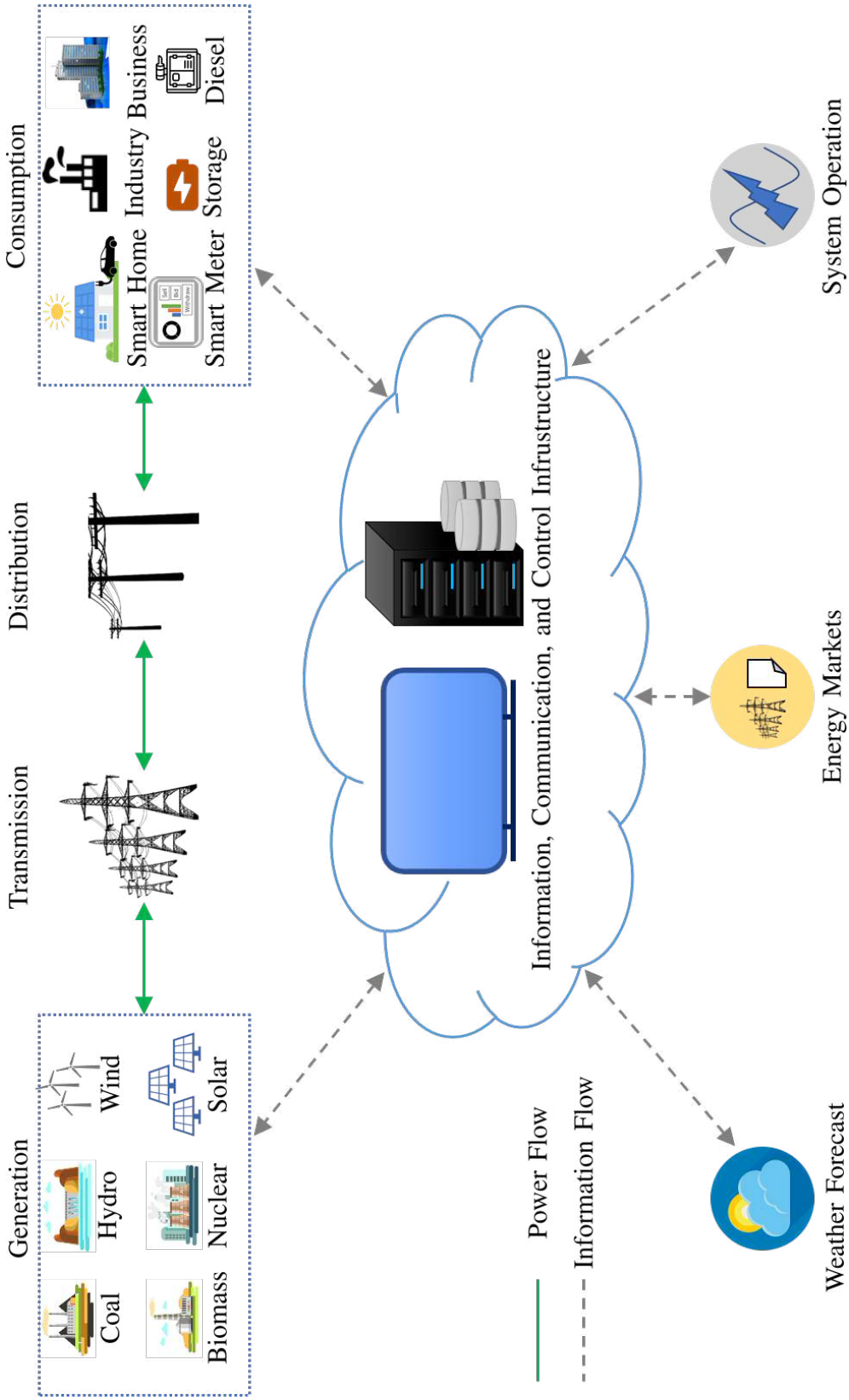

Figure 2.1: Conceptual graph of smart grid.

2.2.1 Components of Smart Grid

Demand Side Management

As one of the key smart grid technologies, the demand side management is defined as reshaping energy behaviours of consumers for supply-demand balance through monetary incentives or education [18]. The demand side management aims to meet peak demand without increasing the capacity of power networks, and balance intermittent generation of renewable energy sources with demand [19].

The concept of demand side management was coined in 1973, following the first energy crisis in American electric power industry [20]. This crisis was caused by the heavy dependence on foreign energy imports and the rise of oil prices. To tackle this energy crisis, the U.S. Congress legislated the National Energy Act [21] to reduce the dependence of foreign energy, improve energy efficiency, facilitate alternative energy sources, and encourage demand side management. The further two energy crises in 1979 and 1990 [22], as well as the California electricity crisis in 2001 amplify the importance of demand side management. Currently, the advanced information and communication technologies of smart grid enhance the feasibility and public involvement for demand side management [23].

The approaches for delivering demand side management can be categorised as follows:

- *Energy Efficiency*: Consumers can deliver the same tasks with fewer energy demand by improving energy efficiency of their loads [24].

- *Demand Response*: The demand response refers to reshaping consumption behaviours in response to the incentive of electricity prices [25]. The management is delivered by curtailing energy demand of consumers during peak time periods or shifting energy demand of consumers from peak time periods to off-peak time periods such as midnight or weekends [26].

- *Dynamic Demand*: The operating cycles of loads can be adjusted by a few seconds without disturbing the consumption of end users to increase the diversity factor of power systems [27]. The loads states, e.g. power factors and

control parameters, are monitored to optimally schedule the operating time of loads and reduce critical power mismatch.

- *Distributed Generation*: Different from the conventional large-scale centralised generation such as coal, gas and nuclear power plants, which requires long-distance transmission, the distributed generation is located in demand side through using renewable energy sources. The distributed generation can strategically dispatch power outputs by incorporating with energy storage devices and smart grid technologies.

Renewable Energy Sources

Renewable energy sources are derived from natural process and can be replenished constantly [28]. The renewable energy sources include wind, solar, hydro, geothermal, and bioenergy [29]. The increasing penetration of renewable energy sources contributes to significant energy security, carbon emissions mitigation, and economic benefits. Nonetheless, the intermittency caused by weather conditions presents a challenge for the integration of renewable energy sources into power systems. Smart grid holds the key to overcome this challenge. The advanced communication and information infrastructures of smart grid incorporating with energy storage devices enable the renewable energy sources to be optimally dispatched.

In the U.K., there are 1,007,427 installations of solar panels by the end of June 2019, providing a total capacity of 13.1 GW [30]. It is expected that the total capacity increases to 15.7 GW by 2023 and 10 millions homes would cover their roof with solar panels [31]. The 12 GW installed capacity of onshore wind has met the annual demand of 7.25 million homes [32]. The offshore wind accounts for over 10 % of the U.K. electricity generation in 2020. The U.K. Government has also committed to 40 GW of installed offshore capacity by 2030 [33].

Energy Storage

The pressure of increasing intermittent renewable energy sources and growing energy demand drives the development of energy storage markets [34]. Energy storage technologies can flexibly absorb or release energy when required with the benefits

for system stability and security of supply [35]. Storage technologies can decrease the need for investing in additional generation capacities, contributing to financial savings and carbon emissions mitigation from power generation. The deployment of energy storage devices also enhances the systems capacities and reduces the costs of updating transmission and distribution systems.

Smart Meters and Home Energy Management

Smart meter is an enabling technology for home energy management, real-time pricing, peer-to-peer trading, and low carbon power systems. With the smart meter installed, consumers can self-read and control their energy use, so as to adopt energy efficiency measures and save energy bills [36]. By 2020, there are 18.1 million smart meters installed in GB, consisting of 11 million electricity meters and 7.1 million gas meters [37]. These smart meters facilitate small-scale energy producers with distributed renewable energy sources (DRESs) to be integrated into the power grid. Additionally, smart meter holds the key to demand side carbon emissions mitigation. From short-term perspective, consumers can be dynamically incentivised by real-time pricing to save their bills by using energy generated from low carbon sources during off-peak periods. From long-term perspective, consumers can cost-effectively invest DRESs and integrate electric vehicles.

The smart control and communication technologies also enhance the efficiency of home appliances to form a home energy management systems. The home energy management systems allow the users to monitor their energy generation and consumption and automatically control the use of energy in a cost-effective manner [38]. The home energy management systems consist of hardware and software. The hardware is the communication infrastructure between the smart appliances and end users. The software collects data from monitored information of energy usage and generates control functions based on users' preferences. For instance, receiving real-time pricing signals, the home energy management systems can help consumers strategically shift or curtail their loads as responses.

2.2.2 Energy Markets Transition Towards Prosumers Era

The advances of smart grid technologies with regulatory supports for low carbon development enable consumers to produce, consume, and store energy through the DRESs, batteries [39], electric vehicles [40], and smart meters [41]. The conventional power systems are transitioning towards prosumers era. The figure of prosumers was coined by Alvin Toffler in 1980 [42]. On the context of energy markets, prosumers are small-sized or medium-sized agents [13], e.g. residential, commercial and industrial users, who actively produce energy and feed surplus energy into a distribution network after self-consumption; When prosumers' demand cannot be met by self-generation, they import energy from main grids or other prosumers [13].

A transition of energy markets towards decentralised generation and consumption is crucial for the integration of emerging role of prosumers. The possible structures of these innovative energy markets have been well investigated. In our literature review, we identify three types of energy markets design towards the prosumers era: peer-to-peer trading markets, intermediary-based trading markets, and microgrid-based trading markets. These three types of energy markets design are based on the information, communication, and control infrastructure of smart grid, and categorised by the functions of control agents and associated manners of information exchange. The schematic illustration of these three types of energy markets design is presented in Fig. 2.2, where each dot represents a control agent and each interconnected line represents the flow of communication and information exchange.

Figure 2.2: Schematic illustration of energy markets design towards the prosumers era. Under peer-to-peer trading markets, prosumers interconnect with each other to trade electricity and other services; Under intermediary-based trading markets, an ensemble of prosumers is organised by an intermediary to pool generation sources, flexible demand, and storage capacities; Under microgrid-based trading markets, prosumers connect to microgrids and microgrids either connect to the main grid or operate at islanded mode as indicated by dashed lines. Dots indicate prosuming agents. Lines indicate information exchange among agents.

Peer-to-Peer Trading Markets

Inspired by the concept of sharing economy [43], the peer-to-peer trading markets are structured as a completely decentralised trading framework. Prosumers can directly trade electricity and other services, e.g. demand side management [44], energy storage [45], and carbon credits [46]. The role of distribution system operator is limited to managing the trading platform and providing distribution function [47]. In comparison to other markets design, the peer-to-peer trading markets are the least structured framework. Instead of using central authorities, e.g. market operators or retailers, as control agents, each individual prosumers become an independent agent to exchange information with each other and perform control functions [48]. Hence, this framework enables a flexible market structure, with more complexed control agents and information flows as indicated by the highest amounts of dots and lines in Fig. 2.2.

Nonetheless, the information exchanges combined with system states monitored by sensors or smart meters and decisions made by prosumers amplify the volumes of information flows. This presents a challenge for the information infrastructure of current power systems [49]. Another challenge of the peer-to-peer trading markets is how to maintain system constraints and guarantee the security of supply without the central authorities. This requires sophisticated rulesets to align individual prosumers' interests with the overall power systems' benefits.

As practical cases, the RWE [50] has developed peer-to-peer trading platforms integrating functions of controlling decentralised generation, grid management, communication, automation, and security. The Power Ledger [51] provides peer-to-peer energy trading for 11,000 participants from residential and commercial consumers in Australia based on software solutions. This peer-to-peer trading market is supported by Australia government, utilities, and distribution system operator.

Intermediary-Based Trading Markets

The intermediary-based trading markets are more structured than the peer-to-peer trading markets. Under the intermediary-based trading markets, an ensemble of prosumers is organised as a community or local organisation, e.g. smart buildings

[52] and virtual power plants [53]. Each community is managed by an intermediary, e.g. aggregators [54] or retailers [55], as an agent to maintain regional energy balance and provide energy services. All generation sources, flexible demand, and storage capacities within a community are pooled to collectively coordinate resources for local benefits. The intermediary can earn bonus from regulators or utilities for providing services to prosumers such as efficiency update, demand response, and setup of renewable energy sources [56].

An example of the intermediary is the Stem [57] which has designed a platform to provide storage services and demand response for consumers in California through real-time optimisation and automated control. The company of Energy and Meteo Systems [58] in Germany has established a virtual power plant via digital control centre with the services of real-time data management, remotely control of wind and solar generation, energy scheduling, demand side management, and balancing group management. The data collection and controlling decisions are managed by the digital control centre without the need of new IT infrastructure.

Microgrid-Based Trading Markets

The microgrid-based trading markets are the most structured framework, under which prosumers are connected to microgrid and the microgrid can either connect to the main grid or operate at islanded mode. When a microgrid connects to the main grid, prosumers can sell surplus generation to the main grid [13]. Prosumers would be incentivised to generate more energy for earning profits through exporting. When a microgrid operates at islanded mode, the surplus generation can be stored within the microgrid or used for load shifting services [59]. Prosumers would be incentivised to strategically schedule their generation and consumption for regional energy balance. The primary difference between microgrid-based trading markets and intermediary-based trading markets is that there is no intermediary in microgrid-based trading markets to pool the sources together. Individual sources of generation and consumption can directly connect to the microgrid and then to the main grid. Rather than seeking for an intermediary's benefits, e.g. maximising the aforementioned bonus, individual microgrids seek for their own benefits, e.g.

maximising energy exporting or achieving energy balance.

As practical implementations, the Asea Brown Boveri Ltd [60] provides microgrid solutions for customers to ensure reliable, stable and affordable power. The LO3 Energy [61] has developed the Brooklyn microgrid integrating 130 buildings on site to facilitate demand response and improve communication infrastructures.

2.3 Low Carbon Policy Design for Energy Market

This section reviews the low carbon policy design from international regulations and existing research. The carbon emissions tracing approaches are also introduced as a foundation of low carbon policy formulation.

2.3.1 A Review of Market Based Low Carbon Policies

The market based low carbon policies, also known as carbon pricing, are an economic instrument to address carbon emissions caused by the combustion of fossil fuels [62]. The carbon pricing enforces the pollutant emitters to compensate the environmental damage in a monetary manner. Therefore, the implementation of carbon pricing increases the costs of using fossil fuels and subsequently stimulates the carbon mitigation. Two primary forms of carbon pricing are carbon tax and emissions trading scheme. By the end of 2019, carbon pricing has been implemented in 46 countries, of which 25 countries adopt carbon tax and the rest 21 countries adopt emissions trading scheme [63]. The carbon pricing helps these countries achieve their low carbon targets by stimulating energy conservation, improvement of the energy efficiency, and investment of low carbon technologies.

Carbon Tax

The carbon tax levies a fixed rate on carbon content of fossil fuels [64]. The rate of carbon tax is determined by the social cost of carbon which quantifies marginal damage costs of carbon emissions to the society [65]. As a revenue of policy maker, carbon tax can be further redistributed for investing low carbon technologies or providing monetary compensation for demand side carbon mitigation, so as to achieve

the carbon revenue neutrality.

Emissions Trading Scheme

The emissions trading scheme, also known as cap-and-trade scheme, is an alternative policy to carbon tax. Under the emissions trading scheme, the policy makers and regulators allocate a certain amount of carbon allowances for a given time period [66]. Emitters are obliged to have an enough amount of carbon allowances covering the amount of their carbon emissions. The surplus or scarcity of carbon allowances can be traded among emitters [67].

Nonetheless, an inappropriate carbon price determined by the emissions trading scheme would inefficiently incentivise the carbon emissions mitigation and fail to achieve low carbon targets. The issue of inappropriate carbon price presents a challenge for the emissions trading scheme in a majority of countries [68]. If the carbon price lies below the social cost of carbon or the rate at which the low carbon targets can be achieved, it would insufficiently stimulate the mitigation of carbon emissions; If the carbon price in one region is higher than that in another region, the market competitiveness of carbon producers in the high-price region would be harmed. The carbon producers are prone to discharging carbon emissions in the low-price region, while the total amount of carbon emissions remains unchanged, which is defined as the carbon leakage issue [69]. Additionally, the carbon producers will pass the cost of carbon allowance onto consumers in the form of higher prices on the products, e.g. higher electricity prices.

To overcome the issue of inappropriate carbon price, carbon price floor and ceiling are implemented in current international carbon markets by setting an additional price limits for the carbon emissions producers in certain regions [70]. For the case of the U.K. carbon market, because the carbon price of the E.U. emissions trading scheme is lower than the social cost of carbon in the U.K., the carbon price has failed to incentivise the U.K. coal-to-gas transition before 2013 [71]. Afterwards, the U.K. has formulated the carbon price support for its own carbon producers as an additional carbon price floor to the E.U. emissions trading scheme. The U.S. set a similar price floor and facilitated carbon auctions in 2009 [72]. By contrast,

in New Zealand, a carbon price ceiling was enacted through fixed price option to prevent high carbon prices and protect market competitiveness of generators [73].

Comparison Remark

As two well-established policy instruments, the carbon tax and emissions trading scheme have following aspects in common:

- Both carbon tax and emissions trading scheme impose a price on carbon emissions for facilitating energy producers and consumers to internalise the social cost of carbon.
- Instead of command-and-control based policy measures that specify actions for carbon mitigation to be taken, the market based policy measures flexibly incentivise carbon producers to strategically respond to the prices.
- Market based low carbon policies can generate public revenue through charging carbon tax or selling carbon allowance.

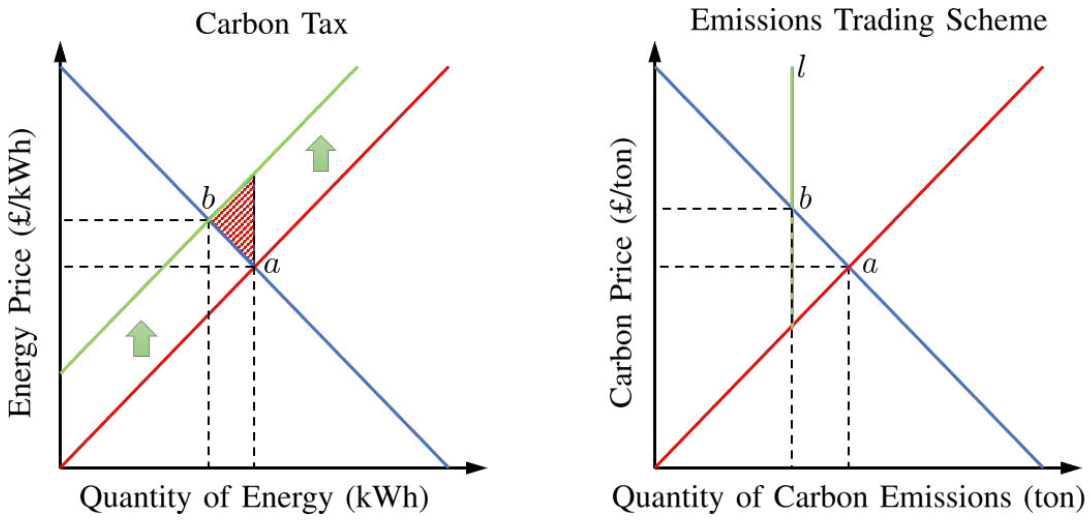

Figure 2.3: Comparison between carbon tax and emissions trading scheme from economics perspective. The implementation of carbon tax would raise energy price and reduce energy demand. The emissions trading scheme would limit the total carbon emissions and raise carbon price.

The differences between carbon tax and emissions trading scheme including the advantages and limitations of each policy design are as follows:

- The carbon tax gives a certainty to the price of carbon emissions through fixed tax rate, whereas the emissions trading scheme gives a certainty to the quantity of carbon emissions through fixed carbon allowance [74].

- Carbon tax is easier to be implemented since it is based on established tax systems. By contrast, emissions trading scheme is more flexible since it can be extended with financial innovation such as peer-to-peer trading, options, banking, and borrowing.

- From economics perspective as indicated in Fig. 2.3, when the carbon tax is implemented, the energy price increases and the energy demand decreases from point a to point b. Consumers would find alternatives, e.g. loads shifting/curtailment, electric vehicles, replacing gas furnace with ground source heat pump. By contrast, under the emissions trading scheme, when the total amount of carbon allowance is fixed according to the target of carbon mitigation as indicated by line l, the carbon price would increase from point a to point b. Facing the uncertainty of carbon price, generators would find alternatives, e.g. improving combustion efficiency, replacing coal by gas, and investing renewable generation.

2.3.2 Carbon Emissions Tracing for Power Systems

Tracing carbon emissions for power systems is a foundation of low carbon development, since it provides options and suggestions that inform low-carbon policy on energy markets and power systems planing [75]. Two primary approaches in literature for tracing carbon emissions from power systems are carbon emissions intensities and carbon emissions flow.

Carbon Emissions Intensities

The carbon emissions from power systems can be evaluated by the usage of fossil fuels and the carbon emissions intensities of related fuels. Evaluation of carbon emissions intensities has been focused by a majority of research [76–79]. For the carbon emissions caused by coal and gas, the displacement by renewable energy sources would

cause part-loaded operation and reduce the generating efficiency. The part-loaded operation consumes more fossil fuels and raises the carbon emissions intensities. The research in [77] investigated the relationship between the dynamic change of carbon emissions intensities and the levels of part-loaded operation using historical data from power systems. For the carbon emissions caused by other sources such as hydro, wind, and biomass, there is no significant impact of part-loaded operation on carbon emissions intensities. The long-term average carbon emissions intensities evaluated by life-cycle carbon analysis [80] are used for calculating carbon emissions. There are three primary approaches to evaluate carbon emissions intensities as follows.

- Average emissions intensity: The average emissions intensity quantifies how much the renewable energy sources displace the annual average carbon emissions from all power generation sources on the power systems [76]. The average intensity is a long-term approximation based on historical observation [81].

- Marginal displacement intensity: The marginal displacement intensity quantifies how much the renewable energy sources displace the carbon emissions from generators operating at the margin [77]. The marginal displacement intensity is evaluated by identifying which power plant responds to changes in outputs of renewable energy sources.

- Marginal emissions intensity: The marginal emissions intensity quantifies how much the renewable energy sources displace the carbon emissions from the marginal changes in power demand [78, 79].

In the GB power systems, the coal and combined cycle gas turbine (CCGT) are the most significant generator types which respond to marginal changes of outputs from renewable energy sources. Hence, the marginal displacement intensity is suitable for evaluating carbon emissions from coal and CCGT. The nuclear is a baseload generator which is only affected by average power generation and corresponding average emissions intensity.

Carbon Emissions Flow

The time-varying and spatial-varying consumption behaviours are a primary driver for the generation from the combustion of fossil fuels. Instead of accounting carbon emissions in generation side, the approach of carbon emissions flow (CEF) targets on individual components of power networks including generators, transmission lines, and consumers. The CEF is a virtual network flow concurrent with power flow to trace carbon emissions caused by generators when transmitting and consuming energy [75]. Analogous to the power flow, the virtual CEF flows along transmission lines from one bus to another under spatial restrictions of power networks. The CEF approach provides a precise information of carbon emissions from specific time and location of power networks and a fair allocation of carbon mitigation responsibilities.

The approach of CEF has been focused in the literature [82–84]. The concept of CEF was initially created from international trades to account carbon responsibilities among countries. Ståhls *et al.* [82] analysed the international carbon flows from a consumption-based perspective and identified the portion of carbon emissions from industrial exports. Further research implemented this concept into power systems to determine the obligation of carbon reduction in energy consumption side. In [83], a CEF tracing approach in power systems was developed to determine the indirect carbon emissions caused by consumption behaviours, by which the regional variation of carbon emissions and locational carbon emissions intensities of individual consumers were identified. Kang *et al.* [84] quantified the carbon emissions accompanying the power delivery process and accumulated the carbon emissions to consumers side. The operational characteristics and the topological features of power networks were considered in this research.

2.3.3 Remark of Research Challenges

Although the market based low carbon policies have been implemented as practical regulations and investigated in the literature, there are still opportunities in designing dynamic low carbon policies. This is because the long-term market policy for overall power systems cannot target on dynamic power profiles and incurred carbon

emissions of individual generators/consumers.

Furthermore, with the participation of prosumers into energy markets, the individual prosumers' carbon emissions caused by generation for self-consumption, consumption from self-generation, and generation (or consumption) for (or from) energy exchange with other prosumers cannot be traced using existing approaches and then incentivised properly. This is more challenging when prosumers trade energy or carbon allowance, because they need to know how much carbon allowance needs to be purchased as carbon cost.

2.4 Approaches of Power Systems Scheduling

The low carbon energy scheduling refers to strategically dispatching power generation from various sources and reshaping power consumption behaviours, for the purpose of carbon emissions reduction, electricity bill saving and generating profit improving [85]. In this section, the state-of-the-art approaches for energy scheduling are reviewed.

2.4.1 Optimisation

The optimisation is an essential approach for power systems scheduling. Under optimisation problems, objectives of energy market participants, e.g. generators, consumers, prosumers, policy makers, system operators, and market operators, are modelled by predefined formulations and parameters, constrained by system capacities, operating conditions and security restrictions. Through solving the optimisation problems, optimal scheduling decisions, e.g. power profiles and electricity prices, can be yielded. In current research for power systems scheduling, the optimisation approaches can be categorised as programming techniques and heuristic algorithms as presented in Fig. 2.4.

The programming techniques include linear programming, integer linear programming, mixed integer linear programming, and non-linear programming. The linear programming refers to an optimisation problem in which all objective functions and constraints are linear functions of decision variables [86]. The integer linear

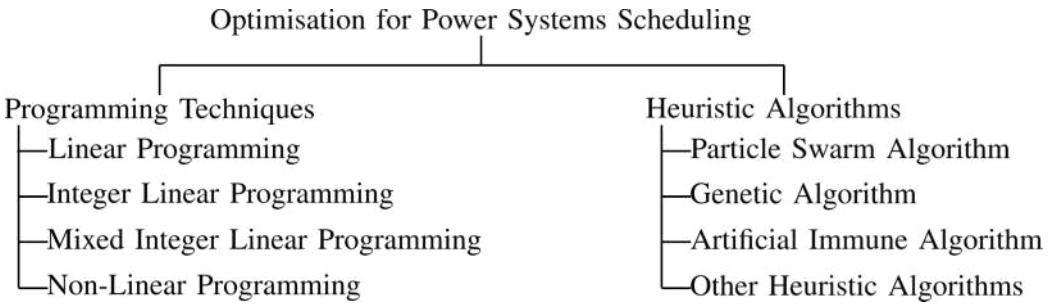

Figure 2.4: Categorises of optimisation approaches for power systems scheduling.

programming differs to linear programming in that only binary values and integers can be used as decisions variables [87]. In the mixed integer linear programming problems, both integers and non-integers can be used as decision variables [88]. The non-linear programming refers to an optimisation problem in which at least one objective function or constraint is non-linear function of decision variables [89].

In the literature, Javaid *et al.* [90] proposed a linear programming model to assign power levels for controllable devices with the objective of costs minimisation, by which the power flows could be optimally controlled to accommodate power fluctuations. In [91], a mixed integer non-linear bi-level programming was formulated to minimise the electricity bills of consumers under a marginal pricing scheme. To solve this problem, the original problem was converted as an equivalent single-level mixed integer linear programming based on the duality theory, integer algebra, and Karush-Kuhn-Tucker optimality conditions. Khushalani *et al.* [92] developed a service restoration algorithm for unbalanced distribution systems, by which the problem was formulated as a mixed integer non-linear programming.

The heuristic algorithms include particle swarm algorithm, genetic algorithm, artificial immune algorithm, and other heuristic algorithms. These algorithms are primarily used for solving non-linear programming problems by iteratively searching over the entire feasible space. The particle swarm algorithm [93] optimises a problem by searching from solution set consisting of particles, and moving particles within the searching space according to predefined functions of particle's position and velocity. The movement of particles is determined by both local best known position and global best known position of searching space. All particle swarm will ultimately move towards the best solution. The genetic algorithm [94] is based on the Darwin's

theory of evolution, by which a population of candidate solutions to an optimisation problem is randomly generated and defined as a generation. The value of objective function for every individual in the population is evaluated and defined as fitness. The highly fitted individuals are selected and mutated to form a new generation. The population is iteratively evolved towards the best solution. Analoguously to the genetic algorithm, in the artificial immune algorithm [95], a population of candidate solutions to an optimisation problem is randomly generated and defined as antigens. The value of objective function for every antigen in the population is evaluated and defined as antibody. The antigens are iteratively cloned towards the best solution.

In the literature, Meng and Zeng [96] formulated a problem for maximising the profits of energy retailers by modelling the effects of real-time electricity prices on shiftable loads and curtailable loads. The problem was solved by genetic algorithm. Olsen *et al.* [97] implemented the weighted sum bisection method to minimise carbon tax rate constrained by maintaining total carbon emissions from power systems below a prescribed target of carbon reduction. This research investigated the relationship between system investments and tax setting process and found that the carbon tax can encourage the investments on cleaner generation, transmission and energy efficiency. Li *et al.* [56] proposed a hierarchical multiobjective scheduling model to integrate renewable energy sources and demand side management. In this model, the utility seeks to minimise operating costs and the customers seek to maximise social welfare. The demand response aggregator as an intermediary seeks to maximise its net profits, which are the difference between bonus from utility for providing demand side management and the cost of offering compensation to customers. A selection criteria was designed to select the optimal solutions yielded by artificial immune algorithm without favouring any market participant. A user-centric multiobjective optimisation problem was further developed in [98] to achieve a tradeoff between residential privacy and energy costs. This research developed a hybrid algorithm by combining a stochastic power scheduling with a deterministic battery control, which addressed the drawbacks of weighted-sum methods, i.e. combing objective functions with various scales, heuristically assigning weight coefficients, and misrepresentation of user preferences.

Nonetheless, the scalability and computational complexity limit the implementation of optimisation approaches on high-complex problems of power systems scheduling. The scalability issue is caused when the scale of power system varies, since each scale requires predefined parameters and mathematical formulations. The computational complexity issue is caused when solving optimisation problems using heuristic algorithms, for which the optimal scheduling decisions are obtained by iteratively searching. At the instance of optimization solved by ι iterations, once it is combined with $|\mathcal{I}|$ types of generators and $|\mathcal{K}|$ types of loads, the computational complexity increases to $O\left(\iota^{|\mathcal{I}|+|\mathcal{K}|}\right)$ [99].

2.4.2 Game Theory

The game theory is gaining increasing attention as an analysis tool for modelling strategic interactions among energy market participants. Cournot and Stackelberg are two classic and common models for analysing actions of market players, e.g. generators or retailers. The Cournot model describes that market players supply homogeneous products, and compete on the amount of supplied products by making decisions independently and simultaneously [100]. On the contrary, the Stackelberg model features a hierarchical two-level or multi-level sequential decision making process [101]. For the two-level decision-making, the players are categorised into a leader level which makes decisions first and a follower level which makes subsequent decisions responding to the leader's strategies. For the multi-level decision-making, after the first level of followers makes responding decisions, they become a leader level to make decisions prioritising the decisions of the next level of followers. This process continues until the last level of followers makes their responding decisions. In energy markets, policy makers, e.g. regulators or system operators, formulate incentive policies prioritising market changes or responses from generators and consumers, so as to achieve certain targets such as reducing carbon emissions or improving social welfare. This sequential action process can be appropriately captured by the two-level Stackelberg model through seizing the strategic interactions of market participants. Additionally, when considering more market participants, e.g. system operators, market operators, and retailers, the multi-level Stackelberg model can

be implemented to capture the interactions among these various participants. For instance, when the policy maker charges the carbon tax from generators, the generators would then increase wholesale prices responding to the increase of generating costs caused by carbon tax. The increase of wholesale prices would incur the increase of retail prices, which results in consumers to change their consumption behaviours for electricity bills saving as responses.

The game theory has been well documented in literature. The game-theoretic models, players and solution approaches in the field of energy scheduling are summarised in Table 2.1. Belgana *et al.* [102] developed a multi-leader and multi-follower Stackelberg game-theoretic problem to find optimal strategies that could maximise the profits of utilities and minimise carbon emissions. The problem was solved by a hybrid multiobjective evolutionary algorithm. Meng and Zeng [103] proposed a 1-leader, n-follower Stackelberg game to maximise the profits of retailers at the leader level and minimise the electricity bills of consumers at the follower level considering the real-time pricing scheme. The genetic algorithm was used to solve the leader's optimisation problem and the linear programming was used to slove the follower's optimisation problem. Ghosh *et al.* [104] formulated a coupled constrained potential game to set the energy exchange prices for maximising the amount of energy exchange among prosumers and reducing the consumption from main grid. A distributed algorithm was proposed enabling individual prosumers to optimise their own payoffs. In [105], an energy trading framework based on repeated non-cooperative game was designed enabling individual microgrids to optimise their own revenues. The reinforcement learning was exploited to estimate the payoff functions under incomplete information. The Cournot game was implemented in [106] to model the competition between customers and utilities in distribution networks for satisfying the system reliability. Similarly, Zhang *et al.* [107] modelled local energy trading as a non-cooperative Cournot game to stimulate regional energy balance and promote the penetration of renewable energy sources.

Table 2.1: Comparison of game-theoretic models, players and solution approaches in the field of energy scheduling.

Literature	Game-Theoretic Model	Player	Solution Approach
Belgana *et al.* [102]	Stackelberg	Microproducers and Consumers	Hybrid Multiobjective Evolutionary Algorithm
Meng and Zeng [103]	Stackelberg	Retailer and Consumers	Genetic Algorithm and Linear Programming
Ghosh *et al.* [104]	Potential Game	Utility and Prosumers	Distributed Algorithm
Wang *et al.* [105]	Stackelberg	Microgrid	Reinforcement Learning
Mohammadi *et al.* [106]	Cournot	Customers and Utilities	Lagrangian function and KKT conditions
Zhang *et al.* [107]	Cournot	Energy Providers	Optimal-Generation-Plan Algorithm

The game theory assumes all players are rational when they compete with each other. Nonetheless, during practical energy markets operation, individual players have various sensitivities to the incentive signals, which causes the individual decisions to deviate from theoretical rational decisions and thus reduces the model accuracy. For instance, when considering the small-scale consumers, e.g. residential users, the price-insensitive consumers normally use energy irrespective of pricing signals.

2.4.3 Data-Driven Learning Approaches

To overcome the aforementioned issues of scalability and computational complexity by using optimisation approach, machine learning has been considered to assist or replace the step of solving optimization problem by the intelligent heuristic algorithm, because it only requires historical data for extracting general features with the advantages of improved scalability and reduced computational complexity.

Using learning approaches for solving energy scheduling problems has been well studied in literature. The learning approaches can be categorised as supervised learning, unsupervised learning, and reinforcement learning. In supervised learning, the input is provided as a labelled dataset, such that the model can learn from the labels to improve the learning accuracy [108]. By contrast, in unsupervised learning, there is no labelled dataset, such that the model explores the hidden features and predicts the output in a self-organising manner [109]. In reinforcement learning, the model learns to react the environment by self-adjusting through travelling from one state to another [110]. Zhang *et al.* [99] developed an online learning approach to replace heuristic algorithms for solving a cost minimisation problem under uncertain DRESs outputs and load demand. Gasse *et al.* [111] proposed a learning model for extracting branch-and-bound variable selection policies to solve combinatorial optimisation, and testified that a series of computational complex problems could be efficiently solved. An energy management system was designed in [112] to provide demand response services, by which the explicit model of consumers' dissatisfaction was replaced by the feature representations extracted through using reinforcement learning. Analogously, Ruelens *et al.* [113] combined heuristic algorithm with re-

inforcement learning to control a cluster of loads and storage devices, and Zhang *et al.* [114] integrated learning mechanism with optimisation techniques to obtain optimal demand response policies. The controller can help consumers reduce energy costs with improved computational efficiency.

Further research implemented deep neural networks as a regression algorithm into learning approaches. The CNN is a class of deep neural networks primarily used for analysing visual imagery, by which the network employs convolution for general matrix multiplication [115]. The convolution operation imports low-level input, e.g. images, to learn general abstractions of a high-complexity problem without the use of manually predefined models [116]. Hence, the CNN is particularly suitable for the high-complexity problems. Owerko *et al.* [117] trained the CNN under imitation learning to approximate an optimal power flow solution. A well trained CNN can scale to various power networks for accurately predicting optimal power flows. Du *et al.* [118] used the CNN to accelerate N-1 contingency screening of power systems, by which the CNN can generalise topological changes and uncertain renewable scenarios with improved computational efficiency. Claessens *et al.* [119] combined the CNN with reinforcement learning for high-complexity load control. The issue of partial observability was addressed through using CNN to extract hidden state-time features. In [120], the CNN was adopted as an online monitoring tool for predicting instabilities in power systems. This research demonstrated that a trained CNN was scalable in terms of varying load conditions, fault scenarios, topology structures, and generator parameters.

When the pattern recognition capability of CNN is exploited, the approach of processing numerical data to CNN input is the key for extracting hidden information. Choi *et al.* [121] processed time-series power systems data from row vector to the matrix of greyscale image by restructuring the original datasets. Liao *et al.* [122] mapped different patches of bus matrix to various areas of power networks for voltage sag estimation. The variables representing power systems configuration were assigned as the dimension of depth from the input image.

Nonetheless, there are primary three issues for data-driven learning approaches. First, when the size of historical data is small, the overfitting issue would be caused

by learning approaches. This would reduce the accuracy for predicting optimal scheduling decisions. Second, although the learning approaches can reduce the computational complexity and improve scalability from solving optimisation by heuristic intelligent algorithms, the predicted optimal decisions may deviate from the theoretical optimal decisions and result in the suboptimal solutions. Third, the predicted optimal decisions may not maintain the system constraints.

2.4.4 Analysis of System Uncertainties

Power system uncertainties caused by the intermittency of renewable energy sources and flexible demand present a challenge for accurately predicting generation and consumption. It is crucial for the reliability of power systems scheduling to consider the possible variations of these uncertainties. The probability approaches have been primarily focused in the literature for incorporating the analysis of system uncertainties into energy scheduling process.

Using a set of scenarios is a potential way to predict possible variations of uncertain variables, by which each variation is defined as a scenario [123]. The uncertain scenarios are generated from probabilistic distribution of historical data by using sampling approaches [124], such as Monte Carlo simulation [125,126], Latin hypercube sampling [127–130] and stochastic analysis [131,132]. Santos *et al.* [125] implemented Monte Carlo simulation to generate renewable scenarios and carried scenarios optimisation by deterministic modelling. Similarly, Hemmati *et al.* [126] analysed the uncertainties of renewable energy resources and load deviation by Monte Carlo simulation, and incorporated uncertainties analysis into decision making process to maximise the profits of distributed generators in microgrids. Nonetheless, the Monte Carlo simulation through randomly sampling would cause the issues of computationally intensive and inefficient. These issues can be further overcome by the Latin Hypercube sampling which can reduce standard deviation of samples through space-filling. In [127], the Latin hypercube sampling was used to generate uncertain scenarios for overcoming the computationally intensive and inefficient issues of Monte Carlo simulation and considered low probable conditions. Mavromatidis *et al.* [131] proposed a two-stage stochastic programming for the design of

distributed energy systems considering the uncertainties of energy prices, emissions factors, heating demand, electricity demand, and solar radiation. In comparison to the deterministic methods, this study demonstrated that the stochastic method can yield a more accurate estimation of costs and carbon emissions. Huang *et al.* [132] designed an economic dispatch model for virtual power plants, by which the uncertainties caused by load prediction and power prediction were described by stochastic intervals. These intervals were subsequently integrated into a costs minimisation problem.

Further research efforts have been dedicated to improving the prediction accuracy and adaptability of scenarios. Liang *et al.* [128] proposed a non-parametric kernel density estimation method to yield the probability density distribution of uncertain variables. The scenarios were generated from the probability density distribution through using Latin hypercube sampling. In [129], a data-driven approach for scenarios generation was developed using generative adversarial networks. This approach can capture both temporal and spatial dimensions of uncertain variables, so as to improve scalability and diversity from probabilistic models. To select high-probable scenarios, Xiao *et al.* [130] proposed an approach to implement synchronous-back-to-generation-reduction for merging scenarios with a minimum probability distance.

2.4.5 Remark of Research Challenges

Although extensive studies have focused on the power systems scheduling, there are four major challenges as follows.

Firstly, for the power systems scheduling, current research has investigated the policy impacts on generation, consumption, and incurred carbon emissions. How policy maker further adjusts incentive measures after receiving the responses from generators and consumers, i.e. an iterative negotiation between policy maker and generators/consumers has not been modelled.

Secondly, with respect to prosumer-centric energy scheduling, it could be useful to connect the intrinsic features of prosumers, e.g. price patterns, with potential scheduling strategies.

Thirdly, when analysing system uncertainties, an approach for using real-time prosumption data to update uncertain scenarios needs to be studied to improve the prediction accuracy for uncertain scenarios.

Fourthly, the pricing schemes investigated in current literature are not prosumer-centric. A new peer-to-peer energy trading needs to be designed, under which the bidding/selling prices of prosumers in energy and carbon markets are able to directly incentivise the reshaping of prosumption profiles to achieve carbon emissions reduction and regional energy balance.

2.5 Blockchain Applications on Peer-to-Peer Trading of Energy and Carbon Allowance

In this section, research and innovations on the blockchain technologies including smart contract, as enabling technologies of peer-to-peer trading, are introduced.

2.5.1 Peer-to-Peer Trading Mechanism

The term of 'peer-to-peer energy trading', similar to the terms of 'transactive energy' and 'community self-consumption', was coined by [133–135] with the aim of energy balance, cost saving and reduction of transmission losses, in a real-time, autonomous and decentralised manner. The mechanism of peer-to-peer energy trading enables the DRESs to be directly managed by prosumers, and aligns individual prosumers' behaviours to the overall benefits of power systems. These benefits include:

- An economically stronger distribution system can be built by using collaborative economy models, by which the profits of supplying energy can be maintained in local communities [136, 137]. Opportunities of training, education and work can be created.

- The local energy resilience and supply-demand balance can be enhanced through facilitating and integrating the small and independent prosumers with DRESs to the grid.

- The carbon emissions caused by long-distance power transmission and fossil-fuelled power generation can be reduced with the increasing penetration of the DRESs.

- The bill saving, profit improving and cost saving can be achieved when prosumers strategically decide their bidding/selling prices and prosumption behaviours.

The design of framework and mechanism of peer-to-peer trading in the energy sector have been well documented. In [138], a two-stage aggregated control framework was designed for peer-to-peer energy sharing in microgrids. Under the designed framework, prosumers could manage their DRESs through the energy sharing coordinator. This research proved the cost saving of community and bill saving of individual prosumers. Morstyn *et al.* [139] proposed a federated power plant to incentivise the coordination of individual prosumers through combining virtual power plants with peer-to-peer energy trading, and addressed the social, institutional and economic issues from the top-down strategies of conventional trading framework. Further research in [48] developed a bilateral contract networks for peer-to-peer energy trading on real-time and forward markets. The developed networks coordinated the upstream larger-scale power plants with downstream small-scale DRESs and considered the forward market uncertainty, so as to ensure an agreed market prices for market participants.

2.5.2 Blockchain Technologies

Blockchain technologies [140], as one of the distributed ledger technologies, have the potential of establishing a decentralised trading platform with automated negotiation procedures, reduced transactional costs, secured information infrastructure and protected residential privacy. The blockchain technologies have three phases of evolutions: cryptocurrency, smart contract and decentralised autonomous organisation [141]. In the field of energy markets, the blockchain can support a platform for energy trading, by which the residential privacy, e.g. address, load patterns, and price patterns, can be protected by the encryption of blockchain. The issues of dou-

ble spending and the same energy supplied twice can be overcome by the collective verification of blockchain networks. The feature disintermediary allows prosumers trade with each other without the interference of market operator. Hence, the role of market operator becomes a neutral facilitator of an open and accessible energy markets.

The most potential technology to be explored in the field of energy and carbon allowance trading is the smart contract. The smart contract, coined by Szabo in 1994 [142], enables executable programs to be performed in a manner of self-enforcing settlement and setting out negotiation [143]. This provides opportunities for both energy and carbon markets to securely automate the trading procedures with standardised contract, and thus reduces the costs of information flows from transactions of a large amount of prosumers. The features of replicable, secure and verifiable of the smart contract [144] ensure the trading, negotiation and agreement to become more trustworthy without the interference of centralised authorities.

A basic principle of the smart contract is that '*If an event A happens, the smart contract pays currency B, deposited by buyer C, to seller D*' [145]. On the context of energy and carbon allowance trading, the event could be the supply of energy or carbon allowance which is monitored by smart meters of prosumers. The pay function is executed in a self-enforcing manner. Hence, the trustworthiness of energy trading is dependent on the trustworthiness of smart meters and programs to be executed on the smart contract.

Overall, the blockchain technologies including smart contract provide a transaction and control foundation for the trading of energy and carbon allowance on the smart grid environment, with the following advantages:

- The blockchain can prevent the risks of which the same energy or carbon allowance is sold twice, or the same digital currency is spent twice, i.e. double spending attack [146], through accounting the ownership of digital and physical assets.

- The distributed feature of blockchain [146] enables a ledger to be held by all participants. Changes to the ledger require the consensus of all participants. Hence, the blockchain network is open and accessible for all participants in

markets including prosumers, energy retailers, power system operators and market operators.

- The properties of trustless and disintermediating [147] require no centralised authorities. Instead of supplying the DRESs, the role of distribution system operators becomes a neutral facilitator to encourage passive customers to be both producers and consumers. This prevents the market manipulation by one or more participants.

- From the cryptographical perspective, the public/private key encryption [148] guarantees private security of a prosumer, including the residential privacy and information security. The computational difficulty of block mining and collective validation through reaching a consensus guarantee the collective security of a trading network.

- The blockchain supports smart control architectures for realising the interoperability of smart contract [149]. The interoperability is defined as multiple agents corporately perform a function through information exchange. The automatically executed control functions written in the smart contract interface with smart meters, distributed computing and fog computing, so as to minimise the latency and enhance the computational efficiency and security.

- The blockchain supports a trading platform that minimises or eliminates costs of handling the information flows from transactions through automatically self-enforcing settlement and setting out negotiation of the smart contract.

- The smart contract with standardised auction procedures has the potential to prevent unforeseen trading behaviours in both energy and carbon markets.

Meanwhile, the blockchain including smart contract remains the following challenges from the technologies' perspective:

- The throughput, i.e. transactions per second, of blockchain is relatively lower than the existing trading technologies. For instance, the throughput of Ethereum

is 15 transactions per second [150] and the throughput of Bitcoin is 7 transactions per second [151], whereas the throughput of Visa is 2000 transactions per second [152].

- The latency, i.e. time per verified transaction, of blockchain is relatively higher than the existing trading technologies. For instance, the latency of Ethereum is 3 min [153] and the latency of Bitcoin is 10 min [154], whereas the latency of Visa is 3 sec [155].

- The users of public blockchain can be identified by analysing their trading patterns or power profiles, which would threaten their data privacy.

- The interface between blockchain network and smart meters requires new protocols and secured communication infrastructures.

The blockchain technologies applied on peer-to-peer trading of energy and carbon allowance are the subject of active research and practical implementation as follows.

Blockchain implementation on Energy Trading

The implementation of blockchain technologies on energy trading is well studied in scientific research. Thomas *et al.* [49] proposed a general form of smart contract for controlling energy transfer process between separate distribution networks. The designed negotiation framework and use case on a DC-link provided a means of applying the smart contract into power systems. In [156], the real-time power losses caused by transactions in microgrids were accounted by the blockchain, by which the prosumers were considered as negotiators of energy transaction and distributors were responsible for computing losses. Li *et al.* [157] applied smart contract into a distributed hybrid energy systems to facilitate energy exchange among end users. The demand side management and uncertainties caused by renewable generation were considered into a framework of peer-to-peer energy trading. Mihaylov *et al.* [158] designed a paradigm for energy trading with a virtual currency generated by energy supply of prosumers. Case studies of this research testified that the designed currency incentivised prosumers to achieve demand response and supply-demand balance. Saxena *et al.* [159] proposed a blockchain based transactive energy

systems to address the incentivising, contract auditability and enforcement of voltage regulation service. The smart contract was used by this research to enforce the validity of each transaction and automate the negotiation and bidding process. In [160], a transparent and safe power trading algorithm executed on the Ethereum blockchain platform was presented for prosumers to trade energy.

Blockchain implementation on Carbon Allowance Trading

In carbon markets, the blockchain has been developed to trade carbon allowance or allocate monetary incentives for decarbonisation. Khaqqi *et al.* [161] customised carbon allowance trading to industries using reputation based blockchain by which the reputation signified participants' performances and commitments for carbon emissions reduction. The reputation system was maintained by the consensus of blockchain networks to guarantee the fairness and security. Pan *et al.* [162] implemented blockchain into carbon emissions trading to reduce the entry threshold for the carbon market and improve the reliability of information exchange. Analogously, Richardson and Xu [163] proposed a blockchain based emissions trading scheme to ensure transparency, tamper-resistance, and high liquidity. With respect to the application of smart contract, a distributed carbon ledger system fitted with existing market-based emissions trading schemes was designed in [164] to strengthen the corporate accounting system for carbon asset management.

2.5.3 Remark of Research Challenges

Based on the aforementioned literature, the difference between the conventional centralised trading and blockchain based peer-to-peer trading in the energy sector is summarised in Table 2.2. This table explains the changes in both energy markets and carbon markets, and the advantages of using blockchain into the peer-to-peer trading, with detailed explanation as follows.

Table 2.2: Comparison between conventional centralised trading and blockchain based peer-to-peer trading.

	Conventional Centralised Trading	Blockchain Based Peer-to-Peer Trading
Primary Energy Supplier	Large Scale Generators	Prosumers with DRESs
Pricing Scheme	Centralised Prices	Bidding/Selling Prices
Contract Type	Idiosyncratic Contract [165]	Standardised Smart Contract
Settlement Enforcement [143]	Legal Restraint	Self-Enforcing
Trustee [143]	Third Party	Smart Meter and Smart Contract
Incentive Supplier	Policy Maker [68]	Consensus of Network
Incentive Update	Long-Term Policy [68]	Real-Time Update

First, the primary energy provider in conventional centralised trading is large scale generators connected to the transmission networks, whereas the primary energy provider in blockchain based peer-to-peer trading is prosumers with DRESs connected to the distribution networks.

Second, the pricing schemes in conventional energy markets and carbon markets are centralised. For the case of the U.K. markets, the carbon price is determined by the E.U. emissions trading scheme plus the U.K. carbon price support [68]. The centralised carbon price applies for all carbon producers without difference; The centralised wholesale energy price is determined by the wholesale market and applies for all energy retailers without difference [166]. The retail energy price is determined by energy retailers in retail markets and applies for all regional consumers without difference [167]. By contrast, the pricing scheme in the blockchain based peer-to-peer network is decentralised. Each individual prosumers can determine their own bidding/selling prices for exchanging energy or carbon allowance, according to their real-time situation of supply-demand balance.

Third, the negotiation and contract processing in the conventional energy markets are idiosyncratic [165], which means that each large-scale generator signs contract with the transmission system operator individually, and the content of each contract varies according to the specific situations of generators. By contrast, in the blockchain based peer-to-peer trading, a standardised contract and negotiation can be formulated by using the nature of smart contract, which reduces the complexity when large amounts of prosumers formulate their own contracts.

Fourth, the settlement of conventional centralised trading is enforced by the legal restraint, which means that if the energy or carbon allowance is not delivered at the agreed time, retailers will be accused or receive penalty from power system operator afterwards. By contrast, in the blockchain based peer-to-peer trading, the self-enforcing nature of smart contract enables the violation of contract to be prevented beforehand by querying the smart meters to ensure that prosumers have enough capacity to supply.

Fifth, in the conventional centralised trading, the carbon accounting and energy trading of generators rely on the third party, e.g. auditing institution or market

operator, whereas in the blockchain based peer-to-peer network, prosumers' trust relies on the automatic interactions between the smart contract and smart meters, under the consensus of the blockchain network.

Sixth, in the conventional centralised trading, the low carbon incentive is formulated by the policy maker, which is a long-term policy. By contrast, in the blockchain based peer-to-peer trading, based on the formulated low carbon incentive mechanism, the real-time low carbon incentive can be allocated by reaching a consensus of the network.

From existing research and aforementioned discussion, separately designing energy or carbon markets is not efficient, because the purchasing of carbon allowance is a part of energy costs. A decentralised trading framework needs to be designed enabling prosumers to trade energy and carbon allowance together.

Chapter 3

Game Theory for Low Carbon Negotiation and Energy Scheduling

3.1 Introduction

The low carbon energy scheduling refers to strategically dispatching power generation from various sources and reshaping power consumption behaviours, for the purpose of carbon emissions reduction, electricity bill saving, and generating profit improving [85]. The low carbon behaviours of consumers and generators are driven by monetary compensation and market-based policy incentives, i.e. carbon pricing, respectively, formulated by the policy maker. In this chapter, a novel model for energy scheduling and low carbon negotiation between the policy maker and consumers/generators is proposed. A Stackelberg game-theoretic problem is formulated to model the dynamic negotiation process, during which the policy maker strategically formulates the monetary compensation rates and carbon prices to reduce total carbon emissions from power systems, and consumers/generators decide their responding strategies, i.e. consumption behaviours/power outputs, to minimise electricity bills/maximise generating profits. An algorithm is proposed based on the artificial immune system for solving the Stackelberg game-theoretic problem to yield an optimal agreement between the policy maker and consumers/generators. Case studies based on the U.K. power systems demonstrate the effectiveness of the proposed model and algorithm, in comparison with the models of multiobjective

optimization and aggregated scheduling.

Overall, this chapter offers the following contributions:

- A novel energy scheduling framework is proposed enabling the dynamic negotiation of carbon reduction between policy maker and consumers/generators, based on the Stackelberg game-theoretic model.
- A decentralised low carbon incentive mechanism is designed based on the developed carbon emissions tracing approach, to reduce the carbon emissions incurred by specific time period and location of individual consumers.
- A bus test system is developed based on the GB power network structures and operations, which demonstrates that the proposed low carbon energy scheduling model can yield better bill saving and carbon emissions reduction, and drive fuel-switching from coal/gas to renewable energy sources.

The rest of this chapter is organised as follows: Section 3.2 introduces the proposed model for low carbon energy scheduling, and discusses the carbon emissions tracing approach and the mechanism of decentralised low carbon incentive. The framework of low carbon energy scheduling is presented in Section 3.3 to analyse the strategies of policy maker and consumers/generators. Section 3.4 formulates the Stackelberg game-theoretic model to describe the process of negotiation and reaching an agreement between the leader and followers. An algorithm is also developed to solve the game-theoretic problem. Section 3.5 provides case studies on the context of the U.K. power systems and energy market. Section 3.6 concludes this chapter.

3.2 Preliminary

In this section, the proposed model for low carbon energy scheduling is illustrated. The approach of carbon emissions tracing and the mechanism of decentralised low carbon incentive are discussed as a preliminary of scheduling framework.

3.2.1 System Model

The proposed model for low carbon negotiation and energy scheduling between policy maker and generators/consumers is presented in Fig. 3.1. The generation sources consist of solar, wind (including onshore and offshore), nuclear, coal, gas (including combined cycle gas turbine (CCGT) and open cycle gas turbine (OCGT)), biomass, hydro (including hydro generation and pumped storage), and interconnectors. The consumers consist of residential, commercial, and industrial users. The policy maker incentivises reshaping power profiles for carbon reduction by charging carbon allowance from generators as carbon cost and provide monetary compensation for consumers. The proposed model is implemented in day-ahead market to enable the energy scheduling for the following day and negotiation between the policy maker and generators/consumers.

The information flows are processed by three types of agents: central data collection/distribution, central/distributed scheduling, and central/distributed decision-making. The central data distribution agent in consumers' side distributes the real-time data of monetary compensation rates and retail electricity prices to the distributed smart meter of each consumer. Analogously, the central data distribution agent in generators' side distributes the real-time data of carbon prices and wholesale electricity prices to the distributed smart meter or sensor of each generator. Receiving this data, the distributed scheduling agents perform optimisation according to the predefined preferences, e.g. minimising electricity bills for individual consumers and maximising profits for individual generators. The optimal scheduling decisions of consumption and generation are sent to the distributed decision-making agents to confirm whether individual consumers/generators accept these decisions. Subsequently, the confirmed decisions are collected by the central data collection agent and sent to the central scheduling agent to perform optimisation according to the policy targets, e.g. carbon reduction and carbon tax neutrality. The optimal policy decisions of monetary compensation rates and carbon prices are sent back to the central data distribution agents. Additionally, the information of retail market prices and wholesale market prices is provided by the market operator. The power balance and system constraints are managed by the power system operator. The

roles of both market operator and power system operator are beyond the scope of this model architecture.

The process of negotiation between policy maker and consumers/generators, and reaching an agreement of low carbon energy scheduling is modelled as the Stackelberg game-theoretic problem. The policy maker acts as a leader with strategies of monetary compensation rates and carbon prices, and the consumers and generators act as followers with responding strategies of consumption and generation, respectively.

Figure 3.1: Model architecture for low carbon energy scheduling. Individual consumers/generators perform their scheduling with own objective functions through distributed agents. The policy maker aggregates the distributed information and analyses the strategies to realise its policy targets through central agents. The process of negotiation and reaching an agreement is described by the Stackelberg game-theoretic model.

3.2.2 Carbon Emissions Tracing

To trace the temporal and spatial variations of carbon emissions from power systems, two metrics are defined as [84]

- *Metric 1 (Carbon Emissions Rate)*: The carbon emissions rate is defined as the amount of carbon emissions from a point of power networks per unit of time as

$$r = \frac{e}{\Delta t}, \tag{3.2.1}$$

  where r is the carbon emissions rate, Δt is the time interval, and e is the amount of carbon emissions during the time interval Δt.

- *Metric 2 (Carbon Emissions Intensity)*: The carbon emissions intensity is defined as the amount of carbon emissions from a specific point of power networks per unit of energy as

$$\rho = \frac{e}{p \cdot \Delta t} = \frac{r}{p}, \tag{3.2.2}$$

  where ρ is the carbon emissions intensity, and p is the active power.

Let $\mathcal{N}$, $\mathcal{I}$, $\mathcal{K}$, and $\mathcal{L}$ denote the index sets of buses, generators, loads, and transmission lines, indexed by integers $n \in \mathcal{N}$, $i \in \mathcal{I}$, $k \in \mathcal{K}$, and $l \in \mathcal{L}$, respectively. Consider a power network with $|\mathcal{N}|$ buses, $|\mathcal{I}|$ generators, $|\mathcal{K}|$ loads, and $|\mathcal{L}|$ transmission lines, under which the CEF is categorised as CEF from generation (CEFG), CEF from transmission (CEFT), CEF from transmission loss (CEFL), and CEF from consumption (CEFC).

Carbon Emissions Flow from Generation

The CEFG traces the carbon emissions caused by electricity generation due to the combustion of fossil fuels. The carbon emissions intensities of generators are determined by the carbon emissions intensities of input fuels and efficiency of electricity supply [79] (Evaluation of carbon emissions intensities for each generation source will be detailed in simulation). Let an $|\mathcal{I}|$-size column vector ρ_{CEFG} denote the carbon emissions intensities of generators. The carbon emissions rates of generators

can be calculated as

$$\mathbf{r}_{\mathrm{CEFG}} = \mathbf{P}_{\mathrm{CEFG}} \times \rho_{\mathrm{CEFG}}, \tag{3.2.3}$$

where $\mathbf{r}_{\mathrm{CEFG}}$ is a $|\mathcal{N}|$-size column vector to denote the carbon emissions rates of generators, and $\mathbf{P}_{\mathrm{CEFG}}$ is a $(|\mathcal{N}| \times |\mathcal{I}|)$-size matrix to denote the power outputs of generators. The indices n and i of each element $p_{\mathrm{CEFG},n,i} \in \mathbf{P}_{\mathrm{CEFG}}$ indicate that the generator i is located at bus n. For the buses without generators, the corresponding elements equal to zero.

Carbon Emissions Flows from Transmission and Consumption

The CEFT and CEFC trace the carbon emissions caused by generators when the electricity is transmitted and consumed, respectively. Firstly, to calculate the carbon emissions rates of transmission and consumption, the corresponding carbon emissions intensities need to be analysed. Analogous to the definition of bus in the context of power flows, a bus in the context of CEF refers to a node connected by various generators, loads, and transmission lines. The CEF flows through a bus from inflows, e.g. generators and inflowing transmission lines, to outflows, e.g. loads and outflowing lines. According to the proportional sharing principle [168] and distribution of the CEF [84], the following two properties hold for the distribution of CEFT and CEFC. A schematic illustration of these two properties are presented in Fig. 3.2.

- *Property 1*: The CEF caused by all power outflows from a bus (including power outflows to the loads connected to this bus) equals to the CEF caused by all power inflows to this bus (including power inflows from the generators connected to this bus).

- *Property 2*: The proportion of the CEF caused by one power inflow to the CEF caused by all power inflows keeps unchanged in the CEFs caused by each power outflow. Hence, all power outflows from the same bus would have the same carbon emissions intensities.

Let a $(|\mathcal{N}| \times |\mathcal{N}|)$-size skew-symmetric matrix $\mathbf{P}_{\mathrm{B}}$ denote the distribution of power inflows from other buses yielded by power flow analysis. The indices n_a and n_b

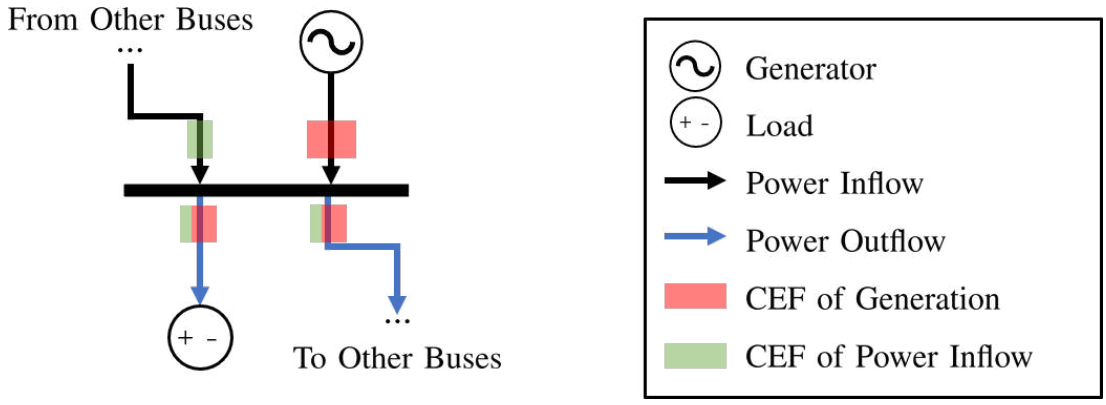

Figure 3.2: Schematic illustration for the distribution of CEFT and CEFC. The CEF caused by all power outflows from a bus equals to the CEF caused by all power inflows to this bus (indicated by the size of CEF box). The bus homogenises the carbon emissions intensities of all power inflows (indicated by the colour of CEF box), so that all power outflows have the same carbon emissions intensities.

$(n_a, n_b \in \mathcal{N})$ of each element $p_{\mathrm{B},n_a,n_b} \in \mathbf{P}_{\mathrm{B}}$ indicate the direction of power inflow in transmission line is from bus n_a to bus n_b. Recall that the $(|\mathcal{N}| \times |\mathcal{I}|)$-size matrix $\mathbf{P}_{\mathrm{CEFG}}$ represents the power inflows from generators. The distribution of power inflows from both other buses and generators can be described as

$$\mathbf{P}_{\mathrm{CEFT}} = \mathrm{diag}\left\{ \mathbf{i}_{(|\mathcal{N}|+|\mathcal{I}|)} \times \begin{bmatrix} \mathbf{P}_{\mathrm{B}} \\ \mathbf{P}_{\mathrm{CEFG}}^{\mathrm{T}} \end{bmatrix} \right\}, \tag{3.2.4}$$

where $\mathbf{P}_{\mathrm{CEFT}}$ is a $(|\mathcal{N}| \times |\mathcal{N}|)$-size diagonal matrix to denote the distribution of the total power inflows from both other buses and generators, $\mathrm{diag}\{\cdot\}$ is the operation to create diagonal matrix, and $\mathbf{i}_{(|\mathcal{N}|+|\mathcal{I}|)}$ is a $(|\mathcal{N}| + |\mathcal{I}|)$-size unit row vector.

According to the *Property 1*, the carbon emissions rates caused by all power inflows to each of buses equal to the carbon emissions rates caused by all power inflows from other buses and generators as

$$\mathbf{P}_{\mathrm{CEFT}} \times \rho_{\mathrm{CEFT}} = \mathbf{P}_{\mathrm{B}}^{\mathrm{T}} \times \rho_{\mathrm{CEFT}} + \mathbf{r}_{\mathrm{CEFG}}, \tag{3.2.5}$$

where ρ_{CEFT} is a $|\mathcal{N}|$-size column vector to denote the carbon emissions intensities of transmission and consumption. Thus, the carbon emissions intensities of

transmission and consumption can be calculated as

$$\rho_{\mathrm{CEFT}} = (\mathbf{P}_{\mathrm{CEFT}} - \mathbf{P}_{\mathrm{B}}^{\mathrm{T}})^{-1} \times \mathbf{r}_{\mathrm{CEFG}}. \tag{3.2.6}$$

Secondly, the carbon emissions rates of transmission and consumption can be calculated as

$$\mathbf{R}_{\mathrm{CEFT}} = \mathrm{diag}\{\rho_{\mathrm{CEFT}}\} \times \mathbf{P}_{\mathrm{B}}, \tag{3.2.7}$$

$$\mathbf{R}_{\mathrm{CEFC}} = \mathrm{diag}\{\rho_{\mathrm{CEFT}}\} \times \mathbf{P}_{\mathrm{CEFC}}, \tag{3.2.8}$$

where $\mathbf{R}_{\mathrm{CEFT}}$ is a $(|\mathcal{N}| \times |\mathcal{N}|)$-size square matrix to denote the carbon emissions rates of transmission, $\mathbf{R}_{\mathrm{CEFC}}$ is a $(|\mathcal{N}| \times |\mathcal{K}|)$-size matrix to denote the carbon emissions rates of consumption, and $\mathbf{P}_{\mathrm{CEFC}}$ is a $(|\mathcal{N}| \times |\mathcal{K}|)$-size matrix to denote the distribution of power loads yielded by power flow analysis. The indices n_a and n_b $(n_a, n_b \in \mathcal{N})$ of each element $r_{\mathrm{CEFT},n_a,n_b} \in \mathbf{R}_{\mathrm{CEFT}}$ indicate the direction of CEFT in transmission line is from bus n_a to bus n_b. The indices n and k of elements $r_{\mathrm{CEFC},n,k} \in \mathbf{R}_{\mathrm{CEFC}}$ and $p_{\mathrm{CEFC},n,k} \in \mathbf{P}_{\mathrm{CEFC}}$ indicate that the load k is located at bus n.

Carbon Emissions Flow from Transmission Loss

According to the *Property 2*, the power loss can be taken as a power outflow from a bus, and has the same carbon emissions intensities with other power outflows from this bus. Recall that $\mathbf{P}_{\mathrm{B}}$ denotes the distribution of power inflows to each of buses in power networks. Let a $(|\mathcal{N}| \times |\mathcal{N}|)$-size square matrix $\mathbf{P}'_{\mathrm{B}}$ denote the distribution of power outflows from each of buses in power networks. The carbon emissions rates of transmission losses can be calculated as

$$\mathbf{R}_{\mathrm{CEFL}} = \mathrm{diag}\{\rho_{\mathrm{CEFT}}\} \times (\mathbf{P}'_{\mathrm{B}} - \mathbf{P}_{\mathrm{B}}), \tag{3.2.9}$$

where $\mathbf{R}_{\mathrm{CEFL}}$ is a $(|\mathcal{N}| \times |\mathcal{N}|)$-size square matrix to denote the carbon emissions rates of transmission losses. The indices n_a and n_b $(n_a, n_b \in \mathcal{N})$ of each element $r_{\mathrm{CEFL},n_a,n_b} \in \mathbf{R}_{\mathrm{CEFL}}$ indicate the direction of CEFL in a transmission line is from bus n_a to bus n_b.

Remark: For simplicity, the matrix calculations of CEF are represented by $f_{\mathrm{CEF}}(\cdot)$ in the following sections. Let $p_{k,t}$ and $r_{k,t}$ denote the power consumption

and corresponding carbon emissions rate of load $k \in \mathcal{K}$ at scheduling time t, and $p_{i,t}$ and $r_{i,t}$ denote the power generation and corresponding carbon emissions rate of generator $i \in \mathcal{I}$ at scheduling time t. Hence, for each load k and generator i, the CEF is a function of power flow as

$$r_{k,t} = f_{\text{CEF}}\left(p_{k,t}\right), \tag{3.2.10}$$

$$r_{i,t} = f_{\text{CEF}}\left(p_{i,t}\right). \tag{3.2.11}$$

3.2.3 Decentralised Low Carbon Incentive Mechanism

Once the carbon emissions of individual consumers are traced, a low carbon incentive can be formulated by the policy maker in the form of monetary compensation. The target of low carbon incentive is on each of individual consumers, instead of an ensemble of consumers as in the centralised incentive approaches. Let $\gamma_k(\cdot)$ denote the function of the monetary compensation for carbon reduction of load k. The following assumptions need to be considered to formulate the low carbon incentive.

- *Assumption 1*: The monetary compensation should be non-negative. When the carbon emissions rate with policy maker's incentive reduces to zero, the monetary compensation of load k should be maximum, i.e. $\gamma_k = \gamma_k^{\max}$, if $r_{k,t} = 0$, where $\gamma_k^{\max}$ is the maximum monetary compensation for carbon reduction of load k.

- *Assumption 2*: If the carbon emissions rate after the policy maker's incentive is higher than or equal to that before the policy maker's incentive, consumers will not receive any monetary compensation as

$$\gamma_k\left(r_{k,t}, r'_{k,t}\right) = 0, r_{k,t} \geq r'_{k,t}, \tag{3.2.12}$$

  where $r'_{k,t}$ is the carbon emissions rate caused by power consumption behaviour of load k at scheduling time t before policy maker's incentive.

- *Assumption 3*: When the carbon emissions rate before the policy maker's incentive $r'_{k,t}$ is known, the monetary compensation should be monotonically

decreasing to the carbon emissions rate after policy maker's incentive $r_{k,t}$ as

$$\frac{\partial \gamma_k \left(r_{k,t}, r'_{k,t}\right)}{\partial r_{k,t}} < 0. \tag{3.2.13}$$

- *Assumption 4*: The loads with high-level of carbon emissions will receive more monetary compensation than the loads with low-level of carbon emissions, because those loads with high-level of carbon emissions are more urgent for carbon mitigation. This means that the marginal monetary compensation should be monotonically increasing to the carbon emissions rate before policy maker's incentive $r'_{k,t}$ as

$$\frac{\partial^2 \gamma_k \left(r_{k,t}, r'_{k,t}\right)}{\partial r'^2_{k,t}} > 0. \tag{3.2.14}$$

Hence, the following function which satisfies all the assumptions is modelled as the decentralised monetary compensation for carbon reduction

$$\gamma_k \left(r_{k,t}, r'_{k,t}\right) := \begin{cases} \alpha_t \cdot \sqrt{\left(r'_{k,t} \cdot \Delta t\right)^2 - \left(r_{k,t} \cdot \Delta t\right)^2}, & r'_{k,t} > r_{k,t}, \\ 0, & r'_{k,t} \leq r_{k,t}, \end{cases} \tag{3.2.15}$$

where α_t is the monetary compensation rate at scheduling time t.

3.3 Framework of Low Carbon Energy Scheduling

This section describes the framework of low carbon energy scheduling. The strategies of consumers/generators and policy maker are analysed in order to model the process of negotiation and reaching an agreement by Stackelberg game theory.

3.3.1 The Role of Consumers

The role of consumers aims to minimise the electricity bills by strategically deciding the consumption behaviours and responding to the low carbon incentive. The carbon emissions caused by time-varying and region-varying consumption behaviours can be traced by the proposed CEF model. By incorporating the monetary compensation into the electricity bills for individual consumers, policy maker can facilitate the reshaping of consumption behaviours in a low carbon manner by eliminating the high-carbon regions and time periods.

The objective function of electricity bills can be modelled as

$$f_k\left(p_{k,t}, r_{k,t}\right) := \sum_{t\in\mathcal{T}} \left[p_{k,t}\cdot\Delta t\cdot\pi_t - \gamma_k\left(r_{k,t}\right)\right], \tag{3.3.16}$$

where $f_k(\cdot)$ is the objective function of electricity bills of consumer k, $\mathcal{T}$ is the index set of scheduling time, and π_t is the retail electricity price at scheduling time t charged by the electricity suppliers. For the scheduling interval of 0.5 h, we have $(\Delta t,|\mathcal{T}|)=(0.5,48)$.

When consumers change their consumption behaviours, the power level of each load should be restricted to certain limits considering the load type as

$$p_k^{\min} \le p_{k,t} \le p_k^{\max}, \tag{3.3.17}$$

where $p_k^{\min}$ and $p_k^{\max}$ are the minimum and maximum power consumption levels of load k, respectively.

Therefore, the objective of individual consumers is to minimise their electricity bills with decision variables of the power consumption behaviours and corresponding carbon emissions rates as

$$\begin{aligned} &\min_{p_{k,t},r_{k,t}} : f_k\left(p_{k,t}, r_{k,t}\right), \\ &\text{s.t.: (3.2.10), and (3.3.17).} \end{aligned} \tag{3.3.18}$$

Remark: Since this chapter focuses on the whole U.K. power systems, in order to represent the technical properties of power systems whilst reducing complexity, an ensemble of regional loads are merged as a consumer. The details of simplified systems will be introduced in case studies.

3.3.2 The Role of Generators

The role of generators aims to maximise their profits by strategically dispatching power outputs and responding to the carbon prices. The profits can be described as the difference between the revenue of selling electricity to the wholesale markets and the generating costs. As one of the generating costs, the carbon cost quantifies how much the generators pay for the allowance of pollutant emissions, and is subject to the variations of carbon prices. By incorporating the carbon prices into the generating costs, policy maker can facilitate the power generation to transit from

using the high carbon sources to using the low carbon sources, e.g. renewable energy sources.

To analyse the incentive effects of carbon prices, the carbon cost is set aside from the operating costs. The function of carbon cost can be modelled as

$$c_{\text{carbon},i}\left(r_{i,t}\right) := r_{i,t} \cdot \Delta t \cdot \pi_{\text{carbon},t}, \tag{3.3.19}$$

where $c_{\text{carbon},i}\left(\cdot\right)$ is the function of carbon cost of generator i, and $\pi_{\text{carbon},t}$ is the carbon price at scheduling time t.

Apart from the carbon cost, other operating costs include costs of operation, maintenance, fuel, and carbon capture and storage [169] (costs of pre-development, construction, decommissioning, and waste are not considered in our dynamic scheduling problem). The coefficients of operating costs for each of energy sources are evaluated by the levelised costs of electricity generation (LCoE) [170]. The LCoE is a discounted lifetime cost of a specific generation source, and quantified by the ratio of the total costs of a source to the total expected amount of electricity generation. Let δ_i denote the coefficient of the total operating costs of generator i. The function of operating costs can be modelled as

$$c_i\left(p_{i,t}\right) := p_{i,t} \cdot \Delta t \cdot \delta_i, \tag{3.3.20}$$

where $c_i\left(\cdot\right)$ is the function of operating costs of generator i excluding the carbon cost.

The objective function of profits can be modelled as

$$f_i\left(p_{i,t}, r_{i,t}\right) := \sum_{t \in \mathcal{T}} \left\{p_{i,t} \cdot \Delta t \cdot \pi_{\text{ws},t} - \left[c_{\text{carbon},i}\left(r_{i,t}\right) + c_i\left(p_{i,t}\right)\right]\right\}, \tag{3.3.21}$$

where $f_i\left(\cdot\right)$ is the objective function of profits of generator i, and $\pi_{\text{ws},t}$ is the wholesale electricity price at scheduling time t purchased by the electricity suppliers.

When generators change their power outputs, the output level of each generator should be restricted to certain limits considering the capacities of generators as

$$p_i^{\min} \leq p_{i,t} \leq p_i^{\max}, \tag{3.3.22}$$

where $p_i^{\min}$ and $p_i^{\max}$ are the minimum and maximum power generation levels of generator i, respectively.

Therefore, the objective of individual generators is to maximise their profits with decision variables of power generation dispatching and corresponding carbon emissions rate as

$$\begin{aligned} &\max_{p_{i,t}, r_{i,t}} : f_i\left(p_{i,t}, r_{i,t}\right), \\ &\text{s.t.: (3.2.11), and (3.3.22).} \end{aligned} \tag{3.3.23}$$

3.3.3 The Role of Policy Maker

The role of policy maker aims to mitigate the total carbon emissions from power systems and facilitate the carbon revenue neutrality, by strategically adjusting the carbon prices and monetary compensation rates. According to the carbon footprint [84], the total carbon emissions rate from power systems equals to the total carbon emissions rate of generators, and is subject to the CEF conservation at any given time as

$$\sum_{i\in\mathcal{I}} r_{i,t} = \sum_{k\in\mathcal{K}} r_{k,t} + \sum_{l\in\mathcal{L}} r_{l,t} = \varrho \cdot \sum_{i\in\mathcal{I}} r_{i,t} + (1-\varrho) \cdot \sum_{i\in\mathcal{I}} r_{i,t}, \tag{3.3.24}$$

where $r_{l,t}$ is the carbon emissions rate caused by the transmission loss of line $l \in \mathcal{L}$, and ϱ is the ratio of the carbon emissions from consumption side to total carbon emissions.

Through solving the objective functions of consumers and generators, the optimal carbon emissions rates of each load k and generator i at scheduling time t, denoted as $r^*_{k,t}$ and $r^*_{i,t}$, respectively, can be obtained by the policy maker. The policy maker subsequently adjusts the carbon prices and monetary compensation rates to abate the total carbon emissions rate of generators by Δr_t. According to (3.3.24), the total carbon emissions rate of consumers would be abated by $(\varrho \cdot \Delta r_t)$ correspondingly.

Firstly, from the economic perspective, the carbon revenue neutrality defines that the revenue from low carbon policy should be redistributed in a manner of monetary incentive [171]. In our research, this means that the difference between the revenue of selling carbon allowance to generators and the cost of monetary compensation to consumers should be eliminated. Hence, the objective function of carbon revenue

neutrality can be modelled as

$$f_n\left(\pi_{\text{carbon},t}, \alpha_t, \Delta r_t, \Delta r_{k,t}\right) := \sum_{t\in\mathcal{T}} \left\{ \sum_{i\in\mathcal{I}} c_{\text{carbon},i}\left(r^*_{i,t} - \Delta r_t\right) - \sum_{k\in\mathcal{K}} \gamma_k \left(r^*_{k,t} - \Delta r_{k,t}, r^*_{k,t}\right) \right\}, \tag{3.3.25}$$

where $f_n(\cdot)$ is the objective function of carbon revenue neutrality, $f_n > 0$, Δr_t is the amount of abatement for the total carbon emissions rate of generators at scheduling time t, and $\Delta r_{k,t}$ is the amount of abatement for the carbon emissions rate of load k at scheduling time t.

There are constraints when the policy maker decides the carbon prices, monetary compensation rates, and the amount of abatement for the total carbon emissions rates of generators as

$$\pi^{\min}_{\text{carbon}} \leq \pi_{\text{carbon},t} \leq \pi^{\max}_{\text{carbon}}, \tag{3.3.26}$$

$$\alpha^{\min} \leq \alpha_t \leq \alpha^{\max}, \tag{3.3.27}$$

$$\Delta r^{\min} \leq \Delta r_t \leq \Delta r^{\max}, \tag{3.3.28}$$

where $\pi^{\min}_{\text{carbon}}$ and $\pi^{\max}_{\text{carbon}}$ are the minimum and maximum levels of carbon prices, respectively, $\alpha^{\min}$ and $\alpha^{\max}$ are the minimum and maximum levels of monetary compensation rates, respectively, and $\Delta r^{\min}$ and $\Delta r^{\max}$ are the minimum and maximum levels of abatement for the total carbon emissions rate, respectively.

Remark: The decision variable Δr_t targets on the overall carbon emissions, instead of the carbon emissions of each generator. This design facilitates the generators with low carbon sources to replace the generators with high carbon sources, so as to achieve overall carbon reduction. On the contrary, due to the design of decentralised carbon incentive mechanism (3.2.15), for the same amount of carbon abatement, the received monetary compensation would be different for consumers at various carbon emissions levels. Hence, the decision variable $\Delta r_{k,t}$ targets on the carbon emissions of each load, and is subject to the following constraint

$$\sum_{k\in\mathcal{K}} \Delta r_{k,t} = \varrho \cdot \Delta r_t. \tag{3.3.29}$$

Secondly, from the environmental perspective, the policy marker should abate the total carbon emissions from power systems. The total carbon emissions can be

modelled as

$$f_c\left(\Delta r_t\right) := \sum_{t\in\mathcal{T}}\left(\sum_{i\in\mathcal{I}} r^*_{i,t} - \Delta r_t\right)\cdot\Delta t, \tag{3.3.30}$$

where $f_c\left(\cdot\right)$ is the objective function of total carbon emissions.

Therefore, the objectives of policy marker are to achieve carbon revenue neutrality, and minimise the total carbon emissions from power systems, with decision variables of carbon prices, monetary compensation rates, and the amount of carbon abatement of generators and each load, which leads to a multiobjective optimisation problem (MOP) as

$$\min_{\substack{\pi_{\text{carbon},t},\alpha_t,\\ \Delta r_t,\Delta r_{k,t}}} : \left\{f_n\left(\pi_{\text{carbon},t},\alpha_t,\Delta r_t,\Delta r_{k,t}\right), f_c\left(\Delta r_t\right)\right\}, \tag{3.3.31}$$

s.t.: (3.3.26), (3.3.27), (3.3.28), and (3.3.29).

3.4 Solution of Game-Theoretic Problem

In this section, the Stackelberg game-theoretic problem is formulated. Through analysing the approaches of solving this problem, an algorithm is developed based on the basic structures of artificial immune system.

3.4.1 Problem Formulation

In the proposed framework, the policy maker acts as a leader to formulate the strategies of carbon prices and monetary compensation rates. By contrast, $|\mathcal{K}|$ consumers and $|\mathcal{I}|$ generators act as followers to decide the generation, consumption and corresponding carbon emissions rates as responding strategies to the leader. This leads to a 1 - leader, $(|\mathcal{K}| + |\mathcal{I}|)$ - follower Stackelberg game-theoretic problem. The procedure of the Stackelberg game between leader and followers is as follows

Step 1: The policy marker initialises its strategies as

$$\pi_{\text{carbon},t} = \pi^{\min}_{\text{carbon}},\ \alpha_t = \alpha^{\min}. \tag{3.4.32}$$

Step 2: With the policy marker's strategies, the consumers and generators decide their responding strategies through solving their optimisation problems as

$$\left\{p_{k,t}^{*}, r_{k,t}^{*}\right\} = \arg\min_{p_{k,t}, r_{k,t}} : f_k\left(p_{k,t}, r_{k,t}\right)|_{\alpha_t=\alpha^{\min}} \tag{3.4.33}$$

s.t.: (3.2.10), and (3.3.17),

$$\left\{p_{i,t}^{*}, r_{i,t}^{*}\right\} = \arg\min_{p_{i,t}, r_{i,t}} : -f_i\left(p_{i,t}, r_{i,t}\right)|_{\pi_{\text{carbon},t}=\pi_{\text{carbon}}^{\min}}, \tag{3.4.34}$$

s.t.: (3.2.11), and (3.3.22).

Step 3: After all the generators and consumers submit their scheduled power generation and consumption, the power system operator performs the power flow analysis under the system constraints to maintain the operational security of the power systems. The system constraints include power balance constraint, voltage limits, apparent power limits, line flow limits, thermal limits, and voltage angle limits with details as studied in [172].

Step 4: With the responding strategies of the generators and consumers, the policy marker adjusts its strategies through solving its optimisation problems as

$$\left\{\pi_{\text{carbon},t}^{*}, \alpha_t^{*}, \Delta r_t^{*}, \Delta r_{k,t}^{*}\right\} = \underset{\substack{\pi_{\text{carbon},t}, \alpha_t, \\ \Delta r_t, \Delta r_{k,t}}}{\arg\min} : \left\{f_n\left(\pi_{\text{carbon},t}, \alpha_t, \Delta r_t, \Delta r_{k,t}\right), f_c\left(\Delta r_t\right)\right\}, \tag{3.4.35}$$

s.t.: (3.3.26), (3.3.27), (3.3.28), and (3.3.29).

Step 5: The policy marker updates its strategies as

$$\pi_{\text{carbon},t} = \pi_{\text{carbon},t}^{*},\ \alpha_t = \alpha_t^{*}. \tag{3.4.36}$$

With the updated policy marker's strategies, the consumers and generators change their responding strategies through solving their objective functions. The iteration continues until the carbon emissions from power systems meet the policy marker's target of carbon abatement ($\Delta r_t^{*} = \Delta r_{k,t}^{*} = 0$), or the maximum number of iteration for negotiation between the policy maker and consumers/generators is reached ($\iota = \iota^{\max}$, where ι is the number of iteration, and $\iota^{\max}$ is the maximum number of iteration). This step indicates the stopping criteria of the Stackelberg game as

$$\Delta r_t^{*} = \Delta r_{k,t}^{*} = 0, \text{or } \iota = \iota^{\max}. \tag{3.4.37}$$

The outputs are final optimal scheduling decisions $\pi^*_{\text{carbon},t}, \alpha^*_t, p^*_{k,t}, r^*_{k,t}, p^*_{i,t}$, and $r^*_{i,t}$. The flowchart of the Stackelberg game between leader and followers is presented in Fig. 3.3.

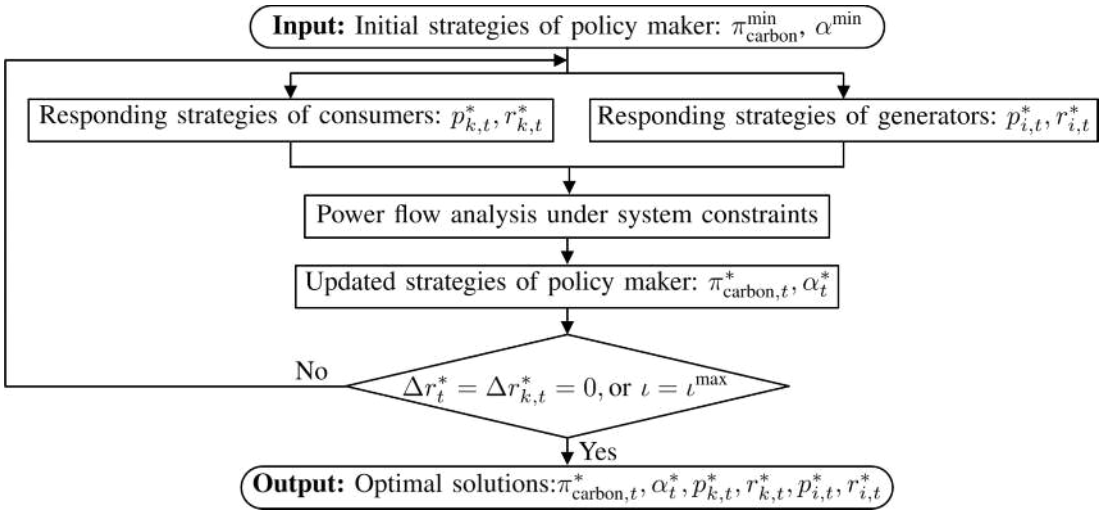

Figure 3.3: Flowchart of the Stackelberg game between leader and followers.

3.4.2 Solution Analysis

To find optimal solutions for both the leader and followers' problems as an agreement of negotiation, the deterministic approaches, such as gradient based algorithms and non-linear programming, are liable to yield sub-optimal solutions for the following reasons:

- The piecewise function of monetary compensation (3.2.15) results in the objective function of consumers to be a non-linear and non-convex function.
- The carbon emissions rates are disproportional to the power outputs due to the dynamic carbon emissions intensities, resulting in the non-linear function of carbon costs and thus the non-linear function of profits.
- The approach of carbon emissions tracing causes the feasible range of carbon emissions rates to be a discrete space.

To overcome these challenges, our research develops an intelligent algorithm based on the basic structure of artificial immune system to search the entire feasible space

of decision variables for finding the global optimal solutions. Given that the followers of individual consumers/generators optimise their own objective functions separately and simultaneously, the followers distributed immune algorithm (FDIA) is developed. For the MOP of the leader, the leader multiobjective immune algorithm (LMIA) is developed to find the trade-off between leader's objectives.

3.4.3 Algorithms

Using the equality constraints (3.2.10) and (3.2.11), the followers' decision variables $r_{k,t}$ and $r_{i,t}$ can be substituted by $p_{k,t}$ and $p_{i,t}$, and these equality constraints can be eliminated. Analogously, using equality constraint (3.3.29), the leader' s decision variable Δr_t can be substituted by $\Delta r_{k,t}$, and this equality constraint can be eliminated.

To facilitate the discussions of algorithms, first, define vector-valued decision variables and objective functions as follows

$$\mathbf{p}_{\text{follower}} = [p_{i,t}, p_{k,t} | i = 1, ..., |\mathcal{I}|, k = 1, ..., |\mathcal{K}|, t = 1, ..., |\mathcal{T}|], \tag{3.4.38}$$

$$\mathbf{p}_{\text{leader}} = [\pi_{\text{carbon},t}, \alpha_t, \Delta r_{k,t} | k = 1, ..., |\mathcal{K}|, t = 1, ..., |\mathcal{T}|], \tag{3.4.39}$$

$$\mathbf{f}_{\text{follower}} = [-f_i(p_{i,t}), f_k(p_{k,t}) | i = 1, ..., |\mathcal{I}|, k = 1, ..., |\mathcal{K}|], \tag{3.4.40}$$

$$\mathbf{f}_{\text{leader}} = [f_n(\pi_{\text{carbon},t}, \alpha_t, \Delta r_{k,t}), f_c(\Delta r_{k,t})], \tag{3.4.41}$$

where $\mathbf{p}_{\text{follower}}$ is a $[(|\mathcal{K}| + |\mathcal{I}|) \times |\mathcal{T}|]$-size row vector to denote the decision variables of followers, $\mathbf{p}_{\text{leader}}$ is a $[(|\mathcal{K}| + 2) \times |\mathcal{T}|]$-size row vector to denote the decision variables of the leader, $\mathbf{f}_{\text{follower}}$ is a $(|\mathcal{K}| + |\mathcal{I}|)$-size row vector to denote the objective functions of followers, and $\mathbf{f}_{\text{leader}}$ is a 2-size row vector to denote the objective functions of the leader. Additionally, the lower bounds and upper bounds of the decision variables of followers as described in (3.3.17) and (3.3.22) are denoted by vectors $\underline{\mathbf{p}}_{\text{follower}}$ and $\overline{\mathbf{p}}_{\text{follower}}$, respectively. The lower bounds and upper bounds of the decision variables of the leader as described in (3.3.26), (3.3.27), and (3.3.28) are denoted by vectors $\underline{\mathbf{p}}_{\text{leader}}$ and $\overline{\mathbf{p}}_{\text{leader}}$, respectively.

Next, the definitions with respect to the artificial immune system [173] and Pareto optimality [174] are introduced as follows

- *Definition 1 (Antigen-Antibody)*: A random vector $\mathbf{p}$ in the decision variable space $\left[\underline{\mathbf{p}}, \overline{\mathbf{p}}\right]$ is termed as an antigen. The corresponding objective function $\mathbf{f}(\mathbf{p})$ is termed as an antibody. All vectors generated from the decision variable space form an antigen population as

$$\mathcal{A} = \left\{\mathbf{p}_1, ..., \mathbf{p}_{|\mathcal{A}|}\right\}, \tag{3.4.42}$$

where $\mathcal{A}$ is the set of antigen population, and $|\mathcal{A}|$ is the number of antigens in this population.

- *Definition 2 (Clone and Mutation)*: The clonal process enables more antigens to be reproduced over the decision variable space $\left[\underline{\mathbf{p}}, \overline{\mathbf{p}}\right]$. Through preserving the diversity of antigens, the entire feasible space of decision variables can be searched to ensure the global optimal solution. The amount of reproduced antigens can be described by clonal rate as

$$r_c := \left\lfloor \frac{|\mathcal{A}^{\max}|}{|\mathcal{A}|} \right\rfloor, \tag{3.4.43}$$

where r_c is the clonal rate, $|\mathcal{A}^{\max}|$ is the maximum number of antigens in the population, and $\lfloor \cdot \rfloor$ is the floor function. Hence, each original antigen in (3.4.42) is cloned by $(r_c - 1)$ antigens through the mutation process to form the set of clonal antigen population as

$$\mathcal{A}_c = \left\{\mathbf{p}_1^1, ..., \mathbf{p}_1^{r_c-1}, ..., \mathbf{p}_{|\mathcal{A}|}^1, ..., \mathbf{p}_{|\mathcal{A}|}^{r_c-1}\right\}, \tag{3.4.44}$$

where $\mathcal{A}_c$ is the set of clonal antigen population, in which each mutant can be calculated as: $\vartheta \cdot \mathbf{p} + (1 - \vartheta) \cdot \mathbf{p}'$, where $\vartheta \in [0, 1]$ is a random number, and $\mathbf{p}'$ is a random vector in the decision variable space $\left[\underline{\mathbf{p}}, \overline{\mathbf{p}}\right]$. Through the clone and mutation process, the antigen population becomes $\mathcal{A}^{\max} = \mathcal{A} \cup \mathcal{A}_c$.

- *Definition 3 (Pareto Dominance)*: A vector of objective function $\mathbf{f}(\mathbf{p}_a)$ dominates another vector of objective function $\mathbf{f}(\mathbf{p}_b)$ in the decision variable space $\mathbf{p}_a, \mathbf{p}_b \in \left[\underline{\mathbf{p}}, \overline{\mathbf{p}}\right]$, denoted as $\mathbf{f}(\mathbf{p}_a) \preceq \mathbf{f}(\mathbf{p}_b)$, if $f(p_a) \leq f(p_b)$, $\forall f(p_a) \in \mathbf{f}(\mathbf{p}_a)$, $f(p_b) \in \mathbf{f}(\mathbf{p}_b)$ holds true and at least one inequality is strict. The vector $\mathbf{f}(\mathbf{p}_b)$ is termed as dominated antibody.

- *Definition 4 (Pareto Optimal Solution)*: A vector of decision variable $\mathbf{p}^* \in [\underline{\mathbf{p}}, \overline{\mathbf{p}}]$ is a Pareto optimal solution, if its objective function $\mathbf{f}(\mathbf{p})$ dominates all objective functions of any other feasible decision variables in $[\underline{\mathbf{p}}, \overline{\mathbf{p}}]$.

- *Definition 5 (Pareto Optimal Set and Pareto Frontier)*: The set of all Pareto optimal solutions is termed as the Pareto optimal set, denoted as $\mathcal{P} = \{\mathbf{p}^*\}$. The graphical presentation of objective functions of the Pareto optimal solutions in the Pareto optimal set is termed as the Pareto frontier.

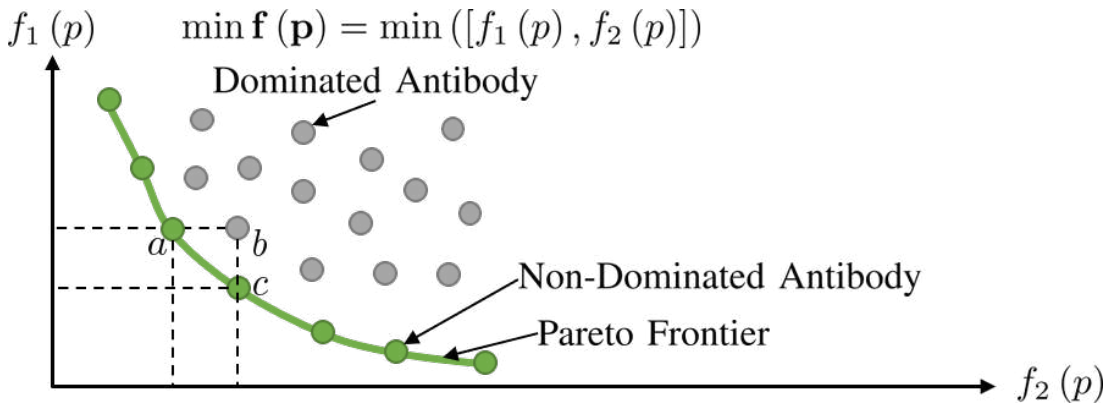

Figure 3.4: Schematic illustration of the Pareto dominance and Pareto frontier. The problem seeks for minimisation of two objective functions. Point b is dominated by points a and c.

A schematic illustration of the Pareto dominance and Pareto frontier for a minimisation problem is presented in Fig. 3.4. Point b is a dominated antibody, whereas points a and c are non-dominated antibodies. Under the same value of $f_1(p)$, point a provides a smaller value of $f_2(p)$ than point b. Analogously, under the same value of $f_2(p)$, point c provides a smaller value of $f_1(p)$ than point b. All the non-dominated antibodies form the Pareto frontier.

The proposed algorithm is performed over the entire scheduling horizon $|\mathcal{T}|$ for the following day. During the operation of the artificial immune algorithm, the antigens are randomly generated and cloned to explore the entire decision variable space. In each iteration, the dominated antigen-antibody pairs are removed to keep the non-dominated ones. Until the iteration ends, the antigens of all non-dominated antibodies form the optimal solution. The results of each generator/consumer serve

as the best solution that maximises/minimises its profits/electricity bills, whereas the results of the policy maker serve as a set of Pareto optimal solutions in the Pareto frontier that achieves a trade-off between the carbon revenue neutrality and carbon emissions reduction. Let ι_{FDIA} and ι_{LMIA} denote the nominal numbers of iterations of the FDIA and LMIA, respectively, and $\iota^{\max}_{\text{FDIA}}$ and $\iota^{\max}_{\text{LMIA}}$ denote the corresponding maximum numbers of iterations. The pseudocode code of the proposed FDIA-LMIA is shown in **Algorithm 1**.

3.5 Case studies

In this section, case studies have been conducted to evaluate the proposed model and algorithms on the context of the U.K. power systems and energy market. The performances of low carbon energy scheduling under various policies are examined to yield an appropriate policy design.

3.5.1 Simulation Setup and Data Availability

The proposed FDIA-LMIA is written in the MATLAB language. The simulations are performed using a machine with Intel$^{\text{R}}$ Core$^{\text{TM}}$ i9-9900K CPU at 3.60 GHz. To improve the computational efficiency, 8-core parallel computing is used during the clone and mutation process of the proposed FDIA-LMIA. The maximum and nominal numbers of antigens are set as 6000 and 3000, respectively, and the numbers of iterations for both the immune algorithm and Stackelberg game-theoretic model are set as 50, based on the empirical study. The simulations are repeated 10 times to eliminate the randomness and outliers.

The GB 29-bus test system is a simplified transmission network developed by [176] to represent the technical properties of the GB transmission network whilst reducing complexity. This test system is adopted by our research to examine the effects of the formulated low carbon policies on the context of the GB power systems. The schematic illustration of this test system is presented in Fig. 3.5. The GB 29-bus test system consists of 29 buses, 98 double-circuit branches, 1 single-circuit branch, and 89 generators. The total installed capacity of each generation source

Algorithm 1 FDIA-LMIA

Input: minimum monetary compensation rate $\alpha^{\min}$, minimum carbon prices $\pi^{\min}_{\text{carbon}}$, and maximum number of iteration $\iota^{\max}$

initialise policy maker's strategies: $\alpha_t = \alpha^{\min}_t, \pi_{\text{carbon},t} = \pi^{\min}_{\text{carbon},t}$

while $\Delta r^*_{k,t} \neq 0$, or $\iota \leq \iota^{\max}$ **do**

  followers distributed immune algorithm:

  Input: monetary compensation rate α_t, carbon prices $\pi_{\text{carbon},t}$, and nominal and maximum number of antigens in the population of followers $|\mathcal{A}_{\text{follower}}|$ and $|\mathcal{A}^{\max}_{\text{follower}}|$, respectively

  randomly initialise the antigen population of followers within the decision variable space $\left[\underline{\mathbf{p}}_{\text{follower}}, \overline{\mathbf{p}}_{\text{follower}}\right]$ as $\mathcal{A}_{\text{follower}}(0) = \left\{\mathbf{p}_{\text{follower},1}, ..., \mathbf{p}_{\text{follower},|\mathcal{A}_{\text{follower}}|}\right\}$

  while $\iota_{\text{FDIA}} \leq \iota^{\max}_{\text{FDIA}}$ **do**

    implement clone and mutation operation according to (3.4.44), and the number of current antigens $|\mathcal{A}_{\text{follower}}(\iota_{\text{FDIA}})|$ increases to $|\mathcal{A}^{\max}_{\text{follower}}|$

    remove dominated antibodies and corresponding antigens from $\mathcal{A}_{\text{follower}}(\iota_{\text{FDIA}})$

    while $|\mathcal{A}_{\text{follower}}(\iota_{\text{FDIA}})| > |\mathcal{A}_{\text{follower}}|$ **do**

      remove the antigen-antibody pairs with small avidities according to [175], i.e. remove the vectors of objective function in a crowded region

    end while

    $\mathcal{A}_{\text{follower}}(\iota_{\text{FDIA}} + 1) = \mathcal{A}_{\text{follower}}(\iota_{\text{FDIA}}), \iota_{\text{FDIA}} = \iota_{\text{FDIA}} + 1$

  end while

  Output: optimal solution $\mathbf{p}^*_{\text{follower}} = \left[p^*_{i,t}, p^*_{k,t} | i = 1, ..., |\mathcal{I}|, k = 1, ..., |\mathcal{K}|, t = 1, ..., |\mathcal{T}|\right]$

  leader multiobjective immune algorithm:

  Input: $\mathbf{p}^*_{\text{follower}}$, $|\mathcal{A}_{\text{leader}}|$, and $|\mathcal{A}^{\max}_{\text{leader}}|$

  randomly initialise the antigen population of the leader within the decision variable space $\left[\underline{\mathbf{p}}_{\text{leader}}, \overline{\mathbf{p}}_{\text{leader}}\right]$ as $\mathcal{A}_{\text{leader}}(0) = \left\{\mathbf{p}_{\text{leader},1}, ..., \mathbf{p}_{\text{leader},|\mathcal{A}_{\text{leader}}|}\right\}$

  while $\iota_{\text{LMIA}} \leq \iota^{\max}_{\text{LMIA}}$ **do**

    implement clone and mutation operation according to (3.4.44), and the number of current antigens $|\mathcal{A}_{\text{leader}}(\iota_{\text{LMIA}})|$ increases to $|\mathcal{A}^{\max}_{\text{leader}}|$

    remove dominated antibodies and corresponding antigens from $\mathcal{A}_{\text{leader}}(\iota_{\text{LMIA}})$

    while $|\mathcal{A}_{\text{leader}}(\iota_{\text{LMIA}})| > |\mathcal{A}_{\text{leader}}|$ **do**

      remove the antigen-antibody pairs with small avidities according to [175]

    end while

    $\mathcal{A}_{\text{leader}}(\iota_{\text{LMIA}} + 1) = \mathcal{A}_{\text{leader}}(\iota_{\text{LMIA}}), \iota_{\text{LMIA}} = \iota_{\text{LMIA}} + 1$

  end while

  Output: Pareto optimal set $\mathcal{P}_{\text{leader}} = \left\{\mathbf{p}^*_{\text{leader}} | \mathbf{p}^*_{\text{leader}} = \left[\pi^*_{\text{carbon},t}, \alpha^*_t | t = 1, ..., |\mathcal{T}|\right]\right\}$

  $\iota = \iota + 1, \alpha_t = \alpha^*_t, \pi_{\text{carbon},t} = \pi^*_{\text{carbon},t}$

end while

Output: $\mathcal{P}_{\text{leader}}, \mathbf{p}^*_{\text{follower}}$

is allocated to each generator, according to the installed capacities and locations of the GB power plants at the end of 2019, published by the Department for Business, Energy, and industrial Strategy [177]. The nuclear operates as baseload plants in the GB power systems. Hence, the power output of nuclear is not considered as a decision variable. The storages are included to dispatch power outputs of solar and wind. The buses with installed generation capacity more than 5000 MW are set as PV buses, the bus 27 is set as a reference bus, and other buses are set as PQ buses. The allocation percentages and power factors of 29 loads in [178] are used to allocate the total consumption to each load. The real-time states of the GB power consumption are obtained from the GridWatch [179]. The power flow analysis is performed by the Matpower using Newton-Raphson method.

Table 3.1: Coefficients of operating costs for generation sources

Source	Onshore Wind	Gas	Nuclear	Solar	Hydro
Costs Coefficients (£/MWh)	15	40	21	9	23
Source	Offshore Wind	Biomass	Coal	Import	
Costs Coefficients (£/MWh)	28	80	42	65	

The £144/MWh of average retail electricity price from the U.K. suppliers [180] is adopted, and the flat electricity pricing scheme is used in our research to specifically investigate the impacts of carbon prices and monetary compensation rates. The wholesale electricity price accounts for 45 % of the retail price [180]. The coefficients of operating costs of generators for project commissioning in 2020 [170] are adopted as shown in Table 3.1. The £18/ton of the U.K. carbon price support is used as the minimum carbon price. Considering the variability of renewable energy sources would cause additional carbon emissions from part-loaded thermal generators, the dynamic carbon emissions intensities are modelled as follows.

- The coal and CCGT which are the dominant sources of carbon emissions primarily operate at part-loaded. The part-loaded operation would reduce unit efficiency, increase fuel consumption, and raise carbon emissions intensity. The

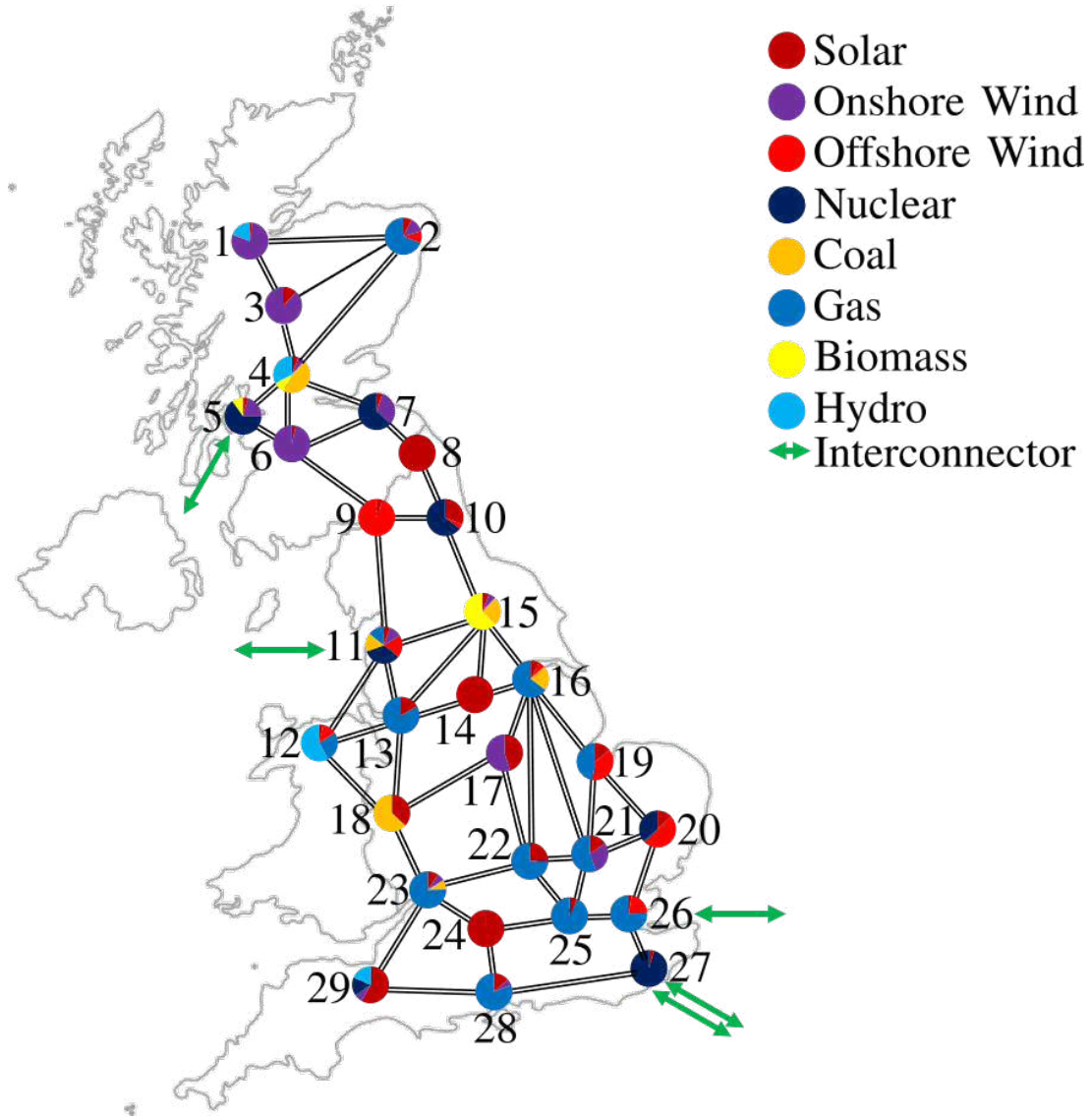

Figure 3.5: Schematic illustration of the GB 29-bus test system and allocation of generation capacities. The allocation is based on the installed capacities of the GB power plants. The percentage of allocated capacities is shown in the pie chart of each bus.

following relationships between carbon emissions intensities and power factors of coal and CCGT are used as studied in [77]

$$\begin{aligned}\rho_{\text{coal},t} =& 6.4 \cdot \cos\theta^6_{\text{coal},t} - 29.0 \cdot \cos\theta^5_{\text{coal},t} + 54.7 \cdot \cos\theta^4_{\text{coal},t} \\ & - 56.1 \cdot \cos\theta^3_{\text{coal},t} + 33.9 \cdot \cos\theta^2_{\text{coal},t} - 12.0 \cdot \cos\theta_{\text{coal},t} + 3.1\end{aligned} \tag{3.5.45}$$

$$\begin{aligned}\rho_{\text{CCGT},t} =& 0.14 \cdot \cos\theta^6_{\text{CCGT},t} - 0.68 \cdot \cos\theta^5_{\text{CCGT},t} + 1.49 \cdot \cos\theta^4_{\text{CCGT},t} \\ & - 1.91 \cdot \cos\theta^3_{\text{CCGT},t} + 1.69 \cdot \cos\theta^2_{\text{CCGT},t} - 1.05 \cdot \cos\theta_{\text{CCGT},t} + 0.71\end{aligned} \tag{3.5.46}$$

where $\rho_{\text{coal},t}$ and $\rho_{\text{CCGT},t}$ are the carbon emissions intensities of coal and CCGT at scheduling time t, respectively, and $\cos\theta_{\text{coal},t}$ and $\cos\theta_{\text{CCGT},t}$ are power factors of coal and CCGT at scheduling time t, respectively.

- For other generation sources, the impact of part-loading on carbon emissions intensities is not found to be significant by the study in [77]. Hence, the average annual carbon emissions intensities are applied to the biomass and nuclear, and evaluated by using the method proposed by Hawkes [79] as

$$\bar{\rho}_i = \frac{\text{Carbon Emissions Intensities of Fuel} \times \text{Fuel Usage}}{\text{Gross Electricity Supply}}, \tag{3.5.47}$$

  where $\bar{\rho}_i$ is the average annual carbon emissions intensity of source i. The data of fuel usage and gross electricity supply is published by the Digest of the U.K. Energy Statistics [181]. The data of carbon emissions intensities of fuel is published by the U.K. Government Greenhouse Gas Conversion Factors for Company Reporting [182].

- The carbon emissions of wind, hydro and solar primarily arise in manufacture and construction. Hence, the operational carbon emissions intensities of these sources are assumed to be zero in our research.

- The carbon emissions of interconnectors are caused by transmission and distribution losses. The data of carbon emissions intensities of transmission and distribution losses is published by the U.K. Government Greenhouse Gas Conversion Factors for Company Reporting [182].

For comparing the results of the policy maker's MOP, a criteria in [183] is used to select a representative solution from the Pareto frontier. An optimal solution that maximises the minimum improvement (after normalisation) of all objective functions is selected as the representative solution as

$$\mathbf{f}_{\text{rep}} = \max_{\mathbf{p}\in\mathcal{A}} \min_{f\in\mathbf{f}} \frac{\overline{f} - f(\mathbf{p})}{\overline{f} - \underline{f}}, \tag{3.5.48}$$

where $\mathbf{f}_{\text{rep}}$ is the vector of representative objective functions form the Pareto frontier, $\overline{f}$ and $\underline{f}$ are the minimal and maximal values of each objective function.

3.5.2 Algorithms Evaluation

To evaluate the performances of the proposed Stackelberg game-theoretic model and FDIA-LMIA, the following cases are used as a comparison:

- *Case 1 (Benchmark)*: The benchmark is yielded by the sum of the GB power system historical data of four representative days in 2019 [179] with equal weight. According to the current GB carbon market design, the £30/ton is used as the carbon prices (the U.K. carbon price support plus the EU ETS) and £0/ton is used as the monetary compensation rate.

- *Case 2 (MOP)*: Instead of using the Stackelberg game-theoretic model to simulate the process of negotiation and yield an optimal scheduling decisions, a MOP is used to perform the scheduling for policy maker, consumers, and generators simultaneously without iteration as studied in [183].

- *Case 3 (Followers Aggregated Immune Algorithm (FAIA))*: Instead of targeting on each individual consumers/generators, the FAIA schedules the aggregated demand/supply to minimise/maximise the overall electricity bills/costs as studied in [54].

The comparison of the aforementioned scheduling models and algorithms in terms of realising the carbon emissions reduction targets of policy maker is presented in Fig. 3.6. For the MOP, without the process of iterative negotiation and reaching an optimal agreement, the policy maker is unable to dynamically adjust

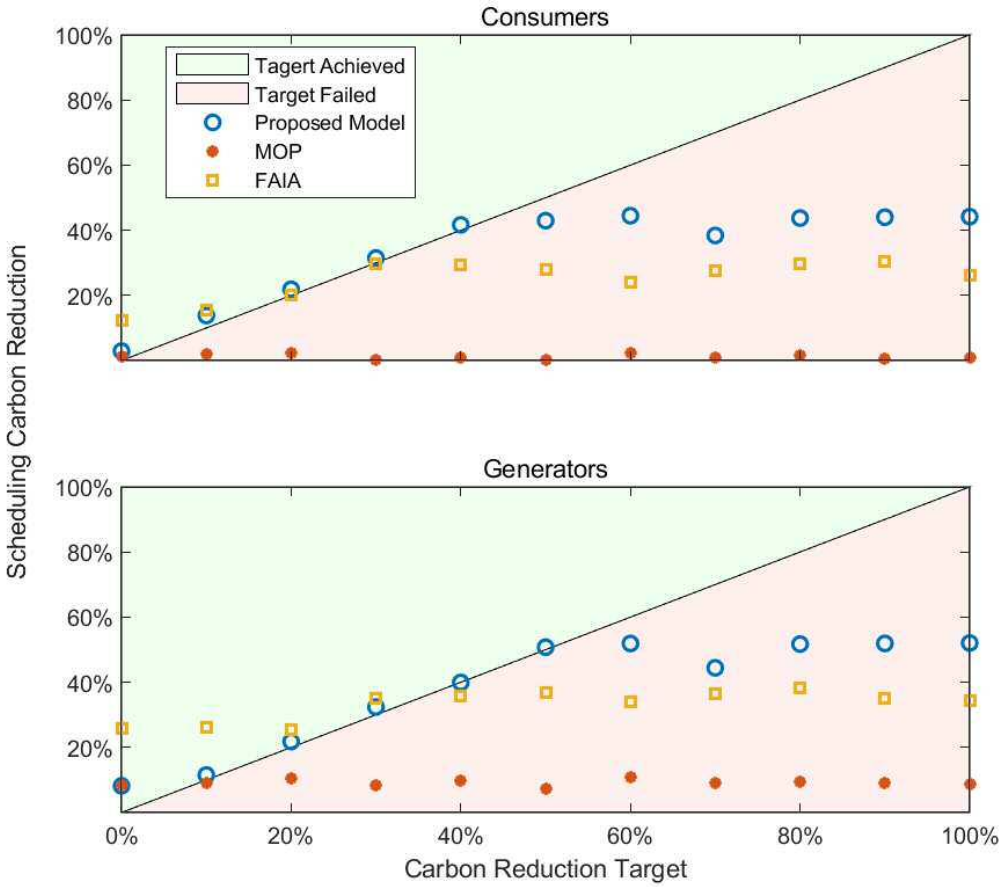

Figure 3.6: Comparison of scheduling models and algorithms in terms of realising the carbon emissions reduction targets. The x axes indicate the percentage of carbon emissions reduction by policy maker's targets, relative to the daily carbon emissions of benchmark. The y axes indicate the percentage of carbon emissions reduction by consumers/generators' scheduling, relative to the daily carbon emissions of benchmark. The green regions indicate the policy maker's targets are achieved by consumers/generators' scheduling, whereas the red regions indicate consumers/generators' scheduling fails to achieve the policy maker's targets. The scheduling results are sampled in every 10 %.

carbon prices and monetary compensation rates, and fails to incentivise the consumers/generators to achieve the carbon reduction targets through scheduling. The percentage of daily carbon emissions reduction of consumers/generators by MOP remains at approximately 10 %, irrespective of the increasing carbon reduction targets. By contrast, through using the proposed scheduling model and the FAIA, consumers/generators can be incentivised to keep reducing their carbon emissions for meeting the increased carbon reduction targets, until above 40 % of carbon emissions reduction. Additionally, as studied in [184], the power system operations resulting from optimising an aggregated objective function may favour a particular participant, whereas our proposed FDIA-LMIA targets on each individual consumers/generators' own objective function. Hence, the proposed model can further improve to approximately 50 % of the carbon emissions reduction.

Table 3.2: Comparison of yielded objective functions by scheduling models and algorithms

	Benchmark	Proposed Model	MOP	FAIA
Daily Electricity Bills (m£)	105.51	95.96	96.97	96.24
Daily Profits (m£)	17.92	16.58	16.68	16.64
Daily Carbon Emissions (kton)	42.92	37.15	38.63	38.56

The comparison of yielded objective functions by the aforementioned scheduling models and algorithms is presented in Table 3.2. The electricity bills of all consumers and profits of all generators are aggregated for comparison. The proposed scheduling model and FDIA-LMIA yield the lowest daily electricity bills and carbon emissions. For the daily profits, the proposed FDIA-LMIA targets on each individual generators, which enables the profits of generators with renewable energy sources to be improved and the profits of generators with coal and gas to be reduced. Since the generators with coal and gas account for a majority of power outputs, the profits of our proposed model are lower than the profits of benchmark and non-negotiation cases.

3.5.3 Scheduling Performances

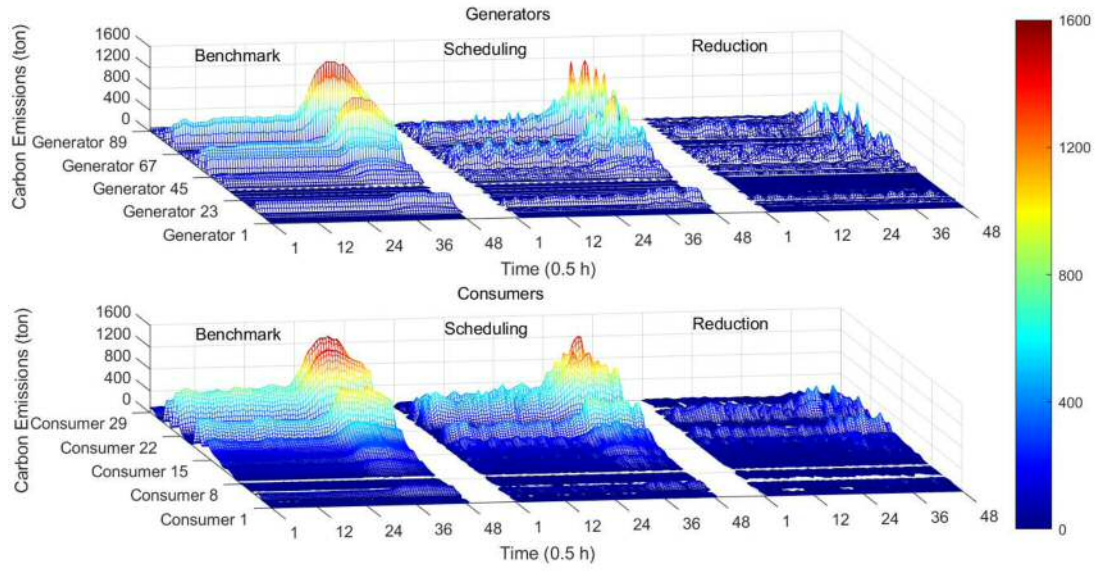

Figure 3.7: Carbon emissions tracing for generators/consumers over the scheduling process. The x axes indicate the scheduling time of day. The y axes indicate the number of generators/consumers. The z axes and colourbar indicate the carbon emissions of individual generators/consumers for a given 0.5 h scheduling interval. 'Benchmark' and 'Scheduling' refer to the carbon emissions before and after the scheduling, respectively. 'Reduction' refers to the difference of carbon emissions before and after the scheduling.

The carbon emissions tracing for individual generators/consumers over the scheduling process is presented in Fig. 3.7. For generation sources with high carbon emissions intensities, i.e. coal and gas, the corresponding generators are incentivised to ramp down the power outputs during the entire scheduling horizon for carbon reduction and cost saving. It is particular for the peak demand period from the twenty-fifth scheduling time to the thirty-sixth scheduling time, during which about 500 tons of carbon emissions per half-hour are reduced, accounting for 31.25 % of the highest carbon emissions rate from generators. Meanwhile, the power outputs of renewable energy sources ramp up to complement the decrease of coal and gas without causing additional carbon emissions. Analogously, for the loads with high-level of carbon emissions, the corresponding consumers are incentivised to shift or curtail

the demand for carbon reduction, in order to earn the monetary compensation and save electricity bills. During the peak demand period, about 200 tons of carbon emissions per half-hour are reduced, accounting for 13.33 % of the highest carbon emissions rate from consumers.

Incentive Effects of Monetary Compensation Rates on Consumers

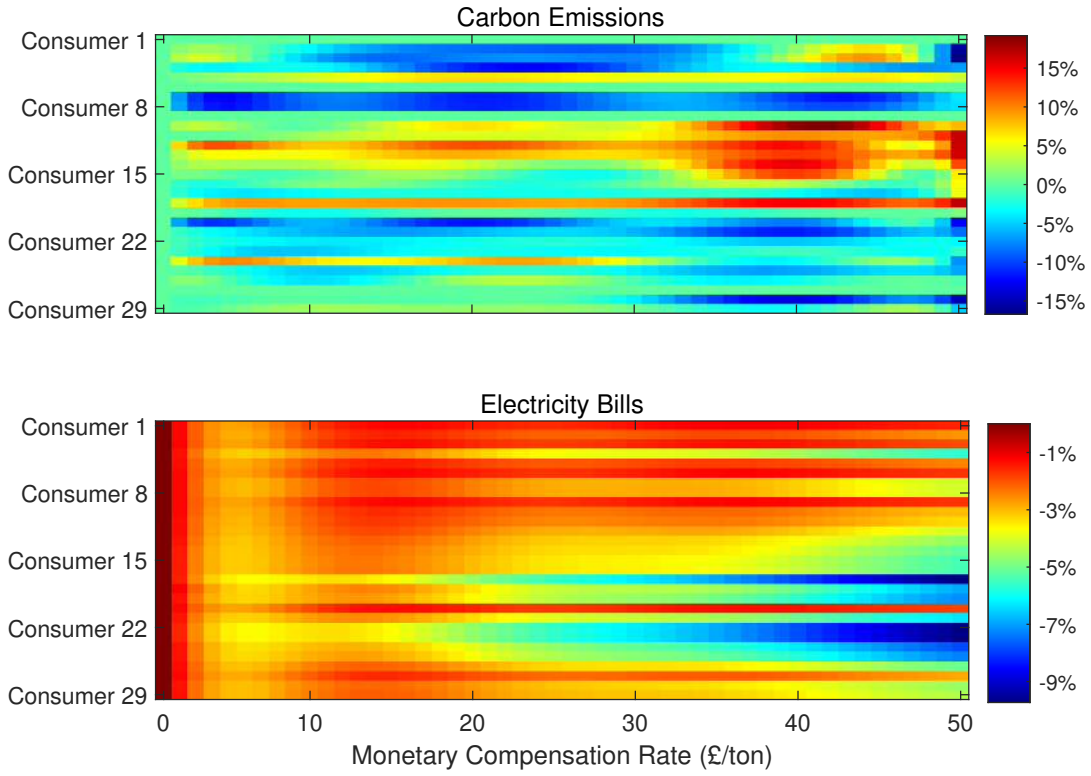

Figure 3.8: Carbon emissions and electricity bills of consumers as a function of monetary compensation rates. The x axes indicate the monetary compensation rates. The y axes indicate the number of consumers. The colourbars indicate the percentage of increase (positive)/decrease (negative) of carbon emissions and electricity bills for each consumer at a given monetary compensation rate, compared to the carbon emissions and electricity bills without the monetary compensation rate, respectively.

The chromatograms in Fig. 3.8 show the trends of carbon emissions and electricity bills of consumers as the monetary compensation rates increase. Each column illustrates the carbon emissions and electricity bills of various consumers at a given

monetary compensation rate. According to our proposed decentralised low carbon incentive mechanism, the consumers with low-level of carbon emissions (as indicated in consumers 10 - 15) would not be significantly incentivised by the monetary compensation. By contrast, the consumers with high-level of carbon emissions (as indicated in rest consumers) would receive more monetary compensations, and therefore curtail or shift their loads for carbon reduction and bill saving. The electricity bills of consumers gradually decrease with the increase of the monetary compensation rates. When the monetary compensation rates exceed £33/ton, the bill saving effects on consumers with extreme high-level of carbon emissions (as indicated in consumer 17 and consumers 22 - 25) would be more significant (at approximately 9 % of bill saving through 10 % of carbon reduction).

Incentive Effects of Carbon Prices on Generators

The chromatograms in Fig. 3.9 show the trends of carbon emissions and profits of generation sources as the carbon prices increase. Each column illustrates the carbon emissions and profits of various generation sources at a given carbon price. For the carbon emissions, with the increase of carbon prices, the generation sources with high carbon intensities, i.e. coal and gas, are incentivised to ramp down power outputs for cost saving. It is noted that the carbon emissions from coal generation increase when the carbon prices rise from £28/ton to £42/ton. The reason is that although the coal generators are incentivised to ramp down the power output for carbon reduction, the slight carbon reduction is offset by the increased carbon intensity caused by part-loaded operation. As a renewable energy source, the power output and incurred carbon emissions of biomass rise to complement the decreased power outputs of coal and gas. However, the carbon emissions intensity of biomass is much lower than the carbon emissions intensities of coal and gas. Analogously, the power outputs of other renewable energy sources ramp up without causing additional carbon emissions; For the profits, the profits of generation from coal, gas, and biomass decrease with the increase of the carbon prices. When the carbon prices exceed £33/ton and £92/ton, the profits of coal and gas generation, respectively, would drop to negative. Additionally, the profits of power import increase with the rise of carbon prices,

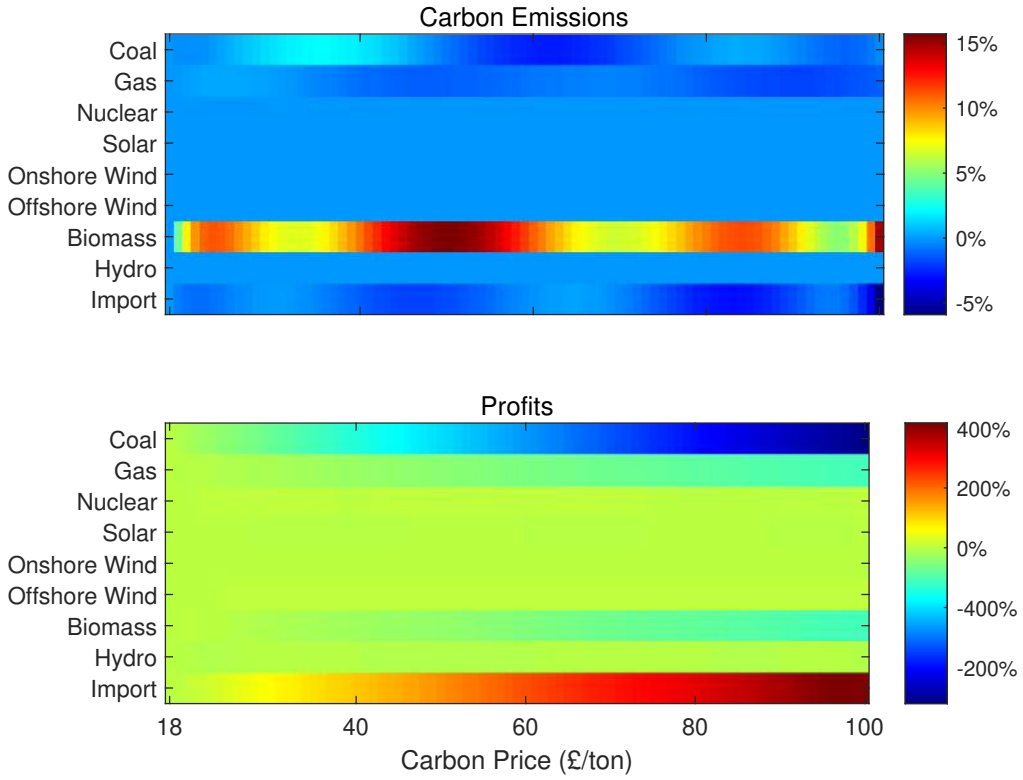

Figure 3.9: Carbon emissions and profits of generators as a function of carbon prices. Generators with the same source are aggregated. The x axes indicate the carbon prices. The y axes indicate the generation sources. The colourbars indicate the percentage of increase (positive)/decrease (negative) of carbon emissions and profits for each source at a given carbon price, compared to the carbon emissions and profits at £18/ton of the U.K. carbon price support, respectively.

because the carbon prices of other regions keep unchanged and are lower than the local carbon prices. It is profitable for generators to emit carbon emissions at the regions with lower carbon prices, and export the power to the regions with higher carbon prices as the study of emissions leakage issue [185].

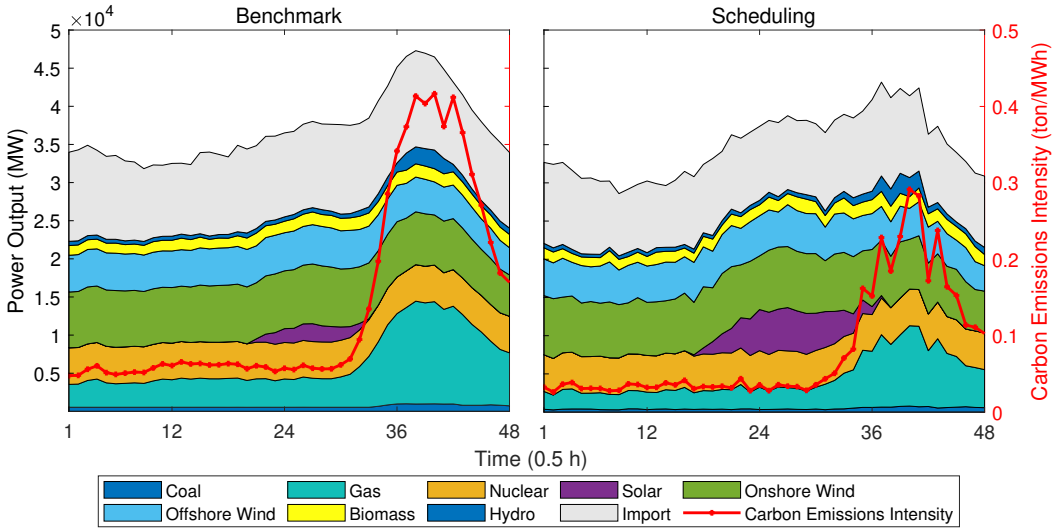

Figure 3.10: Comparison of power outputs by generation sources and average carbon emissions intensity weighted by power outputs between the benchmark and propose scheduling model. The x axes indicate the scheduling time of day. The left y axes indicate the power outputs of generation sources corresponding to the stacked areas. The right y axes indicate the average carbon emissions intensity weighted by power outputs corresponding to the red line.

The comparison of power outputs by generation sources and average carbon emissions intensity weighted by power outputs between the benchmark and proposed scheduling model is presented in Fig. 3.10. Through the proposed energy scheduling, the peak demand is curtailed and shifted to the off-peak demand period. By increasing the proportion of power outputs from renewable energy sources and decreasing the proportion of power outputs from coal and gas, the average carbon emissions intensity of the proposed scheduling model is almost halved compared to that of the benchmark. The daily percentage of renewable energy sources (solar, wind, biomass, and hydro) increases from 39.53 % at benchmark to 45.13 % at the proposed scheduling model.

Trade-off of Policy Maker

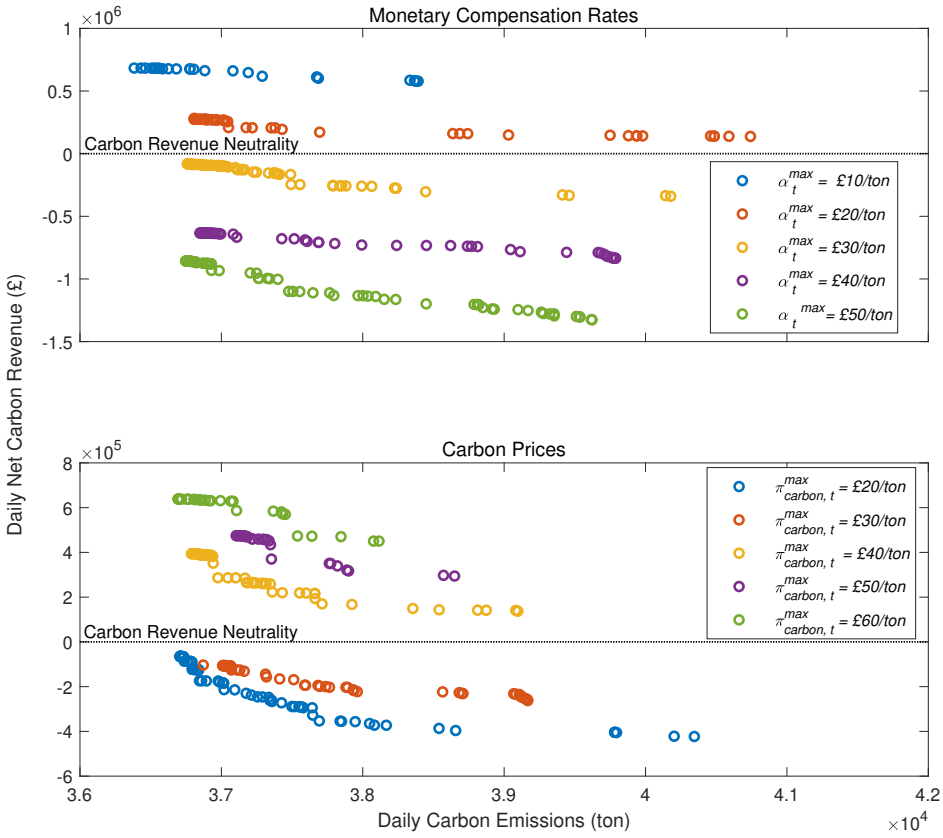

Figure 3.11: Pareto frontiers of the policy maker's objective functions under various maximum bounds of monetary compensation rates and carbon prices. The x axes indicate the objective function of daily carbon emissions. The y axes indicate the objective function of daily net carbon revenue. The dashed line indicates the carbon revenue neutrality is achieved, i.e. the revenue of selling carbon allowance to generators equals to the cost of monetary compensation to consumers.

The Pareto frontiers of the policy maker's trade-off between the carbon revenue neutrality and the carbon reduction are presented in Fig. 3.11. We use the net carbon revenue to describe the difference between the revenue of selling carbon allowance to generators and the cost of monetary compensation to consumers. When the maximum bound of the monetary compensation rates is relaxed from £10/ton to £50/ton (under £20/ton of the fixed maximum bound of carbon prices), both the

net carbon revenue and carbon emissions decrease. The carbon revenue neutrality is achieved when the maximum bound of monetary compensation rates falls into the range between £20/ton and £30/ton. When the maximum bound of the carbon prices is relaxed from £20/ton to £60/ton (under £20/ton of the fixed maximum bound of monetary compensation rates), the net carbon revenue increases whereas the carbon emissions decrease. The carbon revenue neutrality is achieved when the maximum bound of carbon prices falls into the range between £30/ton and £40/ton.

3.6 Chapter Summary

This chapter proposes a novel model for energy scheduling and low carbon negotiation between the policy maker and consumers/generators. The strategical negotiation is modelled as a Stackelberg game-theoretic problem, and the agreement is reached by finding the optimal solutions for both the policy maker and individual consumers/generators. By implementing dynamic monetary compensation rates and carbon prices, the consumers and generators with high carbon emissions intensities can be incentivised to reduce carbon emissions for the propose of bill saving and profit improving, respectively. Case studies based on the U.K. power systems demonstrate that the proposed model and algorithm can achieve up to 50 % of policy maker's targets for carbon emissions reduction, outperforming the models of multiobjective optimization and aggregated scheduling. For consumers, when they receive more than £33/ton of the monetary compensation rates, 9 % of bill saving can be realised through 10 % of carbon emissions reduction by curtailing or shifting the peak demand. For generators, the proposed scheduling improves the percentage of generation from renewable energy sources from 39.53 % to 45.13 % and halves the average carbon emissions intensities through ramping down the power outputs from coal and gas. When the carbon prices exceed £33/ton and £92/ton, the profits of coal and gas generation would drop to negative, respectively. For the policy maker, when the maximum monetary compensation rates and carbon prices are set in the ranges of £20/ton - £30/ton and £30/ton - £40/ton, the revenue of selling carbon allowance can be completely used as monetary compensation, i.e. carbon revenue

neutrality is achieved.

This research remains two directions to be explored in the next chapter: First, in the practical scheduling process, individual consumers/generators have idiosyncratic preferences, e.g. bill saving, utility improving, or cost saving, which requires a scalable model to capture these preferences with diverse parameters and objective functions. However, this would increase the computational burden of our designed intelligent heuristic algorithm. For the case of solving a scheduling problem with ι iterations, once it is combined with $|\mathcal{K}|$ consumers and $|\mathcal{I}|$ generators, the computational complexity would increase to $O\left(\iota^{|\mathcal{K}|+|\mathcal{I}|}\right)$. In the next chapter, this issue is overcome by using the machine learning as a model-free approach to extract idiosyncratic preferences and learn to make the optimal decisions. Second, this chapter assumes the flat electricity pricing scheme to specifically investigate the impacts of carbon prices and monetary compensation rates, which remains the effects of real-time electricity pricing scheme on the generation, consumption, and carbon emissions to be investigated. Next chapter will exploit price elasticities to analyse these effects and capture various energy patterns.

Chapter 4

Data-Driven Prosumer-Centric Low Carbon Energy Scheduling Using Learning Approaches

4.1 Introduction

The advances of smart grids and smart meters enable increasing number of consumers to produce or store energy in distribution networks through exploiting DRESs and batteries, leading to a new figure: prosumers [42]. In the field of energy markets, prosumers are residential, commercial, and industrial users, who actively produce surplus energy and feed it into a distribution network after self-consumption; When prosumers' demand cannot be met by self-generation, they consume energy from the power grids. This chapter proposes a novel data-driven energy scheduling tool for prosumers by using the learning approaches to overcome the issue of computational burden and investigate the effects of real-time electricity pricing scheme, as remained in Chapter 3. The step of solving optimisation problem using intelligent heuristic algorithm is replaced by the learning approaches, including deep neural networks (DNNs) and CNNs. The learning approaches only require historical data for learning to make optimal scheduling decisions with the advantage of improved scalability and reduced computational complexity. The effects of real-time electricity pricing scheme on generation, consumption, and carbon emissions are processed

as corresponding three types of dynamic price elasticities. These dynamic price elasticities represent intrinsic features of individual prosumers, referring as prosumption patterns, which is processed as elasticity images and analysed by using the pattern recognition capability of the CNNs. Additionally, a reliable scheduling tool requires accurate predictions of prosumption behaviours, in particular given uncertainties caused by the intermittency of DRESs and flexible demand. Hence, a real-time scenarios selection approach is developed to predict variations of these uncertainties, by which each variation is defined as a scenario. Case studies based on various IEEE test distribution systems demonstrate the effectiveness of designed neural networks, in comparison with other learning approaches.

Overall, this chapter offers the following key contributions:

- An approach of prosumption patterns processing is designed to analyse local features, temporal transient features, and the correlation of dynamic price elasticities. By exploiting the pattern recognition capability of the CNNs, how these intrinsic features affect individual prosumers' scheduling strategy is investigated.

- Learning approaches are exploited to improve the scalability and computational efficiency of the energy scheduling tool from solving the optimisation problem by the intelligent heuristic algorithms.

- A real-time scenarios selection approach is developed to improve prediction accuracy under uncertainties, by which each scenario provides a possible energy prosumption to be scheduled, and the scheduling decisions provide an update for scenarios set.

- Case studies verify that the proposed energy scheduling tool improves the accuracy of making optimal scheduling decisions with reduced computational complexity, under the various IEEE test systems and uncertain scenarios. The connection between the intrinsic features of dynamic price elasticities and scheduling results is demonstrated.

The rest of this chapter is organised as follows: Section 4.2 introduces an overview of the implementation of the proposed energy scheduling tool. The training phase of

the energy scheduling tool is detailed in Section 4.3 to describe how to use uncertain scenarios, prosumption patterns, and optimal scheduling decisions for training the neural networks. The deploying phase of the energy scheduling tool is detailed in Section 4.4 to describe the real-time scenarios selection and energy scheduling for individual prosumers. Section 4.5 provides case studies under various learning approaches and IEEE test distribution systems to verify the proposed approaches. Section 4.6 concludes this chapter.

4.2 Implementation of Energy Scheduling Tool

The motivation of this research is to design an energy scheduling tool by using learning approaches to reduce computational complexity and capture prosumption patterns of individual prosumers. The prosumers include the residential, commercial, and industrial users in the distribution networks. The proposed energy scheduling tool is deployed in the day-ahead prosumption scheduling to help these prosumers make optimal decisions for the next day, through analysing prosumers' smart meter data. This section introduces the overview of the implementation of the proposed energy scheduling tool, consisting of the training phase and the deploying phase, as presented in Fig. 4.1.

Figure 4.1: Overview of the implementation of the proposed energy scheduling tool. The implementation consists of training phase and deploying phase. At the training phase, the real-time metering data is stored in the data warehouse, and used by the manufacturer of the energy scheduling tool to train the neural networks after pre-processing, i.e. scenarios analysis, prosumption patterns processing, and preferences optimisation. At the deploying phase, the energy scheduling tool with trained neural networks is deployed to individual prosumers' sides to help them schedule generation and consumption.

At the training phase, real-time metering data of individual prosumers is stored in data warehouse, and used by the manufacturer of the energy scheduling tool to train the neural networks under a supervised learning mode. Uncertainties caused by the intermittency of the DRESs and flexible demand are analysed by the developed scenarios analysis approach. The intrinsic features of individual prosumers represented by dynamic price elasticities are processed as elasticity images by using the designed prosumption patterns processing approach. The uncertain scenarios and elasticity images are used as training inputs. The training labels are optimal decision variables yielded from solving the preferences optimisation problems. These preferences are predefined by the users, such as electricity bill saving, utility improving, and generating cost saving.

At the deploying phase, the energy scheduling tool with trained neural networks is deployed to individual prosumers' sides. With real-time data from the prosumer's smart meter, the scheduling tool automatically makes optimal decisions for the next-day prosumption scheduling, and sends these optimal decisions to the controller which controls both generators and loads.

4.3 Training Phase of Energy Scheduling Tool

In this section, the training phase of the proposed energy scheduling tool is discussed. The flowchart of the training phase is shown in Fig. 4.2. The historical metering data is firstly processed by the proposed scenarios analysis approach in Section 4.3.1. The dynamic price elasticities are processed as elasticity images by the proposed prosumption patterns processing approach in Section 4.3.2, in order to extract intrinsic features of prosumers by taking advantage of pattern recognition capability of the CNN. The processed scenarios and elasticity images are used as numerical and image inputs of neural networks, respectively. Meanwhile, each of the analysed scenarios is used to solve the preferences optimisation problem in Section 4.3.3. The preferences in our research are defined as minimising the costs and carbon emissions by optimally modifying the generation and consumption profiles of each scenario. These optimal decision variables are then used as training labels

of the neural networks. This architecture of neural networks is described in Section 4.3.4. The overall algorithm of the training phase is shown in **Algorithm 2**.

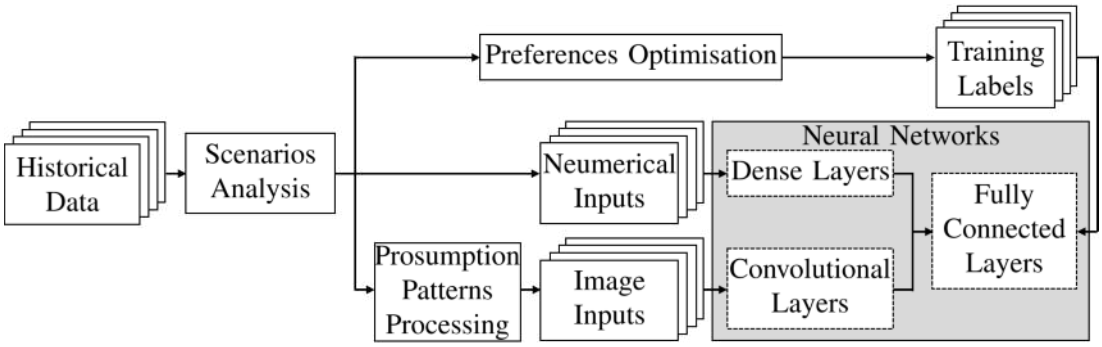

Figure 4.2: Flowchart of the training phase of the energy scheduling tool. Historical data is processed by the scenarios analysis and prosumption patterns processing approaches as training inputs of dense layers and convolutional layers, respectively. The training labels are optimal scheduling decisions yielded by solving the preferences optimisation problems.

Algorithm 2 Algorithm of Training Phase of the Energy Scheduling Tool

Input: historical data $p_{t,m}$, electricity price π_t

1: generate $|\mathcal{X}|$ scenarios, each scenario $p_{t,x}$ with occurrence probability $\Pr(p_{t,x}) = 1/|\mathcal{X}|$

2: **for** $x = 1, ..., |\mathcal{X}|$ **do**

3: process elasticity images $\mathbf{\Phi}_x(t_a, t_b, \Xi)$ as Fig. 4.5

4: solve preferences optimisation problem to obtain optimal decision variables $\Delta\mathbf{p}_x^*$

5: train neural networks as (4.3.23)

6: **end for**

Output: trained neural networks f_{nn}

4.3.1 Scenarios Analysis

At the training phase, the scenarios analysis aims at: 1) data augmentation to avoid the overfitting problem [186] caused by limited samples; 2) accurately analysing

intrinsic features of prosumers by covering more potential information of prosumption patterns under uncertainties. The data augmentation is achieved by generating scenarios using statistical approaches including kernel density estimation and Latin Hypercube sampling. Each each generated scenario represents a possible variation of uncertain variables. Accurately evaluating the distributions of uncertain variables is a prerequisite for scenarios generation. A non-parametric estimation [129] which only relies on historical data can capture the stochastic feature of DRESs and flexible demand, without the need of distributions and assumed parameters in parametric estimation. This research therefore uses the non-parametric kernel density estimation [187] approach to estimate the probability density function of uncertain variables.

With the estimated density function, the Latin Hypercube sampling [188] is then implemented to produce the scenarios. The reason is that compared to random sampling approach, such as Monte Carlo Simulation [189], Latin Hypercube sampling can avoid over-concentration by space-filling so as to reduce the standard deviation of samples, which means that scenarios are generated over the entire feasible range of the historical data to guarantee the accuracy with reduced number of samples.

Recall that $\mathcal{I}$ and $\mathcal{K}$ denote the index sets of generators and loads of a prosumer, respectively. The power generation of generator $i \in \mathcal{I}$ at scheduling time t is denoted by $p_{i,t}$. The power consumption of load $k \in \mathcal{K}$ at scheduling time t is denoted by $p_{k,t}$. The retail electricity price at scheduling time t is denoted by π_t. For simplicity, $p_{i,t}$, $p_{k,t}$, and π_t are represented by an uncertain variable p_t in this subsection. Let $\mathcal{M}$ denote the index set of historical metering data. A data sample $m \in \mathcal{M}$ of uncertain variable p_t is denoted by $p_{t,m}$. The unknown density function of p_t is then fitted from the set of the historical data by using the kernel density estimation [187] as

$$\tilde{f}(p_t) := \frac{1}{|\mathcal{M}| \cdot \varsigma} \sum_{m=1}^{|\mathcal{M}|} f_{\text{kernel}} \left(\frac{p_t - p_{t,m}}{h} \right), \tag{4.3.1}$$

where $\tilde{f}(\cdot)$ is the estimated kernel density function of the uncertain variable p_t, $|\mathcal{M}|$ is the number of historical data, ς is the bandwidth smoothing parameter, and $f_{\text{kernel}}(\cdot)$ is the kernel function. Gaussian kernel function is used due to its high accuracy [190]. The kernel function is placed around each historical data $p_{t,m}$ to

construct $\tilde{f}(p_t)$ by the sum of $|\mathcal{M}|$ kernels as shown in Fig. 4.3.

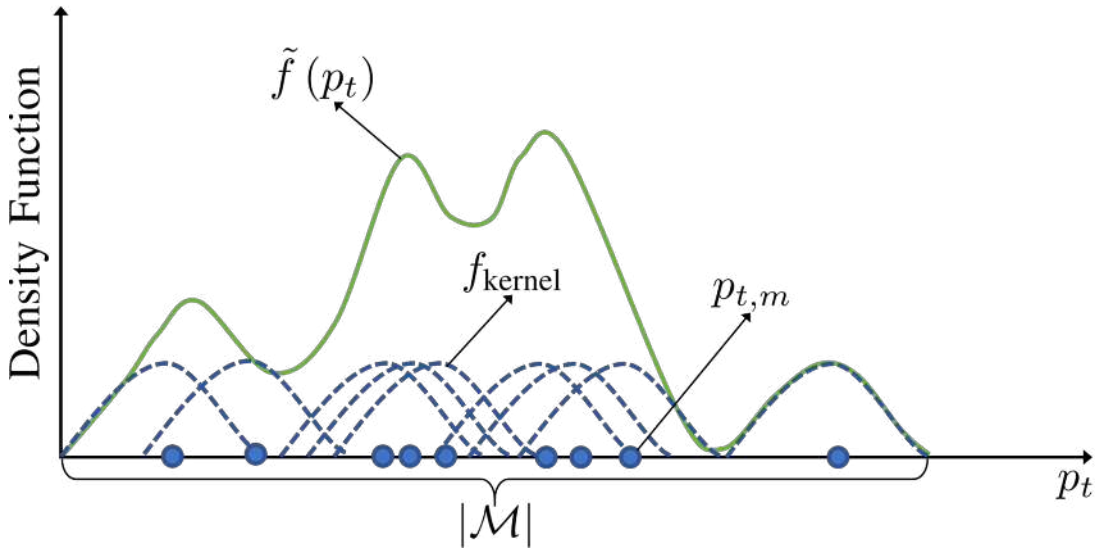

Figure 4.3: Schematic illustration of the kernel density estimation. The kernel function f_{kernel} is placed around each historical data $p_{t,m}$. The estimated kernel density function $\tilde{f}(p_t)$ is constructed by the sum of $|\mathcal{M}|$ kernels.

Let $f_{\text{cumul}}(p_t)$ denote the cumulative density function of the uncertain variable p_t, where $f_{\text{cumul}}(p_t)$ is obtained by the integral of $\tilde{f}(p_t)$. Let $\mathcal{X}$ denote the index set of scenarios and $|\mathcal{X}|$ denote the number of scenarios. To generate the desired $|\mathcal{X}|$ scenarios, the value range of the cumulative density function $f_{\text{cumul}}(p_t)$, i.e. [0,1], is equally divided into $|\mathcal{X}|$ subintervals. The scenario $x \in \mathcal{X}$ of uncertain variable p_t, denoted by $p_{t,x}$, is generated from each subinterval by using the Latin Hypercube sampling [188] as

$$f_{\text{cumul}}(p_t)\,|_{p_t=p_{t,x}} := \left(\frac{1}{|\mathcal{X}|}\right) \cdot \vartheta + \frac{x-1}{|\mathcal{X}|}, \tag{4.3.2}$$

where $\vartheta \in [0,1]$ is a random variable following a uniform distribution. The value of scenario can be calculated by the inverse function as

$$p_{t,x} = f^{-1}_{\text{cumul}}\left[f_{\text{cumul}}(p_t)\,|_{p_t=p_{t,x}}\right], \tag{4.3.3}$$

The occurrence probability of $p_{t,x}$ can be obtained as

$$\Pr(p_{t,x}) = \frac{1}{|\mathcal{X}|}, \tag{4.3.4}$$

where $\Pr(p_{t,x})$ is the occurrence probability of scenario $p_{t,x}$.

The schematic illustration of the Latin Hypercube sampling is presented in Fig. 4.4. The approach of scenarios analysis corresponds to the line 1 in **Algorithm 2**.

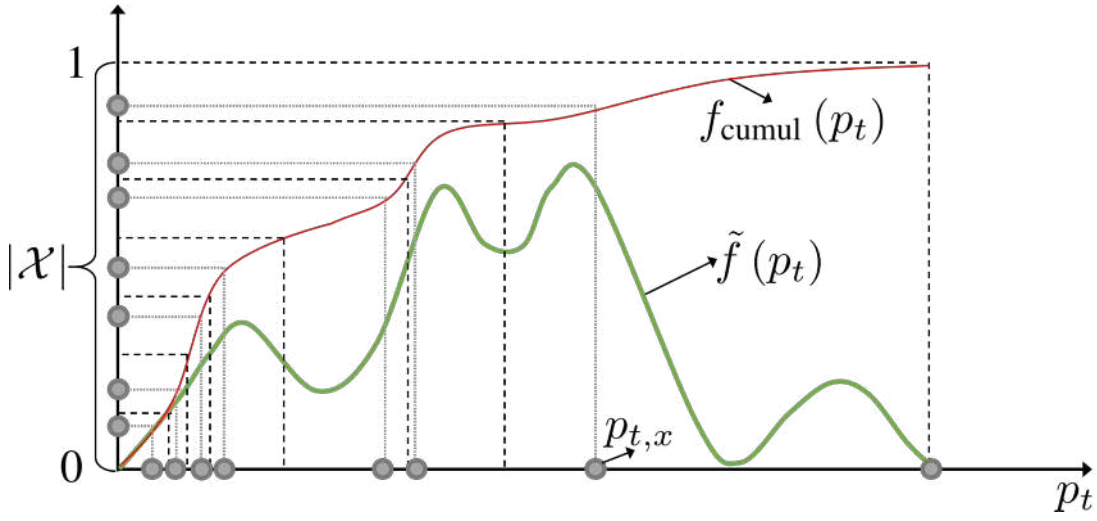

Figure 4.4: Schematic illustration of the Latin Hypercube sampling. The value range of the cumulative density function $f_{\text{cumul}}(p_t)$ is equally divided into $|\mathcal{X}|$ subintervals. Through random sampling from each subinterval, the scenario $p_{t,x}$ can be obtained by the inverse function of $f_{\text{cumul}}(p_t)|_{p_t=p_{t,x}}$. The occurrence probability of each scenario equals to $1/|\mathcal{X}|$.

4.3.2 Prosumption Patterns Processing

Let $p_{i,t,x}$ and $p_{k,t,x}$ denote the power generation of generator i and consumption of load k of scenario x at scheduling time t, respectively. Recall that $\mathcal{T}$ denotes the index set of scheduling time. First, the effects of real-time electricity pricing scheme on generation, consumption, and carbon emissions can be processed to corresponding three types of dynamic price elasticities. These three types of price elasticities describe the percentage change in generation, consumption, and carbon emissions when there is a one percent change in electricity price. Hence, They represent intrinsic features of individual prosumers, defined as the prosumption patterns.

- Price Elasticity of Generation: When the electricity prices change from π_{t_a} at scheduling time $t_a \in \mathcal{T}$ to π_{t_b} at scheduling time $t_b \in \mathcal{T}$, a prosumer's total power generation of scenario x correspondingly changes from $\sum_{i\in\mathcal{I}} p_{i,t_a,x}$ to

$\sum_{i\in\mathcal{I}} p_{i,t_b,x}$. The price elasticity of generation between t_a and t_b can be defined as

$$\xi_{p_{i,x}}(t_a, t_b) := \left(\sum_{i\in\mathcal{I}} \frac{p_{i,t_a,x} - p_{i,t_b,x}}{p_{i,t_a,x}}\right) \cdot \left(\frac{\pi_{t_a}}{\pi_{t_a} - \pi_{t_b}}\right), \tag{4.3.5}$$

where $\xi_{p_{i,x}}(\cdot)$ is the function of price elasticity of generation between any two scheduling time.

- Price Elasticity of Consumption: When the electricity prices change from π_{t_a} at scheduling time $t_a \in \mathcal{T}$ to π_{t_b} at scheduling time $t_b \in \mathcal{T}$, a prosumer's total power consumption of scenario x correspondingly changes from $\sum_{k\in\mathcal{K}} p_{k,t_a,x}$ to $\sum_{k\in\mathcal{K}} p_{k,t_b,x}$. The price elasticity of consumption between t_a and t_b can be defined as

$$\xi_{p_{k,x}}(t_a, t_b) := \left(\sum_{k\in\mathcal{K}} \frac{p_{k,t_a,x} - p_{k,t_b,x}}{p_{k,t_a,x}}\right) \cdot \left(\frac{\pi_{t_a}}{\pi_{t_a} - \pi_{t_b}}\right), \tag{4.3.6}$$

where $\xi_{p_{k,x}}(\cdot)$ is the function of price elasticity of consumption between any two scheduling time.

- Price Elasticity of Carbon Emissions: There are two portions of carbon emissions caused by prosumption behaviours: 1) When a prosumer consumes energy from the main grid, carbon emissions will be caused due to the generation from fossil-fuelled sources, e.g. coal and gas. 2) When a prosumer uses biomass or diesel generators, the carbon emissions are caused by its self-generation. These two portions of carbon emissions can be described as the first and second terms of the following equation as

$$r_{t,x} = p_{\text{main},t,x} \cdot \rho_{\text{main}} + \sum_{i\in\mathcal{I}} p_{i,t,x} \cdot \rho_i, \tag{4.3.7}$$

where $r_{t,x}$ is the carbon emissions rate of a prosumer's scenario x at scheduling time t, $p_{\text{main},t,x}$ is the power exchange of a prosumer with the main grid of scenario x at scheduling time t, ρ_{main} is the average carbon emissions intensity of all generation sources from the main grid, and ρ_i is the carbon emissions intensity of a prosumer's own generator i. The first term of (4.3.7) holds when $p_{\text{main},t,x} > 0$.

Due to the retail electricity prices cover the carbon cost of electricity generation, we define the price elasticity of carbon emissions as

$$\xi_{r_x}(t_a, t_b) := \left(\frac{r_{t_a,x} - r_{t_b,x}}{r_{t_a,x}}\right) \cdot \left(\frac{\pi_{t_a}}{\pi_{t_a} - \pi_{t_b}}\right), \tag{4.3.8}$$

where $\xi_{r_x}(\cdot)$ is the function of price elasticity of carbon emissions between any two scheduling time.

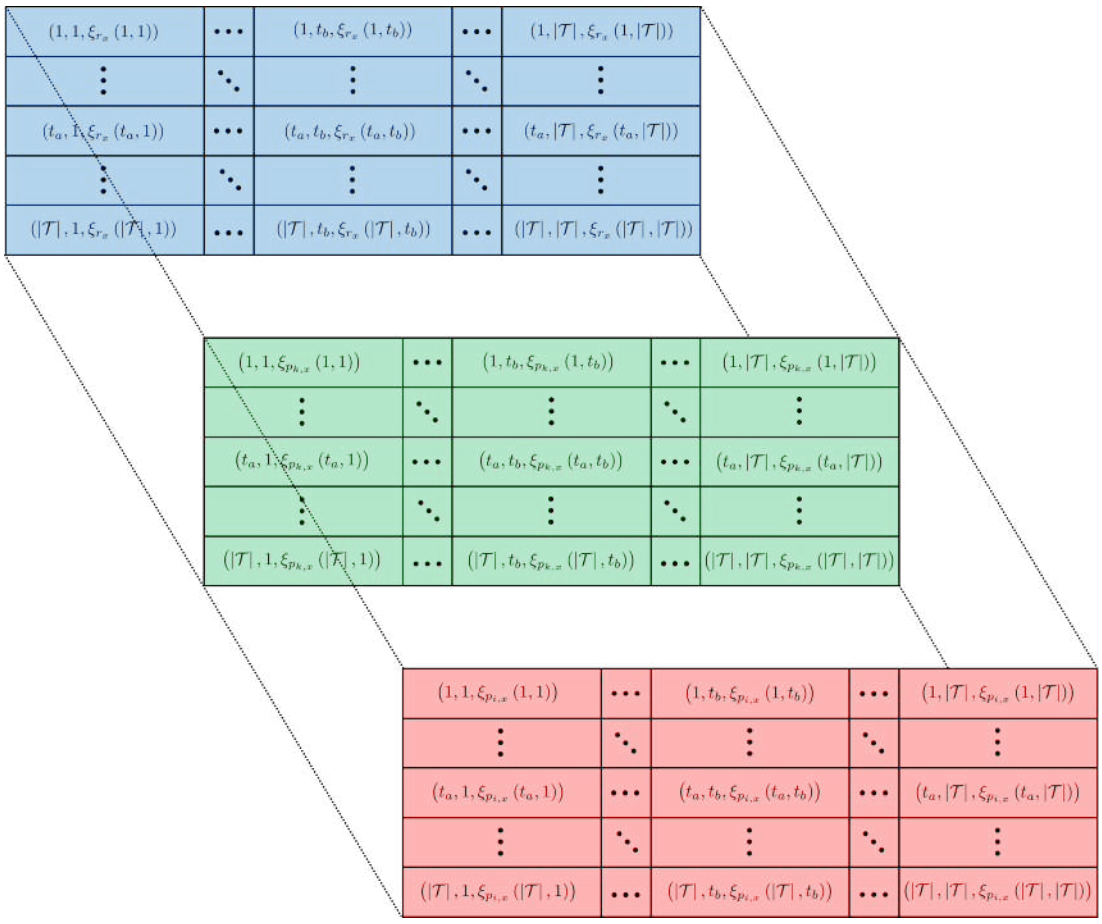

Figure 4.5: Schematic illustration of an elasticity image. The image is in the form of a 3-dimensional array as $\mathbf{\Phi}_x(t_a, t_b, \Xi)$, $\forall t_a, t_b \in \mathcal{T}$. Three elements of Ξ, i.e. $\xi_{p_{i,x}}(t_a, t_b)$, $\xi_{p_{k,x}}(t_a, t_b)$, and $\xi_{r_x}(t_a, t_b)$ correspond to three colour channels. (t_a, t_b) decides the location of a pixel at the elasticity image.

Next, the prosumption patterns processing approach is developed to process this information to be elasticity images as inputs of the CNNs. Unlike the data processing approach as studied by Choi *et al.* [121], to restructure the time-series data

from 1×24 row vector to 4×6×1 matrix as a greyscale image, we use the scheduling time t_a and t_b to locate the position of x-axis and y-axis of a pixel at an image, and assign three types of elasticities to three colour channels (R G B) of z-axis of a pixel by proportionally scaling up to the value range of pixel, i.e. [0,255]. Hence, a 3-dimensional array, i.e. elasticity image, is formed as shown in Fig. 4.5, denoted as $\mathbf{\Phi}_x\left(t_a, t_b, \Xi\right)$, $\forall t_a, t_b \in \mathcal{T}$, where $\Xi = \left[\xi_{p_{i,x}}\left(t_a, t_b\right), \xi_{p_{k,x}}\left(t_a, t_b\right), \xi_{r_x}\left(t_a, t_b\right)\right]$ is the vector of price elasticities between any two scheduling time. These 3 dimensions t_a, t_b, and Ξ correspond to the height, width, and depth of an elasticity image, respectively, and the depth refers to three colour channels. Since a price elasticity from scheduling time t_a to scheduling time t_b does not equal to that from scheduling time t_b to scheduling time t_a according to (4.3.5) (4.3.6) and (4.3.7), the elasticity image is asymmetric with respect to the diagonal. Additionally, since the price elasticities reflect the effects of price change between two scheduling time, the diagonal elements, i.e. t_a=t_b are set as zero. In the elasticity image, a brighter pixel means the prosumption or carbon emissions between scheduling time indicated by its x-axis and y-axis are easier to be scheduled due to a higher price elasticity, whereas a darker pixel means the prosumption or carbon emissions between scheduling time indicated by its x-axis and y-axis are harder to be scheduled due to a lower price elasticity. The approach of prosumption patterns processing corresponds to the line 3 in **Algorithm 2**.

The correlation of $\xi_{p_{i,x}}$, $\xi_{p_{k,x}}$, and ξ_{r_x} is presented at a pixel by combining three colour channels. The temporal transient feature of elasticities is presented as the colour gradient between pixels. Hence, the proposed approach of prosumption patterns processing can take advantage of the pattern recognition capability of the CNN from a high-dimensional array. Another advantage is that the scale difference between prosumption (in a unit of kW) and carbon emissions (in a unit of kg) can be normalised, because three types of elasticities can be treated equally by the CNNs as pixel elements with the same value range.

4.3.3 Preferences Optimisation

The problem of preferences optimisation is only solved at the training phase by manufacturers of the energy scheduling tool, after the historical metering data and pre-defined preferences from individual prosumers are received. At the deploying phase, trained neural networks can replace the step of solving optimisation problems so as to help each prosumer automatically make predicted optimal scheduling decisions. In our research, the preferences of individual prosumers are defined as minimising the costs of using electricity and reducing the total carbon emissions caused by prosumption behaviours for the next day. The following assumptions are made when we consider a prosumer's energy scheduling.

- *Assumption 1*: Since the generators and loads in a distribution network are nearby, and the amount of generation from prosumers is small relative to the total generation in power systems. The transmission losses in the distribution network are neglected.

- *Assumption 2*: When a prosumer sells power to the main grid, i.e. $p_{\text{main},t,x} < 0$, the selling price equals to the retail electricity price at that scheduling time. The reason of this simplified assumption is that this chapter specifically investigates the effects of real-time retail pricing on prosumption behaviours. How individual prosumers strategically decide their selling prices for maximising their profits will be investigated in Chapter 5.

- *Assumption 3*: The energy storage devices are equipped for individual prosumers to help them schedule the non-dispatchable DRESs, e.g. wind and solar. For the prosumers without the energy storage devices, the maximum storage capacity and maximum charging/discharging rate are zero.

Problem Formulation

Firstly, from the economic perspective, a prosumer aims to minimise the costs of using electricity by strategically modifying power exchange with the main grid, generation, consumption, and storage of each scenario. The objective function of costs

of using electricity can be modelled as

$$f_u\left(\Delta p_{\text{main},t,x}, \Delta p_{i,t,x}, \Delta p_{k,t,x}\right) := \sum_{t\in\mathcal{T}} \Bigg[\left(p_{\text{main},t,x} - \Delta p_{\text{main},t,x}\right) \cdot \pi_{t,x} + \sum_{i\in\mathcal{I}} \left(p_{i,t,x} - \Delta p_{i,t,x}\right) \cdot \delta_i + \left|\Delta p_{s,t,x}\right| \cdot \delta_s \Bigg] \cdot \Delta t, \tag{4.3.9}$$

where $f_u(\cdot)$ is the objective function of costs of using electricity by a prosumer, $\Delta p_{\text{main},t,x}$ is the amount of modifying the power exchange from the main grid of a prosumer's scenario x at scheduling time t, $\Delta p_{i,t,x}$ is the amount of modifying the generation by generator i of a prosumer's scenario x at scheduling time t, $\Delta p_{k,t,x}$ is the amount of modifying the consumption by load k of a prosumer's scenario x at scheduling time t, $\pi_{t,x}$ is the retail electricity price of scenario x at scheduling time t, δ_i is the operating cost coefficient of generator i, $\Delta p_{s,t,x}$ is the power charging/discharging rate of a prosumer's energy storage device of scenario x at scheduling time t, and δ_s is the cost coefficient of energy storage devises, and Δt is the scheduling interval. For the scheduling interval of 0.5 h, we have $(\Delta t, |\mathcal{T}|)=(0.5,48)$.

The power dynamics of a prosumer's energy storage device can be described as

$$\Delta p_{s,t,x} = \left(p_{\text{main},t-1,x} - \Delta p_{\text{main},t-1,x}\right) - \sum_{k\in\mathcal{K}} \left(p_{k,t-1,x} - \Delta p_{k,t-1,x}\right) + \sum_{i\in\mathcal{I}} \left(p_{i,t-1,x} - \Delta p_{i,t-1,x}\right), \tag{4.3.10}$$

where

$$\Delta p_{s,t,x} = p_{s,t,x} - p_{s,t-1,x} \tag{4.3.11}$$

indicates the power charging/discharging when the value of $\Delta p_{s,t,x}$ is positive/negative, respectively, and $p_{s,t,x}$ is the stored power of a prosumer's energy storage device of scenario x at scheduling time t. There are two constraints for the energy storage devices as

- *Storage Capacity Constraint*: The maximum storage capacity is determined by the medium of storage devices [191]. The stored power should be restricted to certain limits as

$$0 \le p_{s,t,x} \le p_s^{\max}, \tag{4.3.12}$$

where $p_s^{\max}$ is the maximum storage capacity.

- *Charging/Discharging Rate Constraint*: The charging/discharging rate should be restricted below the maximum limit as

$$|\Delta p_{s,t,x}| \leq \Delta p_s^{\max}, \tag{4.3.13}$$

where $\Delta p_s^{\max}$ is the maximum charging/discharging rate.

Remark 1: According to (4.3.10), the decision variable of modifying power storage can be substituted by $\Delta p_{\text{main},t,x}$, $\Delta p_{i,t,x}$, and $\Delta p_{k,t,x}$. For the prosumers without the energy storage devices, we have $p_s^{\max} = 0$ and $\Delta p_{s,t,x} = 0$.

Remark 2: Recall that in Chapter 3, the operating costs include the costs of operation, maintenance, fuel, and carbon capture and storage (excluding the costs of pre-development, construction, decommissioning, and waste). The coefficients of operating costs are evaluated by the LCoE. In this chapter, the carbon cost is also considered into the operating costs for simplicity, because the flat carbon pricing scheme is used to specifically investigate the effects of electricity prices. Additionally, the storage costs include the costs of operation, maintenance, charging/discharging (excluding the initial installed cost). The coefficient of storage cost is evaluated by the levelised cost of storage (LCoS) [192]. The LCoS is a discounted cost per unit of charged/discharged electrical energy.

Secondly, from the environmental perspective, a prosumer aims to minimise the total carbon emissions caused by prosumption behaviours. The objective function of total carbon emissions can be modelled as

$$\begin{aligned} f_c\left(\Delta p_{\text{main},t,x}, \Delta p_{i,t,x}, \Delta p_{k,t,x}\right) := \sum_{t\in\mathcal{T}} \Bigg[& \left(p_{\text{main},t,x} - \Delta p_{\text{main},t,x}\right) \cdot \rho_{\text{main}} \\ & + \sum_{i\in\mathcal{I}} \left(p_{i,t,x} - \Delta p_{i,t,x}\right) \cdot \rho_i \Bigg] \cdot \Delta t, \end{aligned} \tag{4.3.14}$$

where $f_c(\cdot)$ is the objective function of total carbon emissions caused by prosumption behaviours. The first term of (4.3.14) holds when $(p_{\text{main},t,x} - \Delta p_{\text{main},t,x}) > 0$.

The power exchange, generation and consumption should be restricted to certain limits considering the capacities of power grid, generators and loads as

$$p_{\text{main}}^{\min} \leq p_{\text{main},t,x} - \Delta p_{\text{main},t,x} \leq p_{\text{main}}^{\max}, \tag{4.3.15}$$

$$p_i^{\min} \leq p_{i,t,x} - \Delta p_{i,t,x} \leq p_i^{\max}, \tag{4.3.16}$$

$$p_k^{\min} \leq p_{k,t,x} - \Delta p_{k,t,x} \leq p_k^{\max}, \tag{4.3.17}$$

where $p_{\text{main}}^{\min}$ and $p_{\text{main}}^{\max}$ are the minimum and maximum power exchange levels of power grid, respectively, $p_i^{\min}$ and $p_i^{\max}$ are the minimum and maximum power generation levels of generator i, respectively, and $p_k^{\min}$ and $p_k^{\max}$ are the minimum and maximum power consumption levels of load k, respectively.

Therefore, the objectives of a prosumer are to minimise the costs of using electricity and the total carbon emissions caused by prosumption behaviours, with the decision variables of modifying power exchange, generation, and consumption of each scenario, which leads to a MOP as

$$\min_{\Delta p_{\text{main},t,x}, \Delta p_{i,t,x}, \Delta p_{k,t,x}} : \left\{ f_u \left(\Delta p_{\text{main},t,x}, \Delta p_{i,t,x}, \Delta p_{k,t,x} \right), f_c \left(\Delta p_{\text{main},t,x}, \Delta p_{i,t,x}, \Delta p_{k,t,x} \right) \right\}, \tag{4.3.18}$$

s.t.: (4.3.10), (4.3.11), (4.3.12), (4.3.13),(4.3.15), (4.3.16), and (4.3.17).

Solution Algorithm

Firstly, to include the inequality constraints (4.3.12) and (4.3.13) into the solution of preferences optimisation problem, an additional function is introduced to replace (4.3.12) and (4.3.13) as

$$\begin{aligned} f_a \left(\Delta p_{\text{main},t,x}, \Delta p_{i,t,x}, \Delta p_{k,t,x} \right) := & \max \left\{ -p_{s,t,x}, 0 \right\} + \max \left\{ p_{s,t,x} - p_s^{\max}, 0 \right\} \\ & + \max \left\{ \left| \Delta p_{s,t,x} \right| - \Delta p_s^{\max}, 0 \right\}, \end{aligned} \tag{4.3.19}$$

where $f_a(\cdot)$ is the function of inequality constraints. According to (4.3.10), $f_a(\cdot)$ is a function of $\Delta p_{\text{main},t,x}$, $\Delta p_{i,t,x}$, and $\Delta p_{k,t,x}$. A solution satisfies the inequality constraints (4.3.12) and (4.3.13) if and only if $f_a \left(\Delta p_{\text{main},t,x}, \Delta p_{i,t,x}, \Delta p_{k,t,x} \right) = 0$.

The vector-valued decision variables and objective functions are defined as follows for facilitating the discussion of algorithm.

$$\Delta \mathbf{p}_x = \left[\Delta p_{\text{main},t,x}, \Delta p_{i,t,x}, \Delta p_{k,t,x} | i = 1, ..., |\mathcal{I}|, k = 1, ..., |\mathcal{K}|, t = 1, ..., |\mathcal{T}| \right], \tag{4.3.20}$$

$$\mathbf{f}_x = \left[f_u \left(\Delta \mathbf{p}_x \right), f_c \left(\Delta \mathbf{p}_x \right), f_a \left(\Delta \mathbf{p}_x \right) \right], \tag{4.3.21}$$

where $\Delta\mathbf{p}_x$ is a $[(|\mathcal{I}| + |\mathcal{K}| + 1) \times |\mathcal{T}|]$-size row vector to denote the decision variables of scenario x, and $\mathbf{f}_x$ is a 3-size row vector to denote the objective functions and constraints of scenario x. Additionally, the lower bounds and upper bounds of the decision variables as described in (4.3.15), (4.3.16), and (4.3.17) are denoted by vectors $\underline{\mathbf{p}}$ and $\overline{\mathbf{p}}$, respectively.

Next, the algorithm for solving the preferences optimisation problem is proposed based on the artificial immune system [173]. Readers can refer to the chapter 3 for the detailed definitions of the artificial immune system and Pareto optimality. The proposed algorithm is performed by individual prosumers over the entire scheduling horizon of $|\mathcal{T}|$ for the following day. During the operation of the artificial immune algorithm, the antigens are randomly generated and cloned to explore the entire decision variable space. In each iteration, the dominated antigen-antibody pairs are removed to keep the non-dominated antigen-antibody pairs. Until the iteration ends, the antigens of all non-dominated antibodies form the optimal solution. The results serve as a set of Pareto optimal solution in the Pareto frontier that achieves a trade off between the cost saving and carbon emissions reduction. The criteria of selecting a representative solution from the Pareto frontier as described in (3.5.48) is used. Let ι_{IA} and $\iota_{\mathrm{IA}}^{\max}$ denote the nominal and maximum numbers of iterations of the proposed algorithm, respectively. The pseudocode code of the algorithm for solving the preferences optimisation problem is shown in **Algorithm 3**.

Through solving the preferences optimisation problem, the optimal decision variables are yielded as

$$\Delta\mathbf{p}_x^* = \left[\Delta p_{\mathrm{main},t,x}^*, \Delta p_{i,t,x}^*, \Delta p_{k,t,x}^* | i = 1, ..., |\mathcal{I}|, k = 1, ..., |\mathcal{K}|, t = 1, ..., |\mathcal{T}|\right]. \tag{4.3.22}$$

The optimal decision variables are subsequently used as training labels to train the neural networks. The labels indicate how far the predicted optimal scheduling decisions from the theoretical optimal ones. The Preferences optimisation corresponds to line 4 in **Algorithm 2**.

Algorithm 3 Algorithm for Solving the Preferences Optimisation Problem

Input: set of scenarios $p_{i,t,x}$, $p_{k,t,x}$, and $\pi_{t,x}$, $\forall x \in \mathcal{X}$, nominal and maximum number of antigens in the population of decision variables $|\mathcal{A}|$ and $|\mathcal{A}^{\max}|$, respectively

for $x = 1, ..., |\mathcal{X}|$ **do**
  randomly initialise the antigen population within the decision variable space $\left[\underline{\mathbf{p}}, \overline{\mathbf{p}}\right]$ as $\mathcal{A}(0) = \left\{\Delta\mathbf{p}_{x,1}, ..., \Delta\mathbf{p}_{x,|\mathcal{A}|}\right\}$
  while $\iota_{\mathrm{IA}} \leq \iota_{\mathrm{IA}}^{\max}$ **do**
    implement clone and mutation operation according to (3.4.44), and the number of current antigens $|\mathcal{A}(\iota_{\mathrm{IA}})|$ increases to $|\mathcal{A}^{\max}|$
    remove dominated antibodies and corresponding antigens from $\mathcal{A}(\iota_{\mathrm{IA}})$
    while $|\mathcal{A}(\iota_{\mathrm{IA}})| > |\mathcal{A}|$, or $f_a(\Delta\mathbf{p}_x) \neq 0$ **do**
      remove the antigen-antibody pairs with the highest positive value of $f_a(\Delta\mathbf{p}_x)$
      remove the antigen-antibody pairs with small avidities according to [175], i.e. remove the vectors of objective function in a crowded region
    end while
    $\mathcal{A}(\iota_{\mathrm{IA}} + 1) = \mathcal{A}(\iota_{\mathrm{IA}}), \iota_{\mathrm{IA}} = \iota_{\mathrm{IA}} + 1$
  end while
  remove the antigen-antibody pairs that yield $f_a(\Delta\mathbf{p}_x) > 0$
  select a representative solution from the Pareto frontier
end for

Output: optimal solution $\Delta\mathbf{p}_x^*$

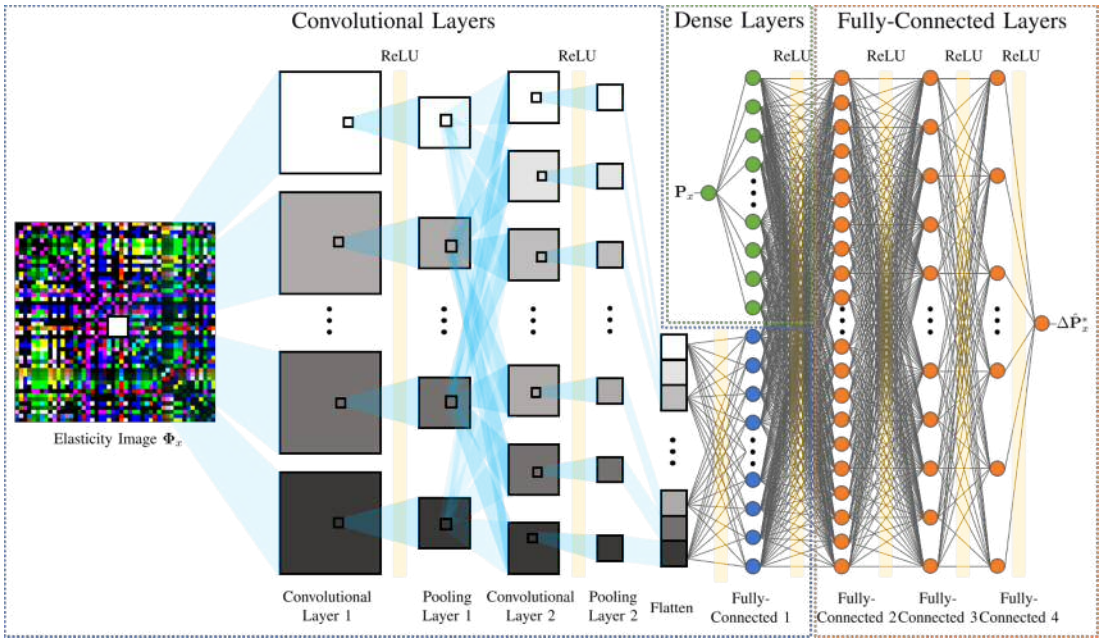

Figure 4.6: Architecture of designed neural networks. The elasticity image is imported to the convolutional layers. The numerical data is imported to the dense layers. The outputs of both layers are merged by fully-connected layers.

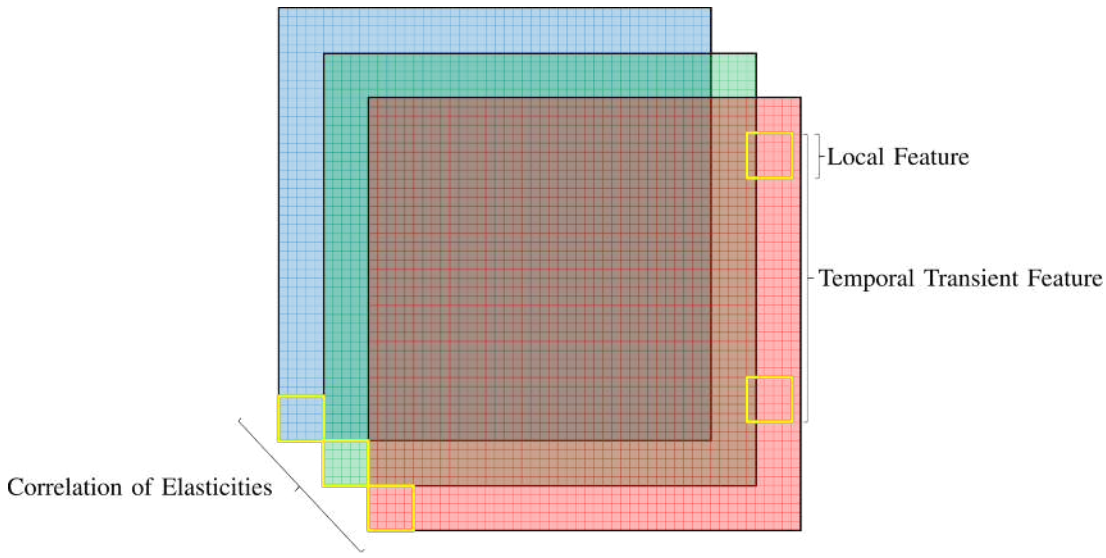

Figure 4.7: Schematic illustration of the local feature, temporal transient feature, and correlation of elasticities. The filter size is indicated by the yellow box.

4.3.4 Neural Networks Architecture

The designed neural networks consist of dense layers to import numerical inputs of each scenario and convolutional layers to extract intrinsic features from each elasticity image. The outputs of these two layers are merged by fully-connected layers to extract combined feature representations. The architecture of the designed neural networks is presented in Fig. 4.6. This structure of paralleled networks [193] has been validated as an efficient approach for extracting information from both numerical data and images in [119]. The training input of dense layers is the original power exchange, generation, and consumption of scenario x, i.e. $p_{\text{main},t,x}$, $p_{i,t,x}$, and $p_{k,t,x}$, $\forall i \in \mathcal{I}$, $k \in \mathcal{K}$, and $t \in \mathcal{T}$, denoted by a $((1+|\mathcal{I}|+|\mathcal{K}|)\times|\mathcal{T}|)$-size matrix $\mathbf{P}_x$. The training input of convolutional layers is an elasticity image of scenario x, denoted by a 3-dimensional array $\mathbf{\Phi}_x$. The training output is the predicted optimal scheduling decisions of scenario x, i.e. $\Delta\hat{p}^*_{\text{main},t,x}$, $\Delta\hat{p}^*_{i,t,x}$, and $\Delta\hat{p}^*_{k,t,x}$, $\forall i \in \mathcal{I}$, $k \in \mathcal{K}$, and $t \in \mathcal{T}$, denoted by a $((1+|\mathcal{I}|+|\mathcal{K}|)\times|\mathcal{T}|)$-size matrix $\Delta\hat{\mathbf{P}}^*_x$. The relationship between the training inputs and output can be described as

$$\Delta\hat{\mathbf{P}}^*_x = f_{\text{nn}}\left(\mathbf{P}_x, \mathbf{\Phi}_x\right), \tag{4.3.23}$$

where $f_{\text{nn}}(\cdot)$ is the relationship function parametrized by tuning neural networks. The process of training the neural networks corresponds to line 5 in **Algorithm 2**.

The convolutional layers convolve the elasticity image with multiple filters to extract the following features as shown in Fig.4.7:

- *Local Feature*: The local feature of each type of price elasticity within the filter size can be detected when the filter is on a patch of image. e.g. If the filter size is 5×5, the local feature within every 5 consecutive scheduling intervals is extracted.

- *Temporal Transient Feature*: The temporal transient feature of each type of price elasticity can be detected when the filter slides through the image by strides. e.g. If the stride is (24,24), the temporal transient feature over every 24 inconsecutive scheduling intervals, i.e. between day and night, is extracted.

- *Correlation of Elasticities*: The correlation of three types of price elasticities

can be detected when multiple filters simultaneously convolve three colour channels.

All these three extracted features are stacked as a feature map and processed by further layers. The feature map of all filters can be described as

$$\mathbf{\Phi}_{\text{map}} = f_{\text{ReLU}}\left(\mathbf{W} \cdot \mathbf{\Phi}_x + \mathbf{b}\right), \tag{4.3.24}$$

where $\mathbf{\Phi}_{\text{map}}$ is the array of the feature map, $f_{\text{ReLU}}(\cdot)$ is the activation function, $\mathbf{W}$ is the weight array, and $\mathbf{b}$ is the bias vector. The rectified linear unit (ReLU) [194] is used as the activation function.

The function of pooling layers is to progressively reduce the spatial size of the feature representations, so as to reduce the parameters and computational burden of neural networks [195]. Each convolutional layer is followed by a pooling layer to downsample the feature map through using max pooling [196]. In order to control the spatial size of convolutional outputs, the same padding is used to pad the input of each convolutional layer with zeros around the border. Over multiple convolutional layers and pooling layers, a global feature map is formed by integrating the feature representations from every layer. The global feature map is subsequently converted to a vector by a flatten layer and processed by fully-connected layers. The function of fully-connected layers is to further extract feature representations from merged feature representations of numerical data and images.

4.4 Deploying Phase of Energy Scheduling Tool

This section introduces the deploying phase of the proposed energy scheduling tool. The flowchart of the deploying phase is shown in Fig. 4.8. The historical data is dynamically updated by the real-time data from a prosumer's smart meter. To provide a prosumer with an accurate prediction that considers the uncertainties of the DRESs and flexible demand for the following day, the scenarios analysis approach in Section 4.3.1 is implemented at the deploying phase, and developed as a real-time scenarios selection approach. This approach can dynamically select the scenarios with current characteristics of uncertainties and discard dated scenarios. The

processed scenarios and elasticity images are subsequently fed into trained neural networks to yield the predicted optimal scheduling decisions. The overall algorithm of the deploying phase is shown in **Algorithm 4**, with detailed steps as follows:

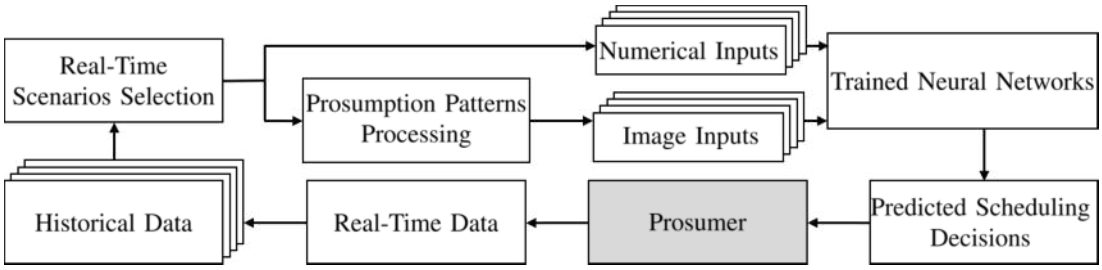

Figure 4.8: Flowchart of the deploying phase of the energy scheduling tool. Historical data is dynamically updated by the real-time data from a prosumer's smart meter. The scenarios are selected by the real-time scenarios selection approach. The processed scenarios and elasticity images are fed into trained neural networks to yield the predicted optimal scheduling decisions.

Algorithm 4 Algorithm of Deploying Phase of the Energy Scheduling Tool

Input: real-time data $p_{\text{main},t}$, $p_{i,t}$, $p_{k,t}$, and π_t

1: use scenarios analysis approach to generate scenarios from updated data
2: **for** $x = 1, ..., |\mathcal{X}|$ **do**
3: update occurrence probabilities using (4.4.25) and (4.4.26)
4: process elasticity images $\mathbf{\Phi}_x(t_a, t_b, \Xi)$ as Fig. 4.5
5: use trained neural networks to obtain predicted optimal decision variables $\Delta\hat{\mathbf{P}}_x^*$ and select predicted optimal decision variables that maintain the optimisation constraints
6: **end for**
7: aggregate the predicted optimal scheduling decisions of $|\mathcal{X}|$ scenarios as (4.4.27), (4.4.28), and (4.4.29), and perform controlling decisions

Output: controlling signals $p_{\text{main},t}$, $p_{i,t}$, $p_{k,t}$

Step 1: The historical data is updated by the real-time data for the current day. The updated data is used to generate scenarios according to the scenarios analysis approach proposed in Section 4.3.1. Let $p_{t,x}$ and $p'_{t,x}$ denote the scenarios generated

from the historical data and updated data, respectively. The occurrence probability of $p'_{t,x}$ is updated as [96]

$$\Pr\left(p'_{t,x}\right) = \Pr\left(p_{t,x}\right) + \frac{1}{|\mathcal{X}|+1}\left[\vartheta_{\Pr} - \Pr\left(p_{t,x}\right)\right], \tag{4.4.25}$$

where $\vartheta_{\Pr} \in \{0,1\}$ is a binary value determined by

$$p'^{*}_{t,x} = \arg\min_{p'_{t,x}} l_{x,x'}, \tag{4.4.26}$$

where $l_{x,x'} = p_{t,x} - p'_{t,x}$ is the distance between $p_{t,x}$ and $p'_{t,x}$. If $p'_{t,x} = p'^{*}_{t,x}$, $\vartheta_{\Pr} = 1$ and the predicted error term $[\vartheta_{\Pr} - \Pr(p_{t,x})]$ becomes positive to reinforce the previous probability; if $p'_{t,x} \neq p'^{*}_{t,x}$, $\vartheta_{\Pr} = 0$ and the predicted error term becomes negative to weaken the previous probability. This step corresponds to the line 1-3 in **Algorithm 4**.

Step 2: Elasticity image $\mathbf{\Phi}_x$ is processed by the prosumption patterns processing approach as described in Section 4.3.2. This step corresponds to the line 4 in **Algorithm 4**.

Step 3: The trained neural networks are used to obtain the predicted optimal scheduling decisions of each scenario. The predicted optimal scheduling decisions are subsequently examined by the constraints of optimisation problem. This step corresponds to the line 5 in **Algorithm 4**.

Step 4: The controlling signals for the next day are yielded by aggregating the predicted optimal scheduling decisions of $|\mathcal{X}|$ scenarios, weighted by the occurrence probabilities as

$$p_{\text{main},t} = \sum_{x\in\mathcal{X}} \left(p_{\text{main},t,x} - \Delta\hat{p}^{*}_{\text{main},t,x}\right) \cdot \Pr\left(p_{\text{main},t,x}\right), \tag{4.4.27}$$

$$p_{i,t} = \sum_{x\in\mathcal{X}} \left(p_{i,t,x} - \Delta\hat{p}^{*}_{i,t,x}\right) \cdot \Pr\left(p_{i,t,x}\right), \tag{4.4.28}$$

$$p_{k,t} = \sum_{x\in\mathcal{X}} \left(p_{k,t,x} - \Delta\hat{p}^{*}_{k,t,x}\right) \cdot \Pr\left(p_{k,t,x}\right). \tag{4.4.29}$$

The controlling decisions are performed by a prosumer's controller and serve as real-time data for the next day. This real-time data is processed by the *Step 1* cyclically. This step corresponds to the line 7 in **Algorithm 4**.

4.5 Case Studies

In this section, case studies have been conducted to evaluate the proposed approaches by comparing various learning approaches and IEEE test distribution systems.

4.5.1 Simulation Setup and Data Availability

The simulations are performed using a machine with Intel^{R} Core^{TM} i9-9900K CPU at 3.60 GHz and a NVIDIA GeForce RTX 2080 GPU. The proposed approaches of scenarios analysis, prosumption patterns processing, and preferences optimisation are written in the MATLAB language and run on the CPU. The proposed neural networks are written in the Python language by using PyTorch and run on the GPU. To improve the computational efficiency, the training process is performed on the GPU, and 8-core parallel computing is used during the scenarios analysis, prosumption patterns processing, and preferences optimisation. The maximum and nominal numbers of antigens are set as 6000 and 3000, respectively, and the number of iterations for the immune algorithm is set as 50, based on the empirical study. The simulations are repeated 10 times to eliminate the randomness and outliers.

Since the scale of energy prosumers varies from the residential houses, commercial areas, industries, to an entire city [42], the following IEEE test distribution systems are adopted by our research to examine the scalability of our proposed energy scheduling tool.

- *Case 1 (Modified IEEE 69-bus distribution network):* The schematic illustration of the modified IEEE 69-bus distribution network is presented in Fig. 4.9. The network is partitioned into 5 prosumers. 15 solar photovoltaics, 6 diesel generators, 4 wind turbines, and 3 biomass generators are arbitrarily assigned to each prosumer, and 69 loads are assigned to each bus.

- *Case 2 (Modified IEEE 33-bus distribution network):* The schematic illustration of the modified IEEE 33-bus distribution network is presented in Fig. 4.10. The network is partitioned into 3 prosumers. 12 solar photovoltaics,

3 diesel generators, 3 wind turbines, and 1 biomass generator are arbitrarily assigned to each prosumer, and 33 loads are assigned to each bus.

- *Case 3 (Modified IEEE 18-bus distribution network):* The schematic illustration of the modified IEEE 18-bus distribution network is presented in Fig. 4.11. The network is partitioned into 3 prosumers. 7 solar photovoltaics, 3 diesel generators, 2 wind turbines, and 1 biomass generator are arbitrarily assigned to each prosumer, and 18 loads are assigned to each bus.

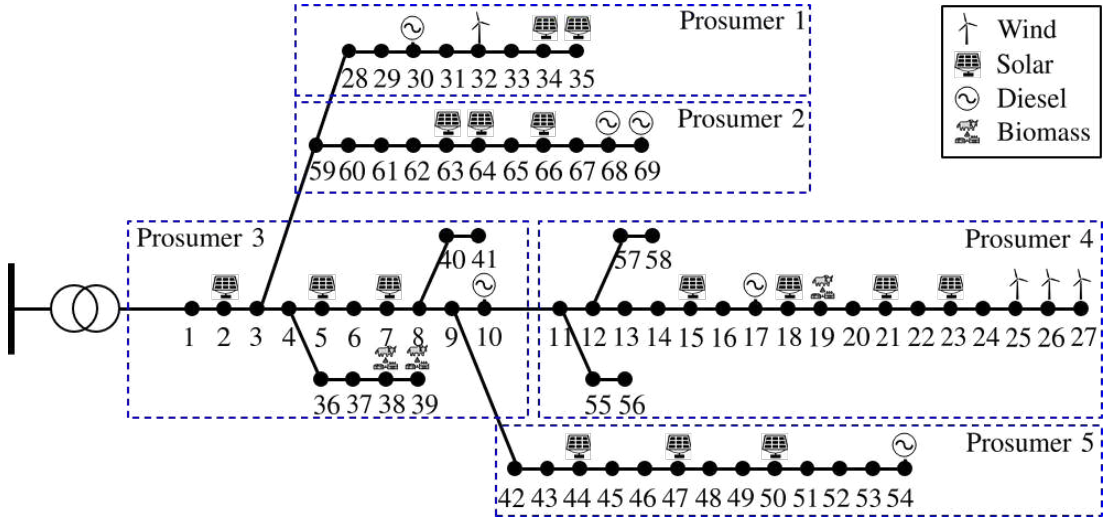

Figure 4.9: Modified IEEE 69-bus distribution network. The network is partitioned into 5 prosumers. 15 solar photovoltaics, 6 diesel generators, 4 wind turbines, and 3 biomass generators are arbitrarily assigned to each prosumer, and 69 loads are assigned to each bus.

To modify the static default data of generation and consumption from these IEEE test distribution systems as dynamic data, the real-time states of the GB power generation and consumption in 2019 from the GridWatch are used [179]. The ratio of peak real-time consumption from the GB power systems to the peak static consumption from these IEEE test distribution systems is used to scale down the GB real-time generation of diesel, solar, wind, biomass, and consumption. The initial stored power is set as zero. The percentages of consumption of each load in the IEEE test distribution systems are used to allocate the total dynamic consumption to each load. The total power outputs of each generation source are equally allo-

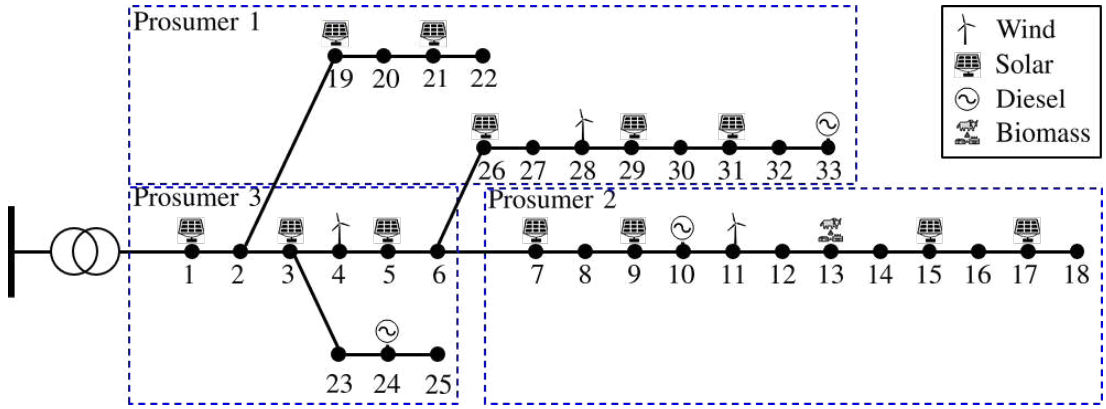

Figure 4.10: Modified IEEE 33-bus distribution network. The network is partitioned into 3 prosumers. 12 solar photovoltaics, 3 diesel generators, 3 wind turbines, and 1 biomass generator are arbitrarily assigned to each prosumer, and 33 loads are assigned to each bus.

cated to the corresponding generators. The lithium energy storage model and cost coefficient studied in [197] is used. The maximum charging/discharging rate is set as 0.3 MWh and maximum storage capacity is set as 2 MWh according to the model of distribution-scale energy storage device in [197].

The half-hourly wholesale electricity prices obtained from the GB energy market [198] are used to calculate the real-time retail electricity prices, by dividing 45 % of the average ratio of wholesale electricity prices to retail electricity prices [180]. The coefficients of operating costs and carbon emissions intensities are presented in Table 4.1. The coefficients of operating costs of generators for project commissioning in 2020 [170] are adopted. The carbon emissions of wind and solar primarily arise in manufacture and construction. Hence, the operational carbon emissions intensities of these sources are assumed to be zero in our research. The average annual carbon emissions intensities are applied to the biomass and diesel, and evaluated by using the method proposed by Hawkes [79] as

$$\bar{\rho}_i = \frac{\text{Carbon Emissions Intensities of Fuel} \times \text{Fuel Usage}}{\text{Gross Electricity Supply}}, \tag{4.5.30}$$

where $\bar{\rho}_i$ is the average annual carbon emissions intensity of source i. The data of fuel usage and gross electricity supply is published by the Digest of the U.K. Energy Statistics [181]. The data of carbon emissions intensities of fuel is published by the

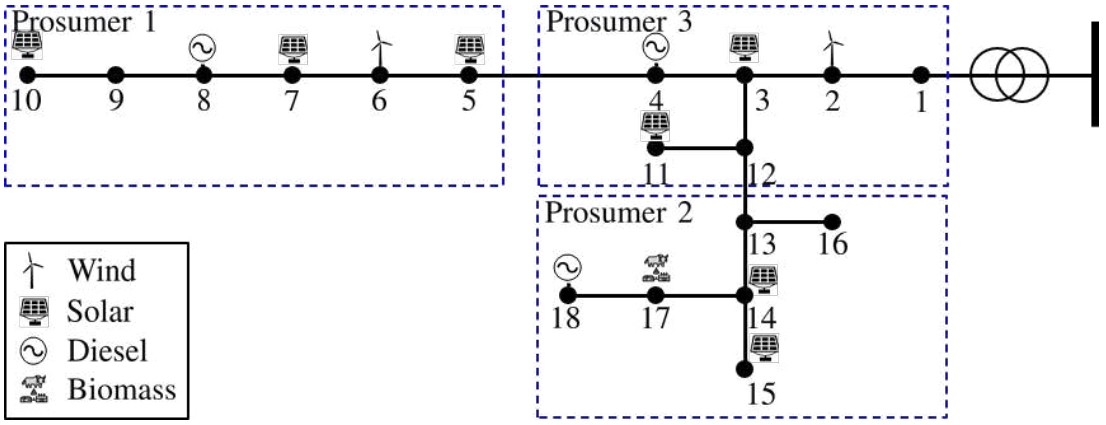

Figure 4.11: Modified IEEE 18-bus distribution network. The network is partitioned into 3 prosumers. 7 solar photovoltaics, 3 diesel generators, 2 wind turbines, and 1 biomass generator are arbitrarily assigned to each prosumer, and 18 loads are assigned to each bus.

U.K. Government Greenhouse gas Conversion Factors for Company Reporting [182].

Table 4.1: Coefficients of operating costs and carbon emissions intensities

Source	Diesel	Wind	Biomass	Solar	Storage
Costs Coefficients (£/MWh)	123	15	80	9	135
Carbon Emissions Intensities (ton/MWh)	1.69	0	0.05	0	0

The inputs of neural networks are separated into 70% of training set and 30% of validation set with randomly sampling. The numerical data is preprocessed by the z-score normalisation [199]. The Adam [200] is used as an optimiser to train the neural networks for 50 epochs, with 4-size of minibatch, 1×10^{-4} of initial learning rate, and 1×10^{-2} of weight decay [201]. The learning rate will be reduced if no improvement of accuracy is seen for 5 epochs. To avoid the overfitting problem caused by parameters of deep structure, 0.5 of dropout [202] is used for each layer to randomly drop units. These training parameters are empirically determined through tuning the neural networks by using validation data. The training labels are used as a benchmark to examine the training accuracy. The mean squared error (MSE) [203] is used as a performance metric to indicate the learning losses. The hyper-parameters

considered in the optimisation of neural networks are shown in Table 4.2.

Table 4.2: Hyper-parameters considered in the optimisation of neural networks

Item	Training Data Size	Validation Data Size	Normalisation	Optimiser
Value	70 %	30 %	Z-score	Adam
Item	Minibatch Size	Initial Learning Rate	Weight Decay	Dropout
Value	4	1×10^{-4}	1×10^{-2}	0.5

The architecture of the proposed neural networks is shown in Table 4.3. The output size of a convolutional layer can be calculated as

$$\text{Output Size} = \frac{\text{Input Size} - \text{Filter Size} + 2 \times \text{Padding}}{\text{Stride}} + 1. \tag{4.5.31}$$

Table 4.3: Architecture of the proposed neural networks

Layer	Input Size	Output Size	Filter Number	Filter Size	Stride	Padding
Convolution 1	48,48,3	48,48,32	32	5×5	(1,1)	2
Pooling 1	48,48,32	24,24,32	1	2×2	(2,2)	0
Convolution 2	24,24,32	24,24,64	64	3×3	(1,1)	1
Pooling 2	24,24,64	12,12,64	1	2×2	(2,2)	0
Flatten	12,12,64	12×12×64	-	-	-	-
Fully-connected 1	12×12×64	1024	-	-	-	-
Dense	$(1 + \lvert\mathcal{Z}\rvert + \lvert\mathcal{K}\rvert) \times \lvert\mathcal{T}\rvert$	1024	-	-	-	-
Fully-connected 2	2048	1024	-	-	-	-
Fully-connected 3	1024	512	-	-	-	-
Fully-connected 4	512	256	-	-	-	-
Output	256	$(1 + \lvert\mathcal{Z}\rvert + \lvert\mathcal{K}\rvert) \times \lvert\mathcal{T}\rvert$	-	-	-	-

4.5.2 Evaluation of Training Phase

To test the convergence performance and learning accuracy, the proposed neural networks are compared with the following learning approaches, under the same training parameters:

- *Approach 1 (Recurrent Neural Network (RNN))*: The convolutional layers of our proposed neural networks are replaced by a RNN [204] with a 1024-node hidden layer to extract information from elasticity images. Different from the CNN to simultaneously convolve three colour channels, the RNN can only import a matrix as an input. Hence, the elasticity image is reshaped as a $(|\mathcal{T}| \times (|\mathcal{T}| \times 3))$-size matrix as shown in Fig. 4.12. At each time step, the RNN imports each row of this matrix and returns a hidden state and an output. The hidden state is used by the next time step to analyse the temporal transient feature of price elasticity. When the RNN processes an entire image, i.e. $|\mathcal{T}|$ time steps, the outputs are stacked as a $(|\mathcal{T}| \times 1024)$-size vector and processed by further layers.

- *Approach 2 (Long Short Term Memory (LSTM)-RNN)*: The convolutional layers of our proposed neural networks are replaced by a LSTM-RNN [144] with a 1024-node hidden layer to extract information from elasticity images. The input matrix of the LSTM-RNN is the same as that of the RNN. However, the LSTM-RNN only returns an output of 1024-size vector at the last time step as shown in Fig. 4.13, since it has the memory of the entire image.

- *Approach 3 (DNN)*: The convolutional layers of our proposed neural networks are excluded. The neural networks become a DNN and only learn from the numerical input.

Performances of Training and Validation

The learning process is considered to be converged when the learning rate drops below 1×10^{-7} and no improvement of accuracy is seen for 5 epochs. Prosumers of the modified IEEE 69-bus distribution network with 5000 scenarios are used as

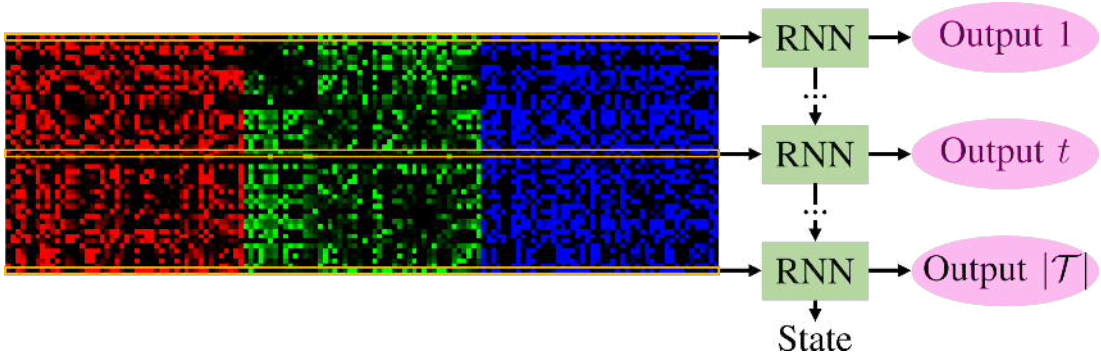

Figure 4.12: Processing of elasticity image as inputs of the RNN. At each time step indicated by the yellow box, the RNN imports each row vector and returns a hidden state and an output. The hidden state is used by the next time step. The RNN has a 1024-node hidden layer, which leads to a $(|\mathcal{T}| \times 1024)$-size vector as stacked outputs.

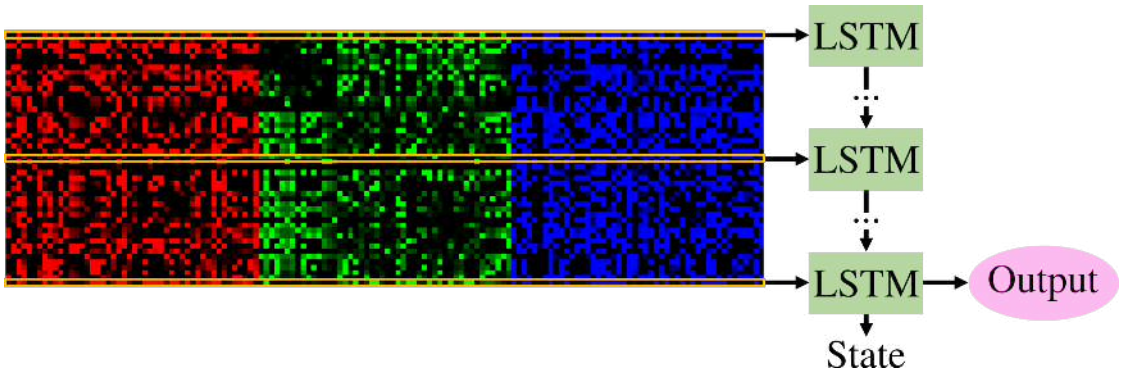

Figure 4.13: Processing of elasticity image as inputs of the LSTM-RNN. At each time step indicated by the yellow box, the LSTM-RNN imports each row vector and returns a hidden state and an output. The hidden state for the entire image is stored and selected by a memory cell. The LSTM-RNN has a 1024-node hidden layer, which leads to a 1024-size vector as an output at the last time step.

samples to demonstrate the performances of training and validation. As shown in Fig. 4.14, both training and validation of these four learning approaches converge within around 30 epochs. With the additional information of prosumption patterns extracted from elasticities images, the training losses of the proposed neural networks, RNN, and LSTM-RNN are lower than the training losses of the DNN. The validation losses of our proposed neural networks are the lowest for all prosumers. By contract, the validation losses of the DNN are the highest for prosumer 1, prosumer 3, and prosumer 5, and the validation losses of the RNN are the highest for prosumer 2, and prosumer 4. The potential reason is that the DNN cannot extract information of prosumption patterns from the elasticity images, and the RNN is incapable of extracting the global features from an entire image without the memory cell of the LSTM-RNN. Therefore, the information of prosumption patterns is a crucial factor for improving the learning accuracy.

Performances of Testing

The testing data is used to evaluate the learning accuracy affected by the number of scenarios. The testing data of load 1 in the modified IEEE 69-bus distribution network is sampled to examine the testing losses with various number of scenarios as shown in Fig. 4.15. With the increasing number of scenarios, the testing losses rise for all learning approaches, because a more diverse set of scenarios would cause a larger bias for the training inputs. However, the proposed neural networks outperform other learning approaches under any scenarios number. To cover the diversity of uncertainties, 5000 scenarios are used in the simulation of the deploying phase in our research. In the practical implementation, an appropriate number of scenarios can be adjusted according to a prosumer's computational power.

4.5.3 Evaluation of Deploying Phase

Analysis of Scheduling and Prosumption Patterns

To demonstrate the connection between the intrinsic features of dynamic price elasticities and a prosumer's energy scheduling, an electricity image and scheduling

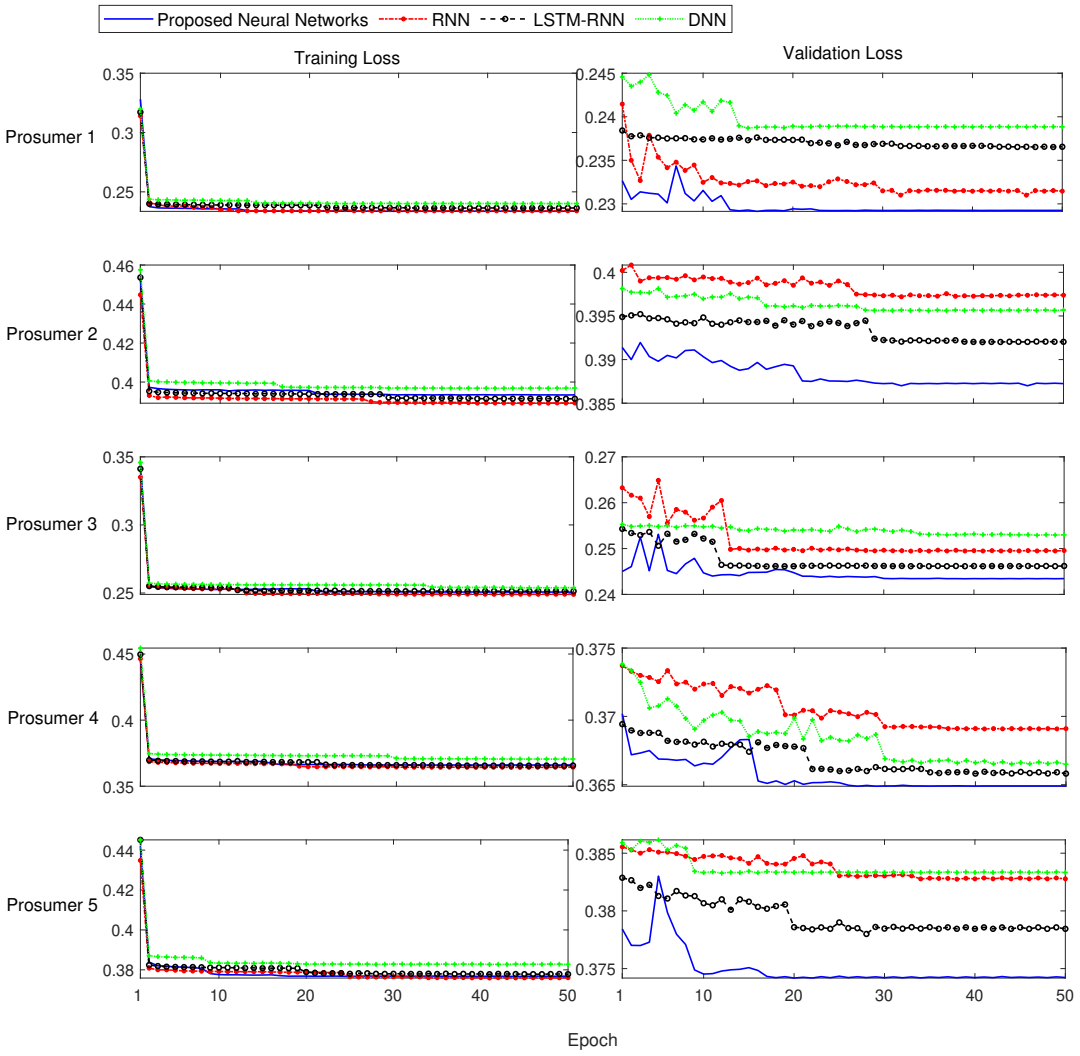

Figure 4.14: Comparison for performances of training and validation. Prosumers of the modified IEEE 69-bus distribution network with 5000 scenarios are sampled to demonstrate convergence and losses under learning approaches of the proposed neural networks, RNN, LSTM-RNN, and DNN. The x axes indicate epochs, and the y axes indicate the MSE losses.

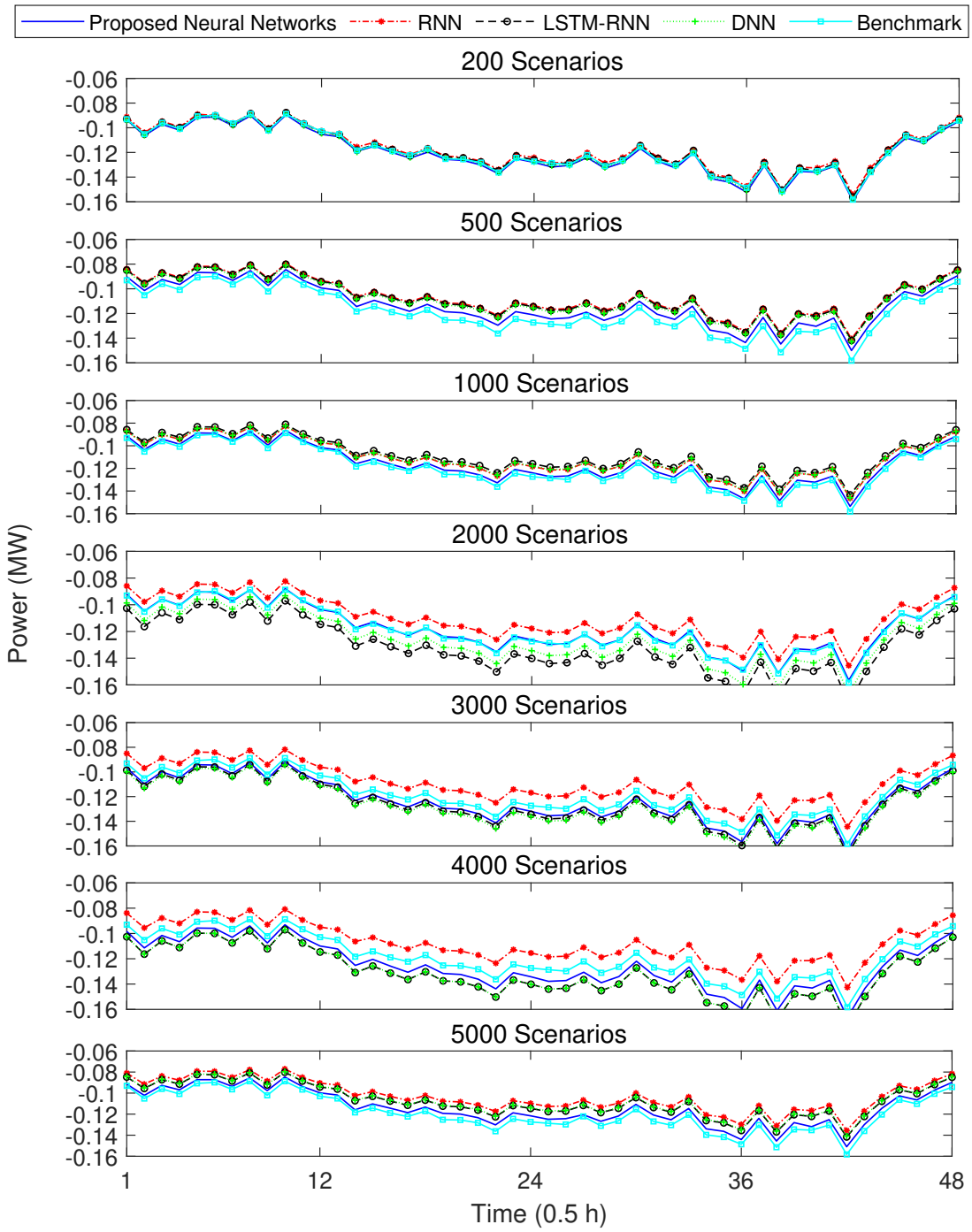

Figure 4.15: Testing accuracy under various number of scenarios. The load 1 in the modified IEEE 69-bus distribution network is sampled to examine the testing losses affected by the number of scenarios under learning approaches of the proposed neural networks, RNN, LSTM-RNN, and DNN. The x axes indicate the scheduling time of day, and the y axes indicate the power demand.

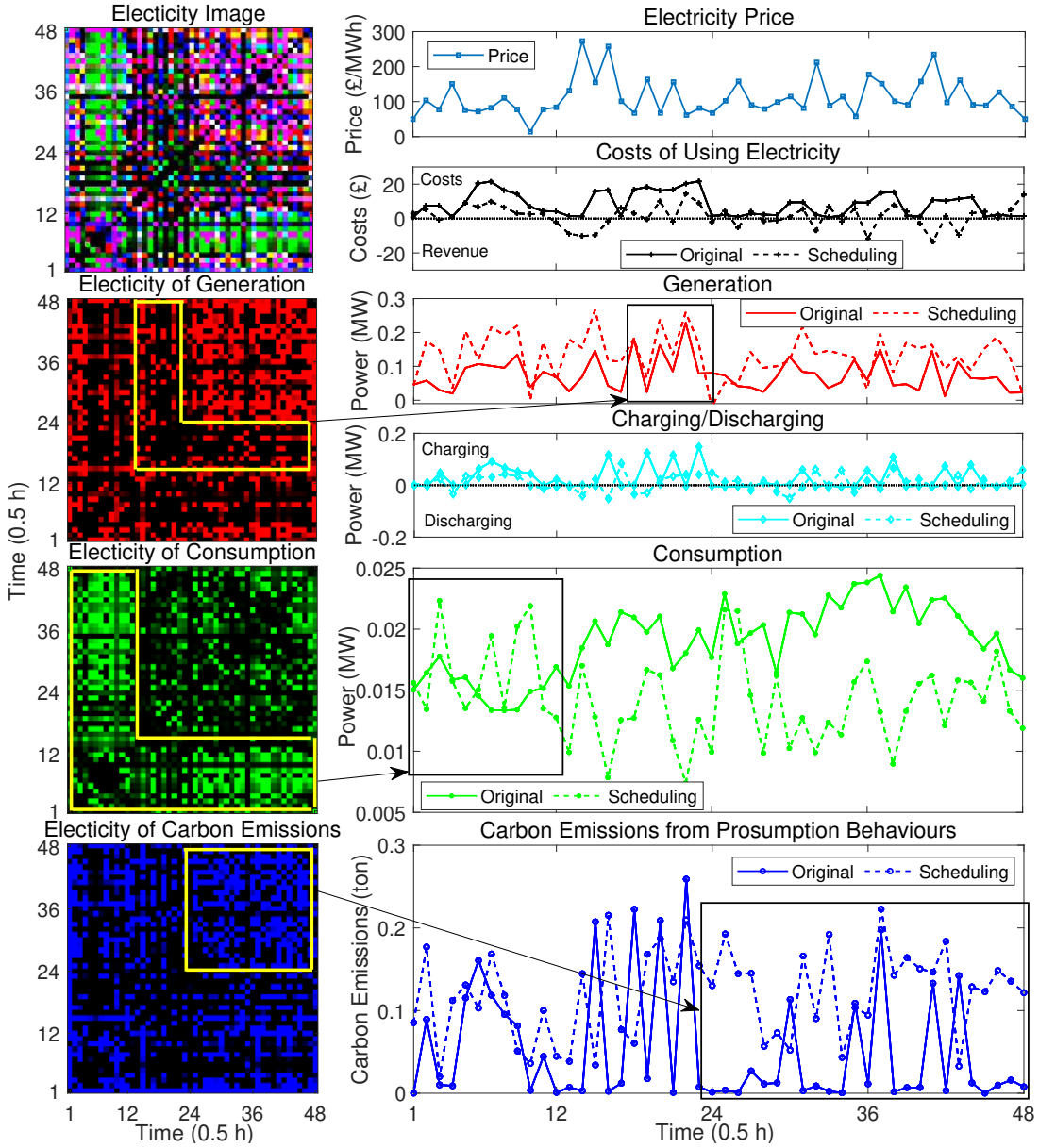

Figure 4.16: Schematic illustration of the connection between prosumption patterns and scheduling results. The left four images show the electricity image and corresponding decomposition of three colour channels, i.e. 'R' for elasticity of generation, 'G' for elasticity of consumption, and 'B' for elasticity of carbon emissions. The elasticity of every two scheduling time is assigned to a pixel indicated by x axes and y axes; The right six figures show the comparison between original prosumption and scheduled prosumption.

results from the same scenario are sampled as shown in Fig. 4.16. The elasticity image is at the left-top and corresponding decomposition of three colour channels are follows, i.e. 'R' for elasticity of generation, 'G' for elasticity of consumption, and 'B' for elasticity of carbon emissions. The brighter region in these images means the prosumption or carbon emissions between scheduling intervals indicated by its x-axis and y-axis are easier to be scheduled due to a higher price elasticity, whereas the darker region means the prosumption or carbon emissions between scheduling intervals indicated by its x-axis and y-axis are harder to be scheduled due to a lower price elasticity. The right figures are information of electricity price, costs of using electricity, power generation, charging/discharging from storage, power consumption, and carbon emissions from prosumption behaviours. The positive value of the second figure means the costs of using electricity, and the negative value of the second figure means the revenue of exporting electricity to the main grid. The positive and negative values of the fourth figure mean the charging and discharging from the storage, respectively.

For the electricity generation, when the electricity price at one scheduling time is higher than that at another scheduling time, a prosumer would reduce the power import from the main grid, and increase the self-generation, or discharging from the storage, so that this prosumer can supplement to its demand and export extra power to the main grid for earning revenue. It can be seen from the second row of the Fig. 4.16, when the electricity price increases, the scheduled generation increases correspondingly with remaining the storage discharging unchanged. For the period from the eighteenth scheduling time to the twenty-forth scheduling time, the price elasticity of generation is relatively low (as indicated by the yellow box on the image of elasticity of generation). Hence, the scheduled generation keeps almost the same as the original generation.

For the electricity consumption, when the electricity price at one scheduling time is higher than that at another scheduling time, the consumption is shifted away or curtailed. By contrast, when the electricity price at one scheduling time is lower than that at another scheduling time, the consumption is shifted to this scheduling time with lower price. It can be seen from the third row of the Fig. 4.16, for

the period from the first scheduling time to the twelfth scheduling time, the price elasticity of consumption is relatively high (as indicated by the yellow box on the image of elasticity of consumption) and the electricity price is relatively low. Hence, the scheduling drives the demand to be shifted from the rest of scheduling time to this period.

For the carbon emissions caused by the prosumption behaviours, a higher price elasticity of carbon emissions indicates the prosumer is more flexible to increase or decrease carbon emissions, as indicated by the yellow box on the image of elasticity of carbon emissions. Additionally, since the overall price elasticity of carbon emissions is lower than that of generation and consumption during the entire scheduling horizon (indicated by the elasticity image which is dominated by the red colour and green colour), the prosumer inherently prefers to save the costs of using electricity, disregarding the increase of carbon emissions.

Accuracy of Scenarios Selection

To test the accuracy of scenarios selection, the data of the first 300 days is taken as the historical data. From day 301 to day 364, the proposed real-time scenarios selection is used to update the scenarios set and occurrence probabilities. The data on day 365 is used as a benchmark to examine the accuracy of the selected scenarios in terms of predicting uncertainties caused by the DRESs and flexible demand. Our proposed real-time scenarios selection approach is compared with the approach of synchronous-back-to-generation-reduction [205]. Both approaches firstly generate 5000 scenarios, and then select the high probable scenarios as a prediction for the current day. The load 34, wind generator 8, and solar generator 2 in the modified IEEE 69-bus distribution network are sampled as presented in Fig. 4.17 to demonstrate the accuracy of scenarios selection. Compared to the synchronous-back-to-generation-reduction, the proposed real-time scenarios selection can more accurately capture the current features of uncertainties, and thus yield precise predictions. This is because the proposed real-time scenarios selection can take advantage of the information from all dynamically generated scenarios by keeping updating the scenarios set and occurrence probabilities with the prosumer's

real-time data. By contrast, the synchronous-back-to-generation-reduction directly deletes the scenarios with low occurrence probabilities, which causes the selected scenarios to be dominated by certain scenarios.

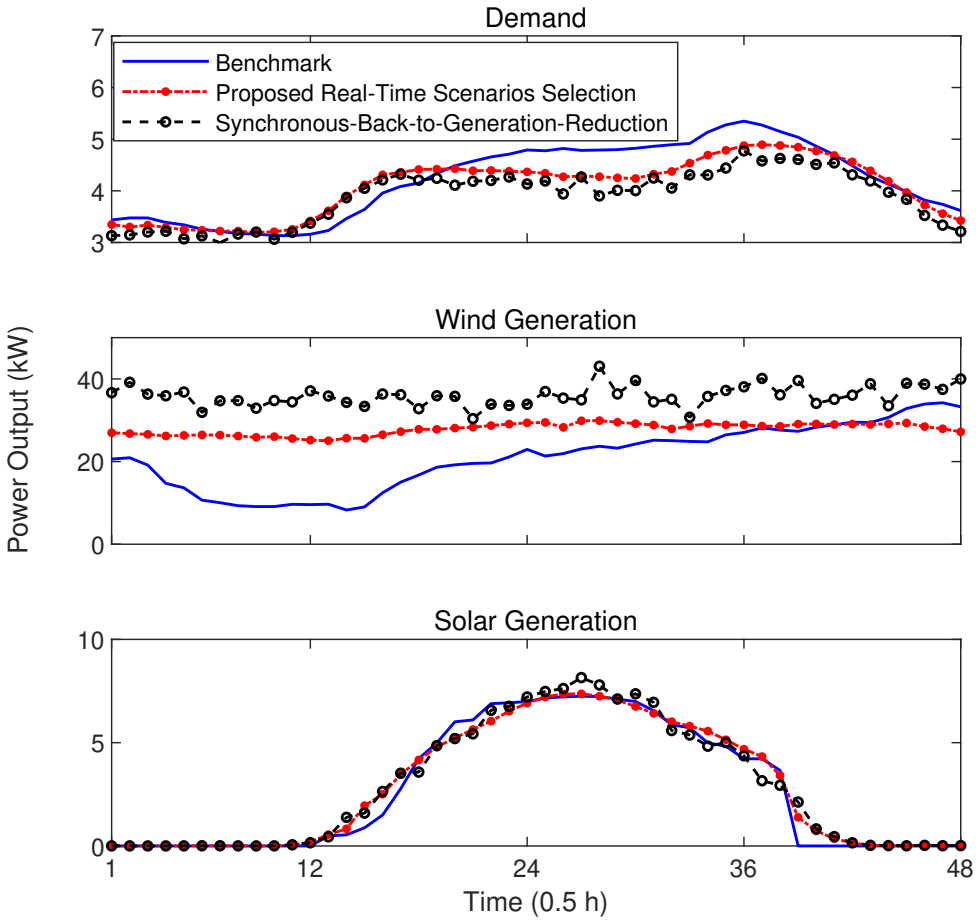

Figure 4.17: Accuracy of Scenarios Selection Approaches. The load 34, wind generator 8, and solar generator 2 in the modified IEEE 69-bus distribution network are sampled. The data on day 365 is used as a benchmark. The x axes indicate the scheduling time of day, and the y axes indicate the power.

Scalability Evaluation

To test the scalability of our proposed energy scheduling tool, the artificial immune algorithm for solving the preferences optimisation problem is used to compare the computational time per scenario of daily energy scheduling under the aforemen-

tioned IEEE test distribution systems. As shown in Table 4.4, with the increase of the system scale including the numbers of prosumers, generators and loads, the computational time of the artificial immune algorithm dramatically increases. On the contrary, once the proposed neural networks are trained, it only requires microseconds to predict the optimal scheduling decisions, irrespective the increase of system scale. This is because the neural networks can generalise high-complexity problems to extract feature representations.

Table 4.4: Scalability and computational time evaluation under various IEEE test distribution systems

IEEE Test Systems		Prosumers	Computational Time (s)		
			Neural Networks		Artificial Immune Algorithm
			Training	Testing	
18-bus	13 generators 18 loads	3	66.58	0.0013	2954.37
33-bus	19 generators 33 loads	3	66.73	0.0021	6533.78
69-bus	28 generators 69 loads	5	67.42	0.0019	17311.61

4.6 Chapter Summary

This chapter proposes a data-driven prosumer-centric energy scheduling by using learning approaches to improve computational efficiency and scalability of the energy scheduling tool. By generating scenarios to analyse variations of uncertainties and using the CNNs to extract prosumption patterns, optimal scheduling decisions can be automatically made by trained neural networks with the strategy of minimizing costs and carbon emissions. Case studies based on various IEEE test distribution systems demonstrate that the designed neural networks outperform other learning approaches in terms of the testing accuracy with any scenarios number. The information of prosumption patterns from elasticity images is a crucial factor for improving the learning accuracy. The connection between the intrinsic features

of dynamic price elasticities and a prosumer's energy scheduling has been testified, and shows that a higher price elasticity indicates a more flexible prosumption or carbon emissions to be scheduled. The proposed real-time scenarios selection approach can accurately capture the current features of uncertainties by using the information from a prosumer's real-time data and generated scenarios. The proposed learning approach is more scalable and computationally efficient compared to solving optimisation by the intelligent heuristic algorithm.

This chapter remains two directions to be explored in the next chapter: First, under practical contexts of the small-scale prosumers, e.g. a household, the cost saving of energy scheduling would be offset by a higher installed cost of energy storage devices. The peer-to-peer energy trading is an alternative solution to balance the surplus/scarcity of energy among prosumers; Second, the centralised wholesale energy pricing is determined by the supply-demand balance between generators and retailers, and the centralised retail energy pricing, e.g. flat pricing, time-of-use pricing, and real-time pricing, is determined by the supply-demand balance between retailers and consumers. The centralised carbon pricing is determined by the emissions trading scheme. These prices dynamically fluctuate with the supply-demand balance of overall markets and are uniform for all customers. Because these prices are independent of the behaviours of individual prosumers, not every prosumer can be efficiently incentivised to reduce carbon emissions and facilitate energy balance. Decentralising these pricing schemes in both energy and carbon markets is a solution, by which the bidding/selling prices of individual prosumers can directly incentivise their behaviours. In the next chapter, a novel blockchain based peer-to-peer trading framework will be introduced enabling prosumers to trade energy and carbon allowance.

Chapter 5

A Blockchain Based Peer-to-Peer Trading Framework Integrating Energy and Carbon Markets

5.1 Introduction

The emerging role of prosumers provides opportunities for local trading of energy and carbon allowance, to achieve regional supply-demand balance of energy and reduce carbon emissions caused by long-distance power transmissions. The blockchain technology [206] (one of the distributed ledger technologies) has the potential of establishing a decentralised trading platform with automated trading procedures and protected residential privacy. The smart contract [143], as one of the key blockchain technologies, enables prosumers to proceed the trading in a manner of self-enforcing settlement and setting out negotiation. For the detailed advantages, challenges, and opportunities of applying the blockchain and smart contract into peer-to-peer trading of energy and carbon allowance, readers can refer to the Section 2.5. This chapter proposes a novel blockchain based peer-to-peer trading framework. This framework enables prosumers to jointly exchange energy and carbon allowance, since purchasing carbon allowance is a part of generating costs. The biding/selling prices of individual prosumers in energy and carbon markets are able to directly incentivise the reshaping of prosumption behaviours for energy balance and carbon saving, which

decentralises the pricing schemes as remained in Chapter 4. Additionally, when prosumers exchange energy as both generators and consumers, they need to know how much carbon allowance would be required. The carbon emissions tracing approach in Chapter 3 is developed to identify the carbon emissions caused by a prosumer' s generation for self-consumption, consumption from self-generation, and generation (or consumption) for (or from) energy exchange with other prosumers. A low carbon incentive mechanism is subsequently designed for individual prosumers. Case studies based on the modified IEEE 37-bus distribution network testify the proposed trading framework, in comparison with the centralised trading scheme and aggregator-based trading scheme. The execution of smart contract on the Ethereum blockchain, and the interface between scheduling algorithms and smart contract are demonstrated.

A conceptual graph of the proposed peer-to-peer trading framework is presented in Fig. 5.1. Overall, this chapter offers the following key contributions:

- A new trading framework is designed enabling the exchange of energy and carbon allowance at both prosumer level and microgrid level, using a smart contract based trading platform. The proposed energy scheduling algorithms interact with the self-enforcing nature of smart contract to automate the standardised auction procedure.

- A carbon emissions tracing approach targeting on individual prosumers' behaviours is developed to ensure a fair allocation of low carbon incentives.

- Case studies show that the proposed trading framework achieves better energy balance and carbon saving than those approaches of centralised trading and aggregator-based trading. The interface between scheduling algorithms and smart contract, and the execution of smart contract are demonstrated.

The rest of this chapter is organised as follows: Section 5.2 introduces the proposed three-layer trading framework. Corresponding to each layer, the details of problem formulation and the smart contract based auction mechanism are described in Section 5.3. Section 5.4 provides case studies to verify the proposed framework and demonstrate the trading platform. Section 5.5 draws the conclusion of this chapter.

Figure 5.1: Conceptual graph of peer-to-peer trading framework.

5.2 Trading Framework

This section describes the overall trading framework under which both energy and carbon allowance are exchanged within distribution networks. According to the commercial relations of market participants, i.e. prosumer and microgrid-trader (MT), as described in [207], the trading procedure is hierarchically categorised into three layers: prosumer-centric trading, MT-centric trading, and peer-to-peer trading platform. Fig. 5.2 shows the architecture and information flows of these three layers. The proposed framework is implemented in the day-ahead market to schedule energy prosumption and perform trading for the following day. The prosumers in the context of our research refer to a master of energy prosumption [42] which seeks for personal benefits, e.g. bill saving or cost saving, and environmental goal, e.g. carbon emissions reduction, by participating in both energy and carbon markets using their DRESs. Ethereum blockchain network [208] is used consisting of full nodes and light nodes. The market operator acts as full nodes to provide and manage the trading platform by offering computing power for blocks mining, storing all blocks, and earning rewards for mined blocks. Prosumers and MTs act as light nodes to store header chain and verify transactions. As the light nodes, prosumers and MTs do not need powerful computers. Hence, the trading process can be supported by smart meters or mobile phones. The specific design of each layer is described as follows and the problem formulation will be detailed in Section 5.3.

Figure 5.2: Architecture and Information flows of the proposed framework for peer-to-peer trading. Individual prosumers trade energy or carbon allowance on the layer of prosumer-centric trading. The residual supply and demand for an ensemble of prosumers in the same microgrid are aggregated and traded by microgrid-traders on the layer of microgrid-trader-centric trading. The trading of energy or carbon allowance is proceeded on the layer of peer-to-peer trading platform.

5.2.1 Prosumer-Centric Trading

The layer of prosumer-centric trading aims at using the collected metering data to help individual prosumers make optimal decisions of reshaping prosumption behaviours and bidding prices. The optimal decisions are yielded by solving optimisation problems with the objective of minimising electricity bills for buyers or maximising profits for sellers. The optimal decisions of reshaped prosumption are implemented by controllers, and the optimal decisions of bidding prices are sent to smart contract for auctions. Through evaluating the carbon emissions behaviours, blockchain automatically updates monetary incentives for individual prosumers. For regional energy balance and reducing transmission losses, prosumer-centric trading only applies for an ensemble of prosumers geographically in the same microgrid by assigning a microgrid index. The advantages of prosumer-centric trading are: 1) The reshaping of prosumption behaviours is directly incentivised by prosumers' bidding or selling prices, instead of central authority, such as aggregator or energy retailer [54]; 2) The monetary incentives for carbon reduction are directly linked with individual prosumers considering their carbon emissions behaviours.

5.2.2 Microgrid-Trader-Centric Trading

A group of physically connected prosumers is managed by a virtual entity, MT [209]. On the layer of MT-centric trading, MT aggregates the residual supply and demand of energy and carbon allowance for its ensemble of prosumers to trade with other MTs. The optimal decisions of bidding prices are also yielded by solving optimisation problems with the same objectives as those of prosumer-centric trading. The aim of MT-centric trading is to help an ensemble of prosumers in the same microgrid balance supply and demand by exchanging with other microgrids.

5.2.3 Peer-to-Peer Trading Platform

The layer of peer-to-peer trading platform aims to provide a standardised negotiation and self-enforcing settlement for enabling buyers and sellers to proceed the trading of energy and carbon allowance. These functions are achieved by smart contract in

the form of '*if an event happens, pay an amount of currency to the receiver on the self-enforcing basis* [143]' . In our research, the event is the delivery of energy or carbon allowance which can be ensured by querying the smart meter.

The execution of smart contract includes initialisation, matching bids and offers, bidding, winner selection, and ownership exchange. The seller initialises the smart contract by specifying offer conditions. Buyers who meet the conditions will be optimally matched to deposit their bids on the smart contract for auction. Until the auction ended, the buyer with the highest bidding price wins the auction. The rest of buyers can withdraw their deposits from the smart contract. The smart contract directly queries the smart meter to ensure that agreed energy or carbon allowance is supplied by the seller at the agreed time, before transferring the highest buyer's deposited bid to the seller.

All the transactions are stored, shared and audited by full nodes to validate authenticity and accuracy. The validated transactions are structured in publicly available blocks. The blocks are chronologically chained to each other through involving the hash of previous block into the current block, forming a blockchain. The validation is collectively achieved by all nodes through reaching a consensus of the proof-of-work [210] which uses secure hash algorithm SHA-256 to protect all blocks. The inputs of SHA-256 are block number, nonce, timestamp, and hash output of previous block, and the output of SHA-256 is a fixed-length digest as a unique identity of a block. This unique identity is guaranteed by specially mined nonce and collectively verification of all nodes, which means that if a malicious node changes one block, a different nonce will result in an unverified block, and if a malicious node changes all blocks, it will be extremely computationally difficult. Therefore, the chaining feature of blockchain and difficulty of solving the proof-of-work enable transactions to be traceable, verifiable and tempering resistance.

5.3 Problem Formulation

This section describes the problem formulation of hierarchical three-layer trading framework.

5.3.1 Prosumer-Centric Low Carbon Incentive Mechanism

Recall that in Chapter 3, for the conventional power systems, the large scale generators report their annual fuel usage and electricity supply to evaluate the efficiency of electricity supply. With the information of the efficiency of electricity supply and carbon intensities of fuels, the carbon emissions intensities of generators can be traced. The proposed carbon emissions tracing approach in Section 3.2.2 is subsequently implemented to evaluate the carbon emissions from generation, transmission, transmission loss, and consumption. By contrast, with the integration of the DRESs in the distribution systems, prosumers play a role as both generators and consumers. This carbon emissions tracing approach needs to be extended to distinguish the following portions of carbon emissions.

- Carbon emissions caused by using a prosumer's own generation for meeting its own demand.
- Carbon emissions caused by using a prosumer's own generation for supplying other prosumers' demand.
- Carbon emissions caused by a prosumer's demand being supplied by other prosumers' generation.

The developed carbon emissions tracing approach aims to evaluate the CEF in microgrids considering these bidirectional power flows caused by energy trading. Recall that $\mathcal{I}$ and $\mathcal{K}$ denote the index sets of generators and loads of a prosumer, respectively, and $r_{i,t}$ and $r_{k,t}$ denote the carbon emissions rates caused by power generation of generator $i \in \mathcal{I}$ and power consumption of load $k \in \mathcal{K}$ at scheduling time t, respectively. A schematic illustration of the aforementioned three portions of carbon emissions is presented in Fig. 5.3. Prosumer A generates surplus energy after meeting its own demand, and supplies the surplus energy to prosumer B who is unable to generate enough energy to meet its own demand. The portion of carbon emissions caused by using prosumer A and prosumer B' s own generation for meeting their own demand can be quantified by $\sum_{k\in\mathcal{K}} r^{\mathrm{A}}_{k,t}$ and $\sum_{k\in\mathcal{K}} r^{\mathrm{B}}_{k,t}$, respectively. In addition, the portion of carbon emissions caused by using a prosumer's

own generation for supplying other prosumers' demand can be described as

$$r_{\text{net},t} = \sum_{i \in \mathcal{I}} r_{i,t} - \sum_{k \in \mathcal{K}} r_{k,t}, \tag{5.3.1}$$

where $r_{\text{net},t}$ is the carbon emissions rate caused by using a prosumer's own generation for supplying other prosumers' demand at scheduling time t. Hence, as indicated in Fig. 5.3, the portion of carbon emissions caused by using prosumer A' s own generation for supplying prosumer B' s demand can be quantified by $r^{\text{A}}_{\text{net},t}$ which is the same amount for the carbon emissions rate caused by prosumer B' s demand being supplied by prosumer A' s generation.

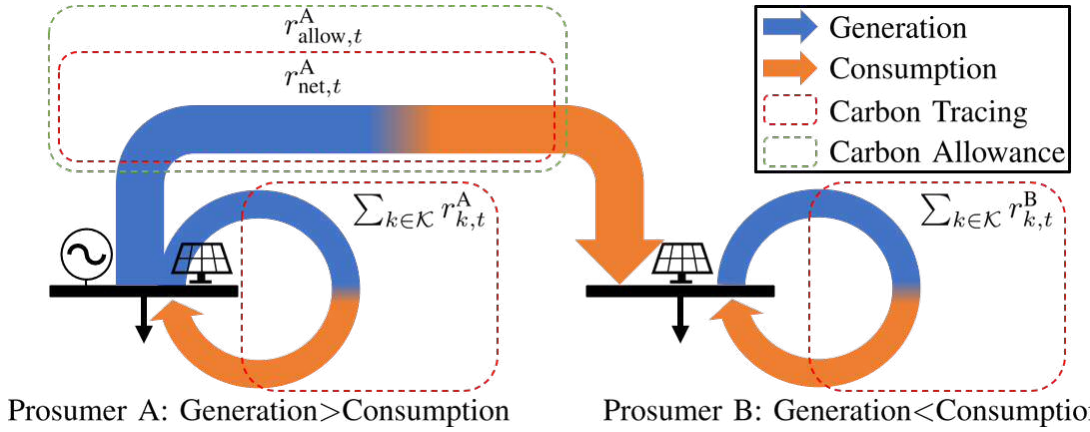

Figure 5.3: Schematic illustration of carbon emissions tracing for prosumers. Prosumer A supplies surplus energy to prosumer B. Prosumer A needs to have the carbon allowance ($r^{\text{A}}_{\text{allow},t}$) when supplying energy to prosumer B.

Once these portions of carbon emissions are traced, the decentralised low carbon incentive mechanism in Section 3.2.3 is extended correspondingly targeting on individual prosumers. According to the principle of carbon accounting [79], when a prosumer supplies energy to other prosumers, this prosumer needs to have the carbon allowance as a permission of pollutant emitting. Let $r_{\text{allow},t}$ denote the carbon allowance of a prosumer at scheduling time t, and $\gamma(\cdot)$ denote the function of the monetary compensation for carbon reduction of a prosumer. The following assumptions need to be considered to formulate the prosumer-centric low carbon incentive.

- *Assumption 1*: If $r_{\text{net},t} > r_{\text{allow},t}$, a prosumer has to buy the carbon allowance

from other prosumers; If $r_{\text{net},t} < r_{\text{allow},t}$, a prosumer can not only sell the extra carbon allowance to other prosumers, but also receive monetary compensation generated by the consensus of peer-to-peer trading networks.

- *Assumption 2*: The monetary compensation should be non-negative. When the net carbon emissions rate reduces to zero, the monetary compensation of a prosumer should be maximum, i.e. $\gamma = \gamma^{\max}$, if $r_{\text{net},t} = 0$, where $\gamma^{\max}$ is the maximum monetary compensation for carbon reduction of a prosumer.

- *Assumption 3*: When the carbon allowance is assigned, the monetary compensation should be monotonically decreasing to the net carbon emissions rate as

$$\frac{\partial \gamma\left(r_{\text{net},t}, r_{\text{allow},t}\right)}{\partial r_{\text{net},t}} < 0. \tag{5.3.2}$$

- *Assumption 4*: Let $\mathcal{N}$ denote the index set of prosumers in the same microgrid. The initial carbon allowance of each prosumer is assigned by the blockchain system based on the carbon emissions intensities of prosumers and carbon reduction target of an ensemble of prosumers as

$$r_{\text{allow},t} = \frac{\rho_n}{\sum_{n\in\mathcal{N}} \rho_n} \cdot \bar{e}, \tag{5.3.3}$$

where ρ_n is the carbon emissions intensity of prosumer n, and $\bar{e}$ is the targeted total carbon emissions of an ensemble of prosumers.

The prosumers with high-level of carbon emissions will receive more monetary compensation than the prosumers with low-level of carbon emissions, because those prosumers with high-level of carbon emissions are more urgent for carbon mitigation. This means that the marginal monetary compensation should be monotonically increasing to the assigned carbon allowance as

$$\frac{\partial^2 \gamma\left(r_{\text{net},t}, r_{\text{allow},t}\right)}{\partial r_{\text{allow},t}^2} > 0. \tag{5.3.4}$$

Hence, the following function which satisfies all the assumptions is modelled as the prosumer-centric monetary compensation for carbon reduction

$$\gamma\left(r_{\text{net},t}, r_{\text{allow},t}\right) := \begin{cases} \alpha_t \cdot \sqrt{\left(r_{\text{allow},t} \cdot \Delta t\right)^2 - \left(r_{\text{net,t}} \cdot \Delta t\right)^2}, & r_{\text{allow},t} > r_{\text{net},t}, \\ 0, & r_{\text{allow},t} \leq r_{\text{net},t}, \end{cases} \tag{5.3.5}$$

where α_t is the monetary compensation rate at scheduling time t, and Δt is the scheduling interval.

5.3.2 Prosumer-Centric Algorithm

The prosumer-centric trading enables prosumers in the same microgrid to exchange energy or carbon allowance with neighbouring prosumers for the purpose of regional balance. The power losses consist of transmission losses and distribution losses. The transmission losses refer to the losses from generators to distribution networks. The distribution losses refer to the losses within the distribution networks, e.g. power losses within a community. From the whole power systems perspective as the focus in Chapter 3, the transmission losses account for about 2 % - 6 % of total power generation [211]. From the distribution systems perspective as the focus of this chapter, the distribution losses are lower than the transmission losses. This is because the generators and loads are nearby, and the amount of distributed generation from prosumers is smaller relative to the amount of large-scale generation in power systems. Therefore, the distribution losses in this chapter are neglected. Recall that $p_{i,t}$ and $p_{k,t}$ denote the power generation of generator $i \in \mathcal{I}$ at scheduling time t, and power consumption of load $k \in \mathcal{K}$ at scheduling time t, respectively. The prosumer-centric algorithm is discussed as follows when a prosumer is an energy buyer or energy seller, respectively.

Prosumer as Energy Buyer

When a prosumer is unable to generate enough energy to meet its own demand, i.e. $\sum_{i\in\mathcal{I}} p_{i,t} < \sum_{k\in\mathcal{K}} p_{k,t}$, this prosumer needs to buy energy from other prosumers as an energy buyer. The objective function of a prosumer as an energy buyer can be modelled as

$$f_b\left(p_{i,t}, p_{k,t}, b_{\text{energy},t}\right) := \sum_{t\in\mathcal{T}_{\text{buyer}}} \left(\sum_{k\in\mathcal{K}} p_{k,t} - \sum_{i\in\mathcal{I}} p_{i,t}\right) \cdot \Delta t \cdot b_{\text{energy},t}, \tag{5.3.6}$$

where $f_b\left(\cdot\right)$ is the objective function of electricity bills of a prosumer, $b_{\text{energy},t}$ is the bidding price of a prosumer at scheduling time t for buying energy, and $\mathcal{T}_{\text{buyer}}$ is the index set of scheduling time when a prosumer is an energy buyer.

When a prosumer participates in the peer-to-peer trading network as an energy buyer, the smart contract requires this prosumer to have enough account balance for purchasing the bided energy as

$$\sum_{t\in\mathcal{T}_{\text{buyer}}}\left(\sum_{k\in\mathcal{K}}p_{k,t}-\sum_{i\in\mathcal{I}}p_{i,t}\right)\cdot\Delta t\cdot b_{\text{energy},t}\leq b_{\text{balance}}, \tag{5.3.7}$$

where b_{balance} is the account balance of a buyer.

Additionally, to proceed the auction, the smart contract requires that a buyer's bidding price is higher than the currently highest bidding prices submitted by other energy buyers for the same offer as

$$b^{\text{highest}}_{\text{energy},t}<b_{\text{energy},t}, \tag{5.3.8}$$

where $b^{\text{highest}}_{\text{energy},t}$ is the currently highest bidding price for the energy selling at scheduling time t over all energy buyers updated by the blockchain network. Let $\mathcal{B}_{\text{energy},t}$ denote the set of bidding prices submitted by all energy buyers for the offer of selling energy at scheduling time t. We have

$$b^{\text{highest}}_{\text{energy},t}=\max:\mathcal{B}_{\text{energy},t}. \tag{5.3.9}$$

Therefore, the objective of a prosumer as an energy buyer is to minimise its electricity bills by strategically deciding the bidding prices of energy and reshaping prosumption behaviours as

$$\min_{p_{i,t},p_{k,t},b_{\text{energy},t}}:f_b\left(p_{i,t},p_{k,t},b_{\text{energy},t}\right), \tag{5.3.10}$$

$$\text{s.t.:(5.3.7), (5.3.8), and (5.3.9).}$$

Prosumer as Energy Seller

When a prosumer generates surplus energy after meeting its own demand, i.e. $\sum_{k\in\mathcal{K}}p_{k,t}<\sum_{i\in\mathcal{I}}p_{i,t}$, this prosumer can sell the surplus energy to other prosumers as an energy seller. Recall that when a prosumer sells energy to other prosumers, this prosumer needs to have the carbon allowance $r_{\text{allow},t}$ which is assigned by the blockchain system. If $r_{\text{net},t}>r_{\text{allow},t}$, the prosumer has to buy the exceeded carbon allowance as a part of generating costs; If $r_{\text{net},t}<r_{\text{allow},t}$, the prosumer can sell the

extra carbon allowance and be compensated as a part of revenue. Let $c_{\text{carbon}}(\cdot)$ denote the function of carbon cost/revenue of an energy seller. The cost/revenue of buying/selling carbon allowance can be described as follows when c_{carbon} is positive/negative.

$$c_{\text{carbon}}(r_{\text{net,t}}) := \begin{cases} (r_{\text{net,t}} - r_{\text{allow},t}) \cdot \Delta t \cdot b^{\text{highest}}_{\text{carbon},t} - \gamma(r_{\text{net},t}, r_{\text{allow},t}), & r_{\text{net},t} < r_{\text{allow},t}, \\ (r_{\text{net,t}} - r_{\text{allow},t}) \cdot \Delta t \cdot b_{\text{carbon},t}, & r_{\text{net},t} > r_{\text{allow},t}, \end{cases} \tag{5.3.11}$$

where $b_{\text{carbon},t}$ is the bidding price of a prosumer at scheduling time t for buying carbon allowance, and $b^{\text{highest}}_{\text{carbon},t}$ is the highest bidding price for the carbon allowance selling at scheduling time t over all carbon allowance buyers updated by the blockchain network. Let $\mathcal{B}_{\text{carbon},t}$ denote the set of bidding prices submitted by all the carbon allowance buyers for the offer of selling carbon allowance at scheduling time t. We have

$$b^{\text{highest}}_{\text{carbon},t} = \max : \mathcal{B}_{\text{carbon},t}. \tag{5.3.12}$$

Apart from the carbon cost, recall in Chapter 3 and Chapter 4 that other operating costs include costs of operation, maintenance, fuel, and carbon capture and storage [169] (costs of pre-development, construction, decommissioning, and waste are not considered in our dynamic scheduling problem). The coefficients of operating costs for each of energy sources are evaluated by the LCoE [170]. The function of operating costs of a prosumer can be modelled as

$$c(p_{i,t}) := \sum_{i \in \mathcal{I}} p_{i,t} \cdot \Delta t \cdot \delta_i, \tag{5.3.13}$$

where $c(\cdot)$ is the function of operating costs of a prosumer excluding the carbon cost, and δ_i is the coefficient of the total operating costs of generator i.

The objective function of a prosumer as an energy seller can be modelled as

$$f_p(p_{i,t}, p_{k,t}, b_{\text{carbon},t}) := \sum_{t \in \mathcal{T}_{\text{seller}}} \left[\left(\sum_{i \in \mathcal{I}} p_{i,t} - \sum_{k \in \mathcal{K}} p_{k,t} \right) \cdot \Delta t \cdot b^{\text{highest}}_{\text{energy},t} - c_{\text{carbon}}(r_{\text{net,t}}) - c(p_{i,t}) \right], \tag{5.3.14}$$

where $f_p(\cdot)$ is the objective function of profits of a prosumer, and $\mathcal{T}_{\text{seller}}$ is the index set of scheduling time when a prosumer is an energy seller.

Analogous to the energy trading, when a prosumer participates in the peer-to-peer trading network as a carbon allowance buyer, the smart contract requires this prosumer has enough account balance for purchasing the bided carbon allowance as

$$\sum_{t \in \mathcal{T}_{\text{seller}}} c_{\text{carbon}}\left(r_{\text{net,t}}\right) \leq b_{\text{balance}}, \tag{5.3.15}$$

Additionally, to proceed the auction, the smart contract requires that a buyer's bidding price is higher than the currently highest bidding prices submitted by other carbon allowance buyers for the same offer as

$$b_{\text{carbon},t}^{\text{highest}} < b_{\text{carbon},t}, \tag{5.3.16}$$

Therefore, the objective of a prosumer as an energy seller is to maximise its profits by strategically deciding the bidding prices of carbon allowance and reshaping prosumption behaviours as

$$\max_{p_{i,t}, p_{k,t}, b_{\text{carbon},t}} : f_p\left(p_{i,t}, p_{k,t}, b_{\text{carbon},t}\right), \tag{5.3.17}$$

$$\text{s.t.:(5.3.12), (5.3.15), and (5.3.16)}$$

The decision variable $b_{\text{carbon},t}$, (5.3.15), and (5.3.16) only hold when a prosumer buys the carbon allowance.

5.3.3 Microgrid-Trader-Centric Algorithm

After the completion of the prosumer-centric trading, there might be residual supply or demand which cannot be met inside the microgrid due to the surplus or scarcity generation of all prosumers in the same microgrid. The MT-centric trading aims to help an ensemble of prosumers in the same microgrid aggregate the residual supply and demand. Through solving the prosumer-centric algorithm, the optimal power generation of generator i and optimal power consumption of load k for a prosumer at each scheduling time t are yielded, denoted as $p_{i,t}^{*}$ and $p_{k,t}^{*}$, respectively. The residual power of prosumer $n \in \mathcal{N}$ can be described as

$$p_{n,t} = \sum_{i \in \mathcal{I}} p_{i,t}^{*} - \sum_{k \in \mathcal{K}} p_{k,t}^{*} \tag{5.3.18}$$

where $p_{n,t}$ is the residual power of prosumer $n \in \mathcal{N}$ at scheduling time t.

Microgrid-Trader as Energy Buyer

When an ensemble of prosumers in the same microgrid is unable to meet their own demand, i.e. $\sum_{n\in\mathcal{N}} p_{n,t} < 0$, MT needs to help its prosumers buy energy from other microgrids or import from the main grid. The objective function of a MT as an energy buyer can be modelled as

$$f_B\left(b_{\text{energy},t}\right) := \sum_{t\in\mathcal{T}_{\text{buyer}}} \sum_{n\in\mathcal{N}} \left(-p_{n,t}\right) \cdot \Delta t \cdot b_{\text{energy},t}, \tag{5.3.19}$$

where $f_B\left(\cdot\right)$ is the objective function of electricity bills of a MT.

Analogous to the prosumer-centric trading, there are account balance constraint and the highest bidding constraint when the MT is an energy buyer as (5.3.20) and (5.3.21), respectively.

$$\sum_{t\in\mathcal{T}_{\text{buyer}}} \sum_{n\in\mathcal{N}} \left(-p_{n,t}\right) \cdot \Delta t \cdot b_{\text{energy},t} \leq b_{\text{balance}}, \tag{5.3.20}$$

$$b^{\text{highest}}_{\text{energy},t} < b_{\text{energy},t}. \tag{5.3.21}$$

Therefore, the objective of a MT as an energy buyer is to minimise overall electricity bills for its prosumers by strategically deciding the optimal bidding price of energy as

$$\begin{aligned} &\min_{b_{\text{energy},t}} : f_B\left(b_{\text{energy},t}\right), \\ &\text{s.t.: (5.3.20), and (5.3.21).} \end{aligned} \tag{5.3.22}$$

Microgrid-Trader as Energy Seller

When an ensemble of prosumers in the same microgrid generates surplus energy after meeting their own demand, i.e. $\sum_{n\in\mathcal{N}} p_{n,t} > 0$, MT can help its prosumers sell energy to other microgrids. Meanwhile, MT can help its energy sellers trade residual carbon allowance with other microgrids. If the net carbon emissions of an ensemble of prosumers in the same microgrid exceed the carbon allowance of this microgrid, MT has to help its prosumers buy carbon allowance from other microgrids. If the net carbon emissions of an ensemble of prosumers in the same microgrid are less than the carbon allowance of this microgrid, MT can help its prosumers sell the extra carbon allowance and earn the monetary compensation for its prosumers. This relationship

has a similar format as (5.3.11). Hence, the objective function of a MT as an energy seller can be modelled as

$$f_P\left(b_{\text{carbon},t}\right) := \sum_{t\in\mathcal{T}_{\text{seller}}}\sum_{n\in\mathcal{N}}\left[p_{n,t}\cdot\Delta t\cdot b^{\text{highest}}_{\text{energy},t} - \left(c_{\text{carbon},n}+c_n\right)\right], \tag{5.3.23}$$

where $f_P\left(\cdot\right)$ is the objective function of profits of a MT, $c_{\text{carbon},n}$ is the carbon cost/revenue of prosumer n, and c_n is the operating costs excluding the carbon cost of prosumer n.

There are account balance constraint and the highest bidding constraint when the MT is a carbon allowance buyer as (5.3.24) and (5.3.25), respectively.

$$\sum_{t\in T_{\text{seller}}}\sum_{n\in\mathcal{N}} c_{\text{carbon},n} \leq b_{\text{balance}}, \tag{5.3.24}$$

$$b^{\text{highest}}_{\text{carbon},t} < b_{\text{carbon},t}. \tag{5.3.25}$$

Therefore, the objective of a MT as an energy seller is to maximise the overall profits for its prosumers by strategically deciding optimal bidding prices of carbon allowance as

$$\begin{aligned}&\max_{b_{\text{carbon,t}}} : f_P\left(b_{\text{carbon},t}\right),\\ &\text{s.t.: (5.3.24), and (5.3.25).}\end{aligned} \tag{5.3.26}$$

The decision variable $b_{\text{carbon},t}$, (5.3.24), and (5.3.25) only hold when a MT buys the carbon allowance.

Remark: The optimisation problems of both the prosumer-centric algorithm and the MT-centric algorithm are solved by the artificial immune algorithms as proposed in Chapter 3 and Chapter 4. To improve the scalability and computational efficiency, the learning approach as proposed in Chapter 4 is further implemented to make predicted optimal scheduling decisions.

5.3.4 Smart Contract Based Auction Mechanism

In the layer of peer-to-peer trading platform, the proposed smart contract based auction mechanism is applicable for both prosumers and MTs to trade either energy or carbon allowance, under the standardised negotiation and self-enforcing of smart

contract. The auction consists of the following steps: initialisation, matching, bidding, withdrawal, and pay-to-seller. Each step is performed by a function of smart contract, denoted as $f_{\text{init}}(\cdot)$, $f_{\text{match}}(\cdot)$, $f_{\text{bid}}(\cdot)$, $f_{\text{withdraw}}(\cdot)$, and $f_{\text{pay}}(\cdot)$, respectively. Let $\mathcal{U}$ denote the index set of sellers, and $\mathcal{V}$ denote the index set of buyers. The trading algorithm, as shown in **Algorithm 5**, is written in the Solidity language and stored in the Ethereum blockchain [212]. Detailed steps of executing the auction are described as:

Step 1: Each seller calls the initialisation function $f_{\text{init}}(\cdot)$ from smart contract to specify the seller address, trading type (energy or carbon allowance), seller type (prosumer or MT), microgrid number, selling amount, minimal accepted bidding price, the currently highest bid, and the time of auction ended as

$$\mathcal{O}_u = f_{\text{init}}\left(\text{id}_u, \varepsilon, \beta, m_u, s_u, b_{u,t}^{\min}, b_{u,t}^{\text{highest}}, \tau_u\right), \tag{5.3.27}$$

where $\mathcal{O}_u$ is the offer initialised by seller $u \in \mathcal{U}$, id_u is the encrypted address of seller u, $\varepsilon \in \{0,1\}$ is a binary value indicating if the trading type is energy ($\varepsilon = 0$) or carbon allowance ($\varepsilon = 1$), $\beta \in \{0,1\}$ is a binary value indicating if the seller type is prosumer ($\beta = 0$) or MT ($\beta = 1$), m_u is the microgrid index of seller u which enables buyers to find sellers in the same microgrid, s_u is the amount of energy or carbon allowance to be supplied by seller u, $b_{u,t}^{\min}$ is the minimal accepted bidding price specified by seller u for the energy or carbon allowance to be provided at scheduling time t, $b_{u,t}^{\text{highest}}$ is the currently highest bidding price ($b_{u,t}^{\text{highest}} = b_{u,t}^{\min}$ at the initialisation) for the energy or carbon allowance to be provided by the seller u at scheduling time t, and τ_u is the time of auction ended specified by seller u. The blockchain network stores and updates the offers of all the sellers. This step corresponds to the line 1-3 in **Algorithm 5**.

Step 2: In the proposed auction mechanism, each buyer needs to bid with a higher price than the currently highest bidding price over all the buyers. Hence, the matching function $f_{\text{match}}(\cdot)$ aims to help buyers automatically match the optimal offers combination to submit their bids, according to the following criterion.

- The demand of energy or carbon allowance for a buyer can be met by the summation of selected offers.

Algorithm 5 Smart Contract Based Auction Procedure

function: initialisation $f_{\text{init}}(\cdot)$

input: $\text{id}_u, \varepsilon, \beta, m_u, s_u, b_{u,t}^{\min}, b_{u,t}^{\text{highest}}, \tau_u$

output: $\mathcal{O}_u$

function: matching $f_{\text{match}}(\cdot)$

for $v \in \mathcal{V}$ **do**

  find optimal offers combination $\mathcal{U}_v^*$ by (5.3.28) and (5.3.29)

end for

function: bidding $f_{\text{bid}}(\cdot)$

input: $\tau_{\text{now}}, b_v^*, m_v, b_{\text{balance},v}$

while $\tau_{\text{now}} \leq \tau_u$, $m_v = m_u$, $b_{u,t}^{\text{highest}} \cdot s_u < b_v^* \cdot s_u \leq b_{\text{balance},v}$ **do**

  submit bids and update the highest bidding price by (5.3.31)

end while

output: $b_{u,t}^{\text{highest}'}$

function: withdrawal $f_{\text{withdraw}}(\cdot)$

input: $\tau_{\text{now}}, b_v^*, b_{\text{balance},v}$

while $\tau_{\text{now}} > \tau$, $v \in \mathcal{V}$, $v \neq v^*$ **do**

  unsuccessful buyers withdraw their bids by (5.3.33)

end while

output: $b'_{\text{balance},v}$

function: pay-to-seller $f_{\text{pay}}(\cdot)$

input: $\tau_{\text{now}}, b_v^*, b_{\text{balance},u}$

while $\tau_{\text{now}} > \tau$, $v = v^*$ **do**

  pay the deposited highest bid to seller by (5.3.35)

end while

output: $b'_{\text{balance},u}$

- The selected optimal offers have the minimal summation of the currently highest bidding prices, which allows buyers to bid with minimal bidding prices.

The optimal offers combination can be yielded as

$$\mathcal{U}_v^* = \arg\min_{u} : \sum_{u \in \mathcal{U}} b_{u,t}^{\text{highest}} \cdot s_u, \tag{5.3.28}$$

$$\text{s.t.} \sum_{u \in \mathcal{U}} s_u \geq d_v, \tag{5.3.29}$$

where $\mathcal{U}_v^*$ is the set of optimal offers combination that can meet buyer v' s demand with minimal required bidding prices, and d_v is the demand of energy or carbon allowance of buyer v. This step corresponds to the line 4-7 in **Algorithm 5**.

Step 3: The bidding function $f_{\text{bid}}(\cdot)$ enables buyers to submit their bids after checking the following conditions.

- The auction is not ended, i.e. $\tau_{\text{now}} \leq \tau_u$, where τ_{now} is the current time.
- The microgrid index of buyer v, denoted as m_v, matches m_u, i.e. $m_v = m_u$.
- The buyer has enough balance to provide a higher bid than the currently highest bidding price as

$$b_{u,t}^{\text{highest}} \cdot s_u < b_v^* \cdot s_u \leq b_{\text{balance},v}, \tag{5.3.30}$$

  where b_v^* is the optimal bidding price of buyer v yielded by solving the optimisation problems in prosumer-centric algorithm or MT-centric algorithm, and $b_{\text{balance},v}$ is the account balance of buyer v.

After a buyer successfully submits a bid, the highest bidding price of seller u' s offer is updated as

$$b_{u,t}^{\text{highest}'} = f_{\text{bid}}\left(\tau_{\text{now}}, b_v^*, m_v, b_{\text{balance},v}\right), \tag{5.3.31}$$

where $b_{u,t}^{\text{highest}'}$ is the updated currently highest bidding price for the energy or carbon allowance to be provided by the seller u at scheduling time t. Before the auction is ended, all the bids are frozen by the smart contract, which means that the buyers are unable to withdraw their bids back to their account. This step corresponds to the line 8-13 in **Algorithm 5**.

Step 4: When the auction is ended, i.e. $\tau_{\text{now}} > \tau$, the buyer with the highest bidding price wins the auction as

$$v^* = \arg\max_{v} : \mathcal{B}_t, \tag{5.3.32}$$

where v^* is the buyer with the highest bidding price, and $\mathcal{B}_t$ is the set of bidding prices submitted by all buyers for the energy or carbon allowance provided at scheduling time t.

The rest of unsuccessful buyers $v \in \mathcal{V}, v \neq v^*$ withdraw their previously submitted bids by calling the withdrawal function $f_{\text{withdraw}}(\cdot)$ as

$$b'_{\text{balance},v} = f_{\text{withdraw}}\left(\tau_{\text{now}}, b^*_v, b_{\text{balance},v}\right), \tag{5.3.33}$$

where

$$b'_{\text{balance},v} = b_{\text{balance},v} + b^*_v \cdot s_u, \tag{5.3.34}$$

is the updated account balance of buyer v after withdrawing the bid for seller u' s offer. This step corresponds to the line 14-19 in **Algorithm 5**.

Step 5: Once the smart contract confirms that the energy or carbon allowance is delivered by querying the smart meter, the deposited final highest bid for offer u, denoted as $b^{\text{highest}*}_{u,t}$ is paid to the seller by the pay-to-seller function $f_{\text{pay}}(\cdot)$ as

$$b'_{\text{balance},u} = f_{\text{pay}}\left(\tau_{\text{now}}, b^{\text{highest}*}_{u,t}, b_{\text{balance},u}\right), \tag{5.3.35}$$

where

$$b'_{\text{balance},u} = b_{\text{balance},u} + b^{\text{highest}*}_{u,t} \cdot s_u, \tag{5.3.36}$$

is the updated account balance of seller u after receiving the payment. This step corresponds to the line 20-25 in **Algorithm 5**.

5.4 Case Studies

In this section, case studies have been conducted to evaluate the proposed blockchain based peer-to-peer trading framework.

5.4.1 Simulation Setup and Data Availability

The proposed prosumer-centric algorithm and MT-centric algorithm are written in the MATLAB language. The proposed smart contract is written in the Solidity 0.6.0 and executed on the Remix-IDE. Individual deposit accounts are created for each prosumer and MT. An overview of testing environment for our proposed blockchain based peer-to-peer trading framework is presented in Fig. 5.4. The simulations are performed using a machine with Intel$^{\mathrm{R}}$ Core$^{\mathrm{TM}}$ i9-9900K CPU at 3.60 GHz.

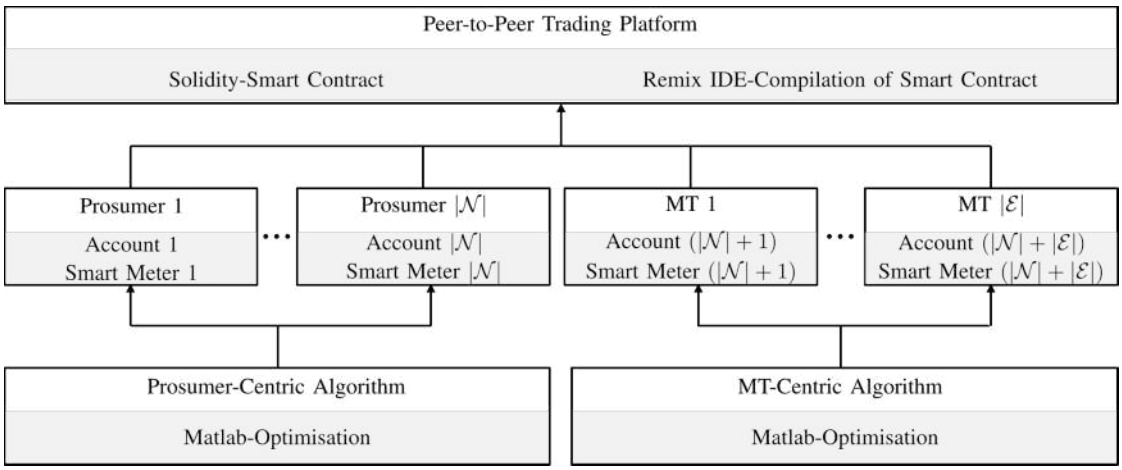

Figure 5.4: Overview of testing environment for blockchain based peer-to-peer trading framework. The smart contract is written in the Solidity language and executed on the Remix-IDE. The prosumer-centric algorithm and MT-centric algorithm are written in the MATLAB language. Individual deposit accounts are created for each prosumer and MT.

The modified IEEE 37-bus distribution network is adopted by our research as shown in Fig. 5.5. The network is partitioned into 5 interconnected microgrids. Each bus represents a prosumer. 7 solar photovoltaics, 4 diesel generators, 4 wind turbines, and 2 biomass generators are arbitrarily assigned to each microgrid, and 33 loads are assigned to each bus. The static default data of generation and consumption from the IEEE 37-bus distribution network is replaced by dynamic data. The demand data of residential loads is collected by using EFERGY monitor hub and allocated to each prosumer as shown in Fig. 5.6. The data of solar generation is obtained from the U.K. rooftop solar generation of endpoint consumers [76]. The

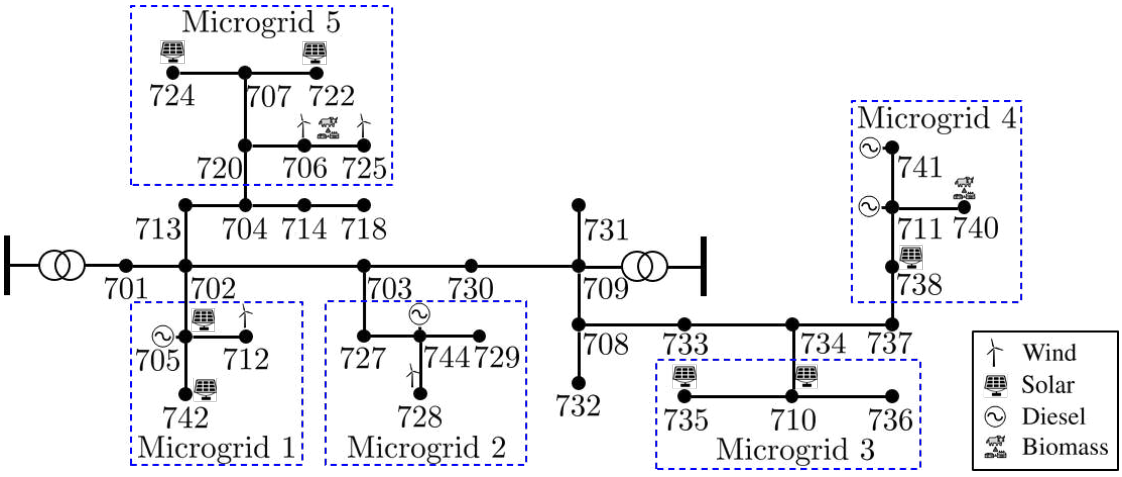

Figure 5.5: Modified IEEE 37-bus distribution network. The network is partitioned into 5 microgrids. Each bus represents a prosumer. 7 solar photovoltaics, 4 diesel generators, 4 wind turbines, and 2 biomass generators are arbitrarily assigned to each microgrid by connecting to prosumers' buses. 33 loads are assigned to each bus.

real-time states of the GB generation in 2019 from the GridWatch are used [179]. The ratio of peak real-time demand to the peak static demand from the IEEE 37-bus distribution network is used to scale down the generation of diesel, wind, and biomass. The total power outputs of each generation source are equally allocated to the corresponding generators. The generation allocation for prosumers and microgrids in the modified IEEE 37-bus distribution network is shown in Fig. 5.7.

The coefficients of operating costs and carbon emissions intensities are the same as Table 4.1 in Chapter 4. The data of centralised prices of energy and carbon allowance is obtained from the U.K. energy retail market [180] and the U.K. carbon market [213], i.e. the E.U. emissions trading scheme plus the U.K. carbon price support, respectively. These centralised prices are set as the minimal accepted bidding price of each seller, such that during the auction process, the buyers can provide a higher price than the centralised prices through solving their own objective functions. As studied in [104], this design encourages more prosumers to sell their surplus energy or carbon allowance, and reduces the import from central markets.

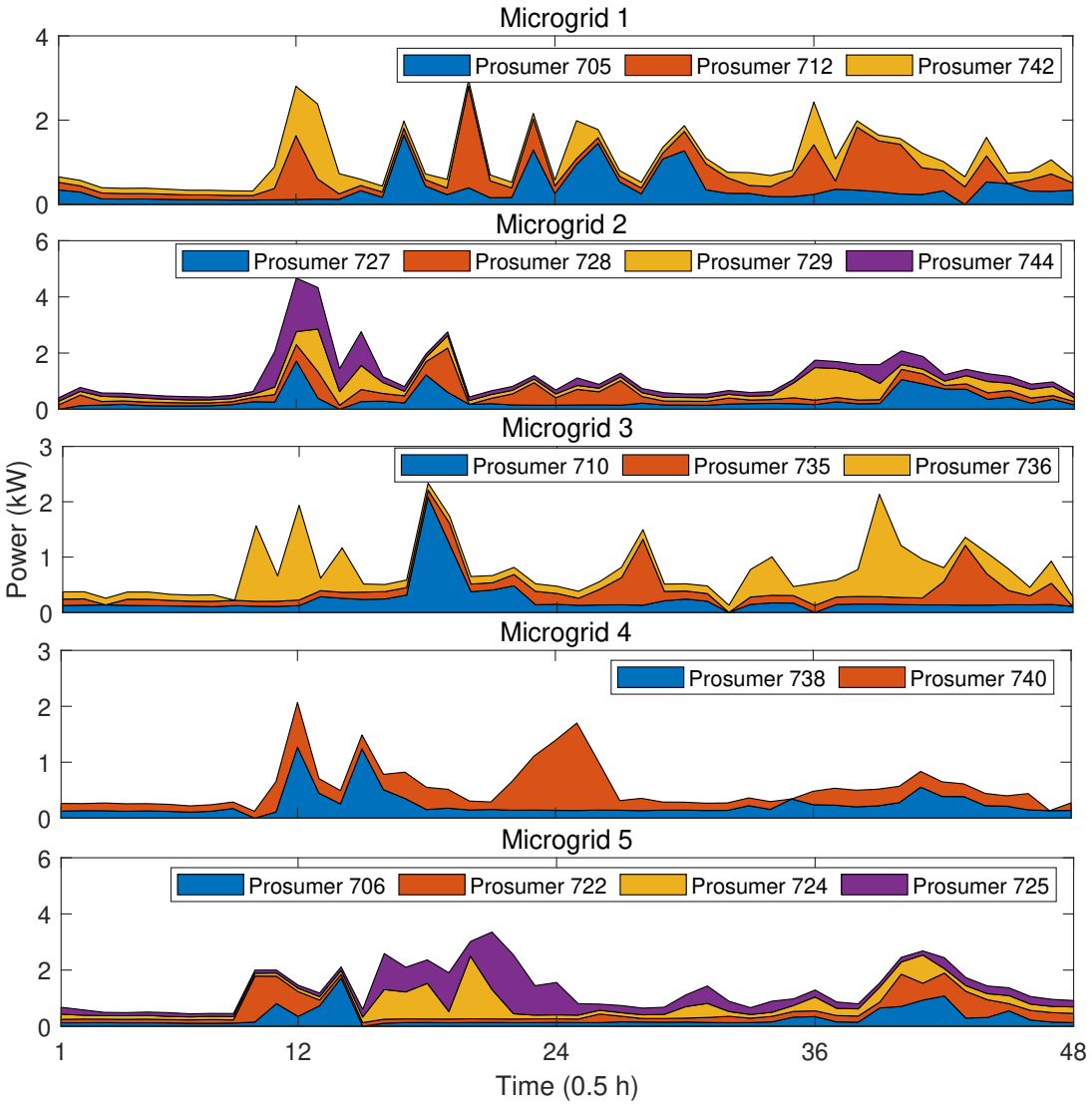

Figure 5.6: Demand allocation for prosumers and microgrids in the modified IEEE 37-bus distribution network.

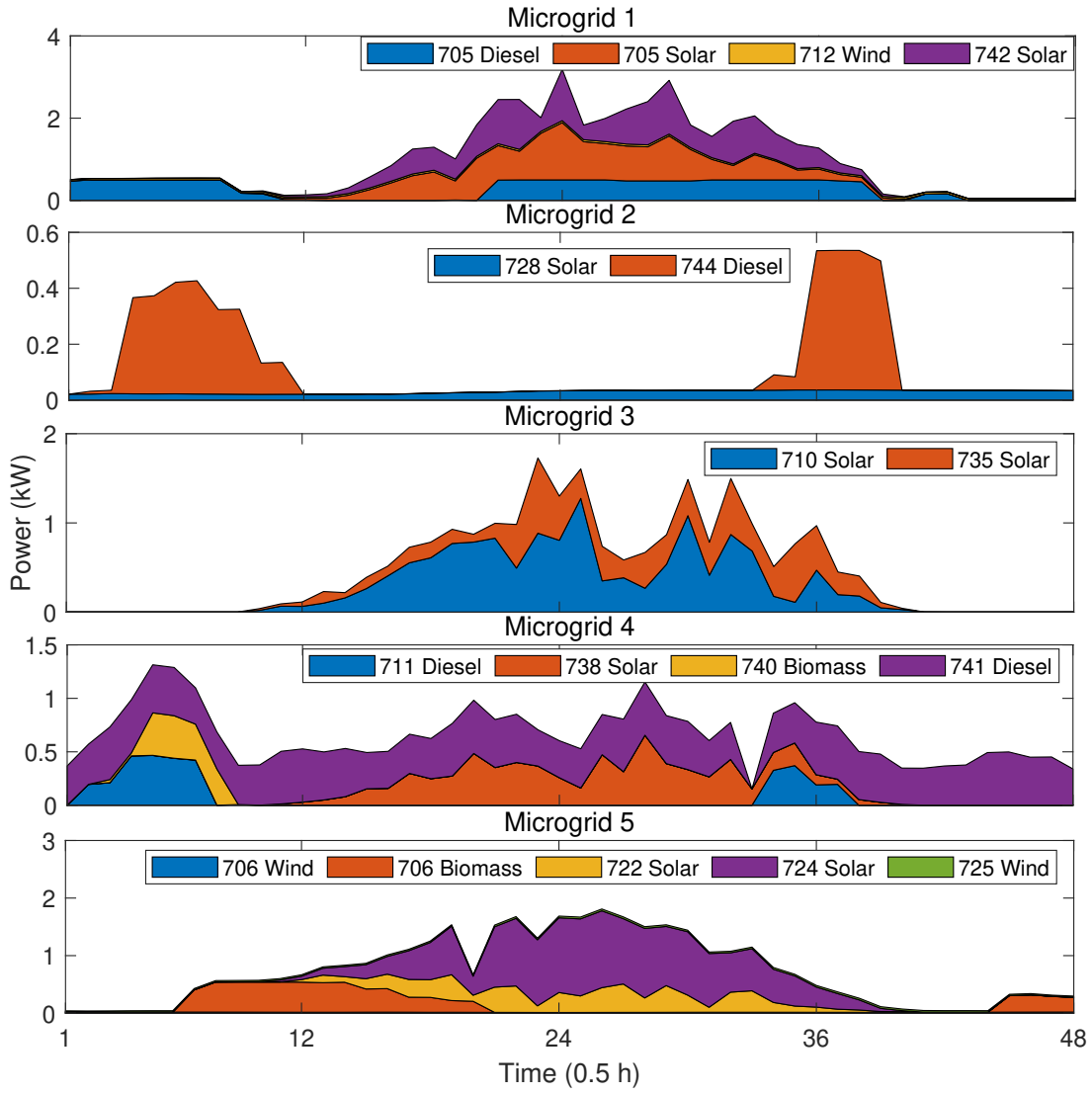

Figure 5.7: Generation allocation for prosumers and microgrids in the modified IEEE 37-bus distribution network.

5.4.2 Balancing Performances of Energy and Carbon Allowance

To evaluate the balancing performances of energy and carbon allowance, the proposed trading framework is compared with the following trading schemes:

- *Scheme 1 (Centralised Trading)*: The trading of energy or carbon allowance is only performed on the centralised markets. The prices of energy [180] and carbon allowance [213] in central markets are applied in the centralised trading.
- *Scheme 2 (Aggregator-Based Trading)*: As the trading scheme in [54, 56], the reshaping of prosumption behaviours is managed by relatively decentralised agents, i.e. aggregators, with the same objectives of minimising bills for buyers or maximising profits for sellers. Aggregators then pay prosumers the monetary compensation for the reshaping. The trading of energy or carbon allowance is only performed by aggregators.

The net power of the modified IEEE 37-bus distribution network, i.e. the total power generation minus the total power consumption, is presented in Fig. 5.8. The positive net power indicates the total generation is greater than the total demand. The negative net power indicates the total generation is less than the total demand, and the distribution network has to import power from the main grid. Through the proposed peer-to-peer trading framework, the summation of daily net energy is 0.99 kWh, which indicates a better energy balance, compared to -4.50 kWh in the aggregator-based trading and -46.44 kWh in the centralised trading.

The surplus of carbon allowance of the modified IEEE 37-bus distribution network, i.e. the total assigned carbon allowance minus the total carbon emissions, is presented in Fig. 5.9. The positive surplus of carbon allowance indicates the total carbon emissions produced by the distribution network are less than the total assigned carbon allowance, whereas the negative surplus of carbon allowance indicates the total carbon emissions produced by the distribution network exceed the total assigned carbon allowance. The proposed peer-to-peer trading framework can save total daily carbon emissions from the carbon allowance by 1465.90 g, approximately 6 times higher than the aggregator-based trading (385.91 g) and 9 times higher than the centralised trading (168.65 g). It is particularly for the period from the

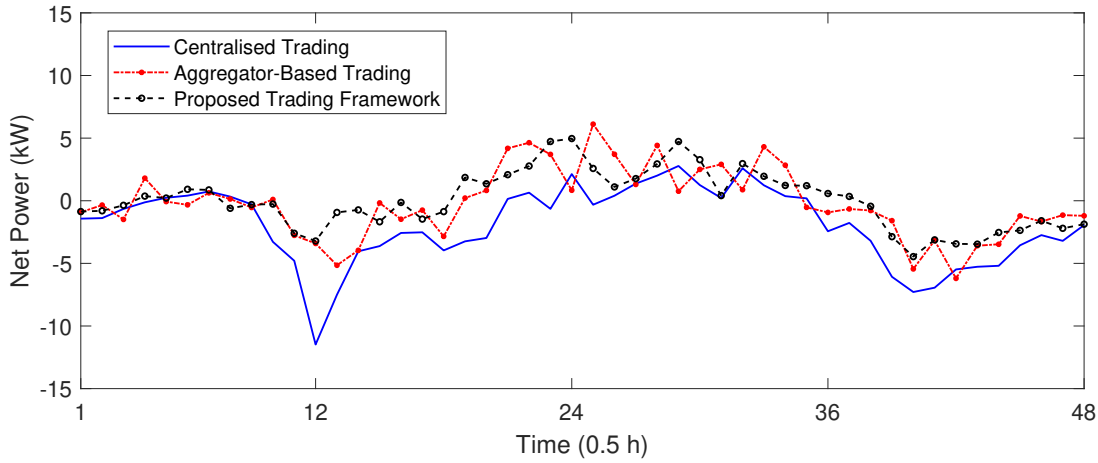

Figure 5.8: Net power of the modified IEEE 37-bus distribution network. The positive value of y-axis indicates the total generation is greater than the total demand. The negative value of y-axis indicates the total generation is less than the total demand. The x-axis indicates the scheduling time of day.

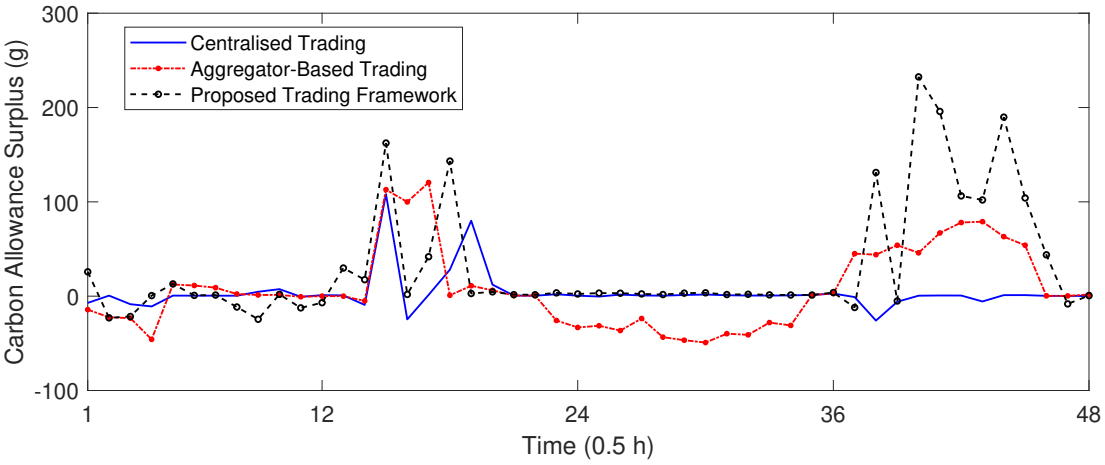

Figure 5.9: Surplus of carbon allowance of the modified IEEE 37-bus distribution network. The positive value of y-axis indicates the total carbon emissions are less than the total assigned carbon allowance. The negative value of y-axis indicates the total carbon emissions exceed the total assigned carbon allowance.

thirty-sixth scheduling time to the forty-eighth scheduling time, during which more carbon emissions are saved. Although the aggregator-based trading also achieves the carbon saving during this period, it results in that the carbon emissions exceed the carbon allowance during the period from the twenty-second scheduling time to the thirty-fifth scheduling time.

5.4.3 Demonstration of Interface Between Scheduling Algorithms and Smart Contract

The optimal energy scheduling and bidding prices for each of the individual prosumers obtained by the prosumer-centric algorithm are shown in Fig. 5.10, relative to the cases with no scheduling, i.e. original prosumption. For the microgrid at scheduling intervals during which all prosumers of this microgrid cannot generate surplus energy to trade, there is no energy seller and bidding price. By comparing the scheduled prosumption and original prosumption, it can be observed that during the peak demand periods for a majority of prosumers, i.e. from the twelfth scheduling time to the thirty-sixth scheduling time, the generation is scheduled to increase whereas the consumption is shifted to the off-peak demand periods, i.e. the rest of scheduling time. When the prosumers experience high power consumption and low power generation and thus become the energy buyers, by appropriately scheduling, the bidding prices stabilise at around 10 pence/kWh without dramatic increase. The slight fluctuation of bidding prices dynamically reflect the actual supply-demand balance in energy markets.

The interface between scheduling decisions and smart contract is shown in Fig. 5.11. Through solving the prosumer-centric algorithm, the optimal bidding prices of prosumers as buyers (indicated by the colourbar) are automatically sent to the smart contract for auction. The highest bidding prices (indicated by the red line) would be accepted by sellers. For the microgrid at scheduling intervals during which all prosumers of this microgrid cannot generate surplus energy to trade, there is no auction proceeded (indicated by the scheduling intervals without the red line). It can be seen from Fig. 5.11 that the auctions are proceeded over all the scheduling intervals of day at microgrid 4, whereas the auctions are only proceeded at a few

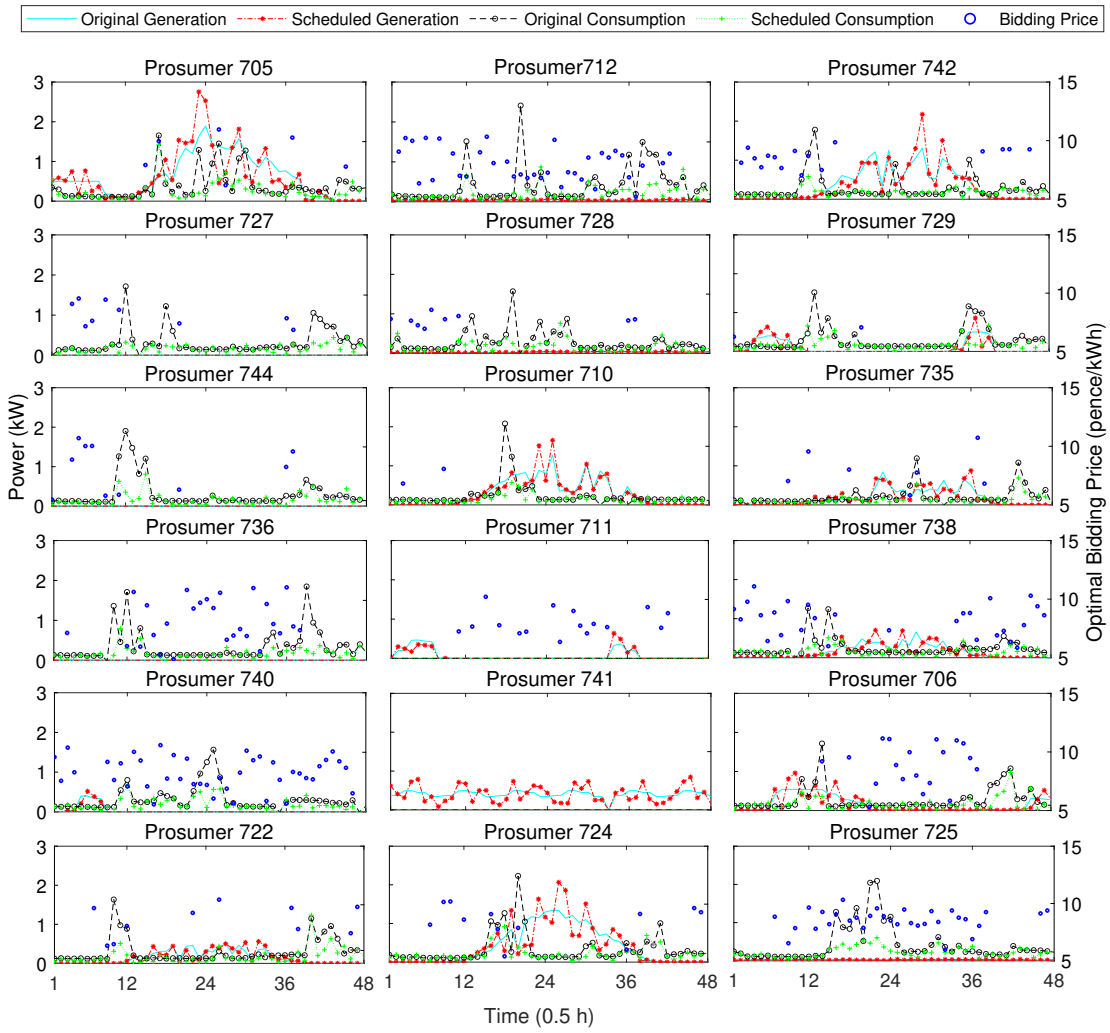

Figure 5.10: Optimal energy scheduling and bidding prices obtained by prosumer-centric algorithm. The left y axes indicate the power of original prosumption and scheduled prosumption of individual prosumers, and the right y axes indicate the optimal bidding prices. The x axes indicate the scheduling time of day.

scheduling intervals at microgrid 2. This is because the generation capacity of microgrid 2 cannot meet its demand. The MT 2 has to help its prosumers buy energy from other MTs. Additionally, through the proposed peer-to-peer trading framework, the selling prices are stabilised between 6 pence/kWh and 10 pence/kWh over all the scheduling intervals, which is different from the aggregator-based trading [54,56] with dramatic peak prices and off-peak prices. The auction prices decided by individual prosumers can accurately target on the actual supply-demand relationship of prosumers.

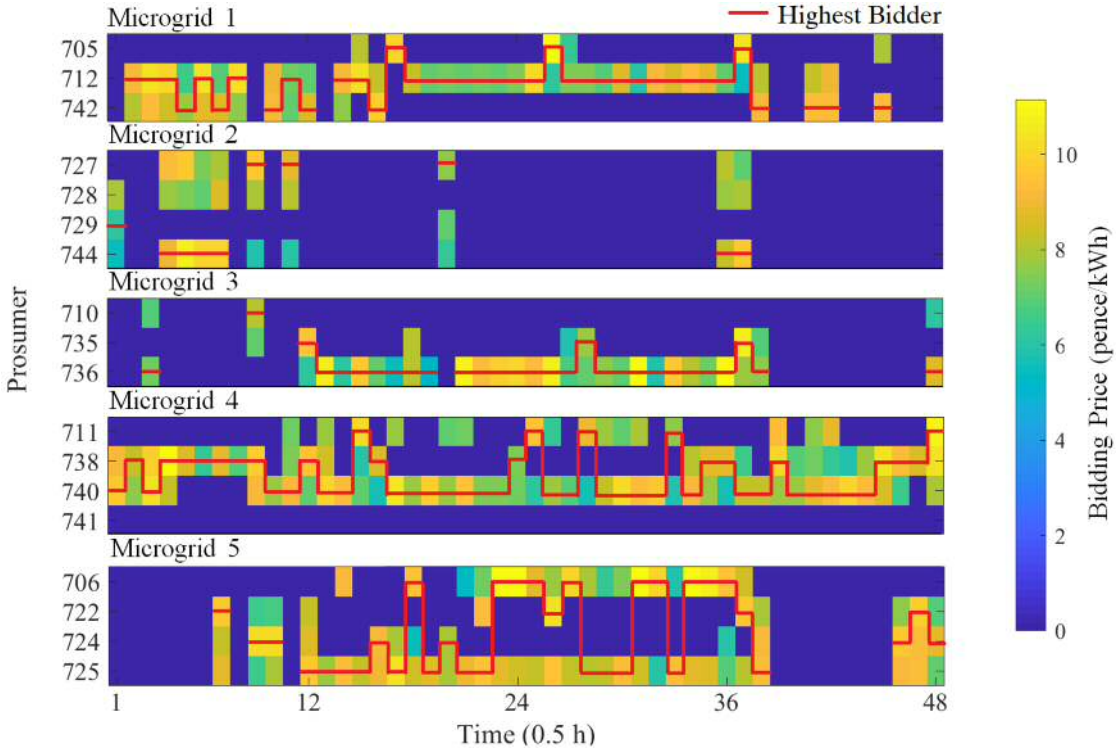

Figure 5.11: Optimal bidding prices of energy buyers as inputs of smart contract. The y axes indicate the bus number of prosumers, assigned to corresponding microgrids. The x axes indicate the scheduling time of day. The colourbar indicates the optimal bidding prices from each prosumer for a given 0.5 h scheduling interval. The red line indicates the highest bidding prices accepted by energy sellers. The scheduling interval without the red line means there is no surplus energy on the microgrid to trade.

5.4.4 Demonstration of Smart Contract Execution

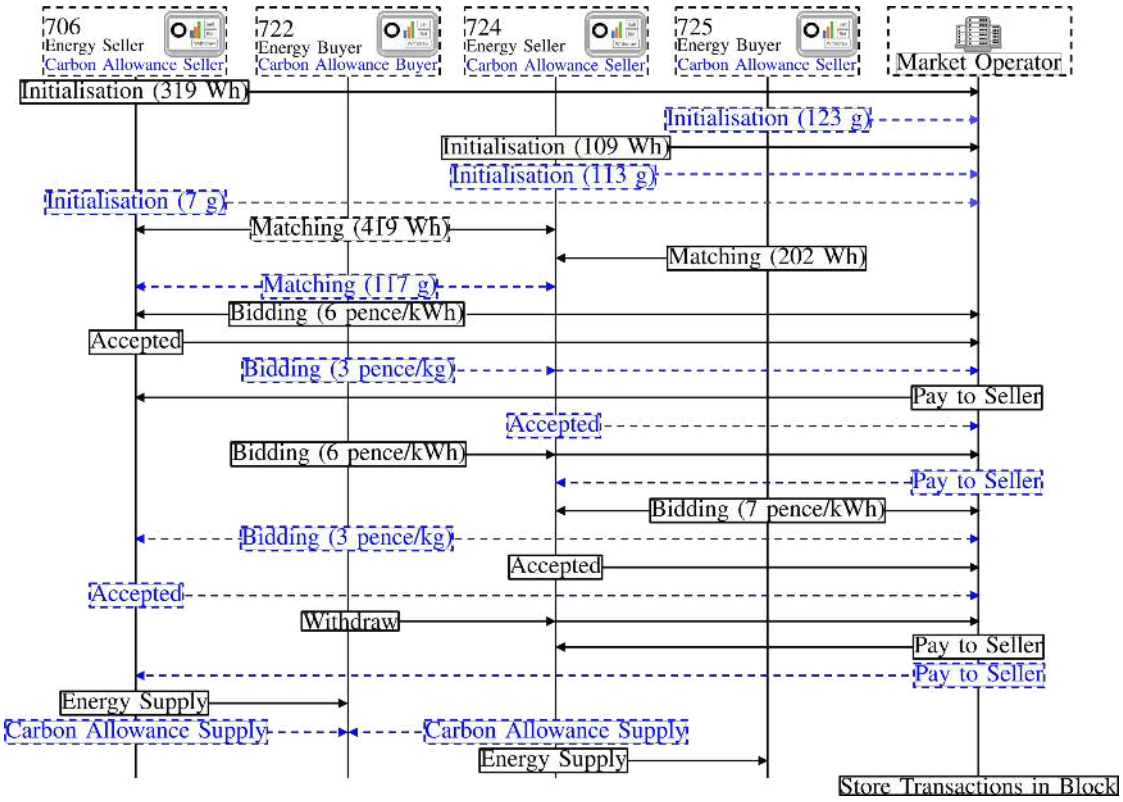

Figure 5.12: Execution of smart contract based auction on the peer-to-peer trading platform. The black line is the execution of the energy trading, and the dashed blue line is the execution of the carbon allowance trading.

The proposed auction mechanism is performed in the form of smart contract on the Ethereum blockchain. Fig. 5.12 demonstrates the procedure of executing the auctions of energy and carbon allowance on the microgrid 5. Prosumers at bus 706 and bus 724 are energy sellers to supply 319 Wh and 109 Wh energy, respectively. Prosumers at bus 706, bus 724, and bus 725 are carbon allowance sellers to supply 7 g, 113 g, and 123 g carbon allowances, respectively. The sellers call the initialisation function from the full node to specify offer conditions. Prosumer at bus 722 and bus 725 are energy buyers with the demand of 419 Wh and 202 Wh, respectively. Prosumer at bus 722 is a carbon allowance buyer with the demand of 117 g. The bids and offers are matched by the proposed matching criteria.

For the auction of carbon allowance, there is a single buyer with multiple sellers. To meet the 117 g demand of carbon allowance, the prosumer at bus 722 has the

options as

- Buying 123 g carbon allowance from the prosumer at bus 725 with 4 pence/kg of bidding price.
- Buying 113 g from the prosumer at bus 724 with 3 pence/kg of bidding price and buying another 7 g from the prosumer at bus 706 with 3 pence/kg of bidding price.

According to the matching criteria, the second option would be selected.

For the auction of energy, there are multiple buyers with multiple sellers. For the offer of selling 109 Wh energy by prosumer at bus 724, prosumers at bus 725 and bus 722 attempt to bid as buyers. The prosumer at bus 725 wins this auction with the 7 pence/kWh of the highest bidding price. The unsuccessful buyer at bus 722 then calls the withdrawal function from the full node to withdraw its bid. Once confirming the energy or carbon allowance is supplied, the smart contract pays to the sellers with the highest bids.

The residual 123 g carbon allowance from prosumer at bus 725, 93 Wh energy demand from prosumer at bus 725, and 100 Wh energy demand from prosumer at bus 722 are aggregated by the MT 5 to trade with other MTs.

5.5 Chapter Summary

This chapter proposes a blockchain-based peer-to-peer trading framework to achieve the regional energy balance and reduction of carbon emissions on distribution networks. The framework enables the energy and carbon allowance to be exchanged simultaneously. The carbon emissions tracing approach is developed targeting on specific prosumption behaviours, so that the low carbon incentive can be allocated to individual prosumers properly. The optimal bidding/selling prices of prosumers and energy reshaping decisions are yielded by the proposed prosumer-centric algorithm and MT-centric algorithm. The auction is proceeded under the standardised and self-enforcing smart contract. Case studies based on the modified IEEE 37-bus distribution network testify that the proposed trading framework can export

0.99 kWh of daily energy to the main grid and save 1465.90 g daily carbon emissions. The balancing performance of the proposed trading framework on energy and carbon allowance outperforms the centralised trading scheme and aggregator-based trading scheme. The proposed scheduling algorithms drive up the prosumers' self-generation, shift away the peak demand, and stabilise the energy prices below 10 pence/kWh. The auction prices of individual prosumers can accurately target on the actual supply-demand relationship of prosumers. The execution of smart contract on the Ethereum blockchain, and the interface between scheduling algorithms and smart contract are demonstrated.

Chapter 6

Conclusions and Future Work

This thesis has contributed to address how smart grid enables the realisation of future low carbon power systems and facilitates the emerging role of prosumers to be integrated into energy markets. In this concluding chapter, the primary findings and results from this thesis are summarised. The potential extensions based on this thesis will be indicated to help researchers further explore in the future work.

6.1 Conclusions

Firstly, from the regulatory perspective, Chapter 3 has developed a novel model for energy scheduling and low carbon negotiation between the policy maker and consumers/generators. The process of dynamic negotiation of policy measures and determining optimal power profiles of generators and consumers is modelled as a Stackelberg game-theoretic problem, which is solved by the developed FDIA-LMIA based on the artificial immune systems. The policy maker in the leader level formulates monetary compensation rates and carbon prices to incentivise consumers and generators with high carbon emissions intensities, for the purpose of electricity bill saving and generating profit improving. Case studies show that the proposed scheduling model outperforms the models of multiobjective optimization and aggregated scheduling in terms of achieving policy maker' s target for carbon emissions reduction and improving the percentage of generation from renewable energy sources. It is worth noting that by considering the effects of part-loaded generation

on the carbon emissions intensities, this research finds that the slight decrease of carbon emissions by ramping down the power outputs from coal and gas would be offset by the increased carbon emissions intensities.

Secondly, from individual prosumer's perspective, a data-driven energy scheduling tool is developed in Chapter 4 by using learning approaches to reduce computational complexity and improve scalability from solving the optimisation problem by intelligent heuristic algorithm. The CNNs are exploited to extract hidden prosumption patterns from elasticity images processed by the developed prosumption patterns processing approach. Scenarios are dynamically generated and updated to predict the possible variations of uncertainties caused by the intermittency of DRESs and flexible demand. The trained neural networks can automatically predict the optimal scheduling decisions with the strategy of minimising costs and carbon emissions. Case studies show that the designed neural networks provide an accurate prediction of optimal scheduling decisions, compared to other learning approaches including the RNN, LSTM-RNN, and DNN. The proposed learning approach improves scalability and computational efficiency from solving the optimisation problem by intelligent heuristic algorithm. The uncertainties caused by the DRESs and flexible demand can be accurately predicted by the proposed real-time scenarios selection approach. It is worth noting that this research finds the connection between the intrinsic features of dynamic price elasticities and scheduling results, and demonstrates the importance of the elasticity information for improving the learning accuracy.

Thirdly, from community's perspective, a blockchain-based peer-to-peer trading framework is designed in Chapter 5 enabling prosumers to trade energy and carbon allowance simultaneously. The trading platform is based on the self-enforcing and setting out negotiation of smart contract. Under the proposed trading framework, the bidding/selling prices of individual prosumers can directly incentivise the reshaping of prosumption behaviours for regional energy balance and carbon emissions mitigation. The carbon emissions tracing approach is also developed targeting on specific prosumption behaviours to ensure a fair allocation of low carbon incentives. Case studies demonstrate that the proposed peer-to-peer trading framework outper-

forms the aggregator-based trading and the centralised trading in terms of exporting energy to the main grid and saving carbon emissions from carbon allowance. The proposed trading framework and demonstrated benefits can encourage more passive consumers to invest in the DRESs and participate in the local energy exchange.

6.2 Future Work

This section presents the potential extensions based on the results and findings of this thesis. Some new ideas based on our work are also indicated to be explored in the future research.

6.2.1 Reducing Information Burdens

The interoperability of smart grid enables bidirectional information exchange between the policy maker and generators/consumers to cooperatively achieve energy systems scheduling. Nonetheless, the system states monitored by sensors or smart meters and decisions made by generators/consumers amplify the volumes of information flows. This presents a challenge for the information infrastructure of current power systems. To overcome this issue, a potential future work is to design a standardised protocol, e.g. smart contract, for automatic information exchange and self-enforcing execution of controlling decisions towards large-scale power systems. This would reduce the costs of processing information flows and enhance security of power systems. A potential direction to do this is to scale our designed smart contract from the distribution system level to overall power system level.

6.2.2 Long-Term Planing of Carbon Revenue

In chapter 3, the objective function of policy maker for carbon revenue neutrality specifies that the revenue from charging carbon allowance is completely redistributed as a monetary compensation. As future work, this revenue can serve for multiple purposes. For instance, in addition to using a portion of carbon revenue for monetary compensation, the rest portions of carbon revenue can be used for long-term investment of low carbon technologies. In doing this, the day-ahead scheduling

proposed by our research needs to be incorporated with long-term planing to find optimal strategies for redistributing the carbon revenue.

6.2.3 Diverse Behaviour Learning

This thesis has attempted to process price elasticities as an intrinsic feature of prosumers, and connected this feature with the energy patterns. As future work, more features of prosumers can be extracted and mapped to energy patterns. For instance, consumers' dissatisfaction can be captured from social media data through using machine learning with target-specific dictionary. With analogous approaches, the spike demand can be also connected to extreme social events.

6.2.4 Multiple Auction Mechanisms

This thesis has designed a general form of standardised smart contract by which the energy sellers initiate the smart contract and the buyers compete for bidding with a higher price. Future work can integrate multiple forms of smart contract and allow prosumers to choose the most appropriate form according to the supply demand relationship. For instance, the energy buyers can initiate the smart contract with specified demand. The sellers can subsequently compete for providing energy with a lower price.

6.2.5 Incorporating Hardware of Energy Trading

The blockchain based peer-to-peer trading platform proposed in Chapter 5 is based on the software including Ethereum blockchain network, Solidity for coding smart contract, and Remix IDE for compilation of smart contract. As future work, the hardware, e.g. PXI/NI, can be exploited for supporting peer-to-peer trading. The interface between blockchain network and hardware as well as associated protocols can be also developed.

Bibliography

[1] "World population prospects 2019," United Nations, Department of Economic and Social Affairs, Tech. Rep., 2019.

[2] "International energy outlook 2019," U.S. Energy Information Administration, Tech. Rep., 2019.

[3] R. E. Zeebe, A. Ridgwell, and J. C. Zachos, "Anthropogenic carbon release rate unprecedented during the past 66 million years," *Nature Geoscience*, vol. 9, no. 4, pp. 325–329, 2016.

[4] J. Rogelj, M. Den Elzen, N. Höhne, T. Fransen, H. Fekete, H. Winkler, R. Schaeffer, F. Sha, K. Riahi, and M. Meinshausen, "Paris agreement climate proposals need a boost to keep warming well below 2 c," *Nature*, vol. 534, no. 7609, pp. 631–639, 2016.

[5] "Kyoto protocol," *UNFCCC Website. Available online: http://unfccc.int/kyoto_protocol/items/2830. php (accessed on 1 January 2011)*, 1997.

[6] T. Bruckner, I. A. Bashmakov, Y. Mulugetta, H. Chum, A. De la Vega Navarro, J. Edmonds, A. Faaij, B. Fungtammasan, A. Garg, E. Hertwich *et al.*, "Energy systems," 2014.

[7] J. A. de Chalendar, J. Taggart, and S. M. Benson, "Tracking emissions in the us electricity system," *Proceedings of the National Academy of Sciences*, vol. 116, no. 51, pp. 25 497–25 502, 2019.

[8] "The carbon plan - reducing greenhouse gas emissions," HM Government, Tech. Rep., 2011.

[9] electricinsights.co.uk, Mar. 2020.

[10] H. Farhangi, "The path of the smart grid," *IEEE power and energy magazine*, vol. 8, no. 1, pp. 18–28, 2009.

[11] Y. Yan, Y. Qian, H. Sharif, and D. Tipper, "A survey on smart grid communication infrastructures: Motivations, requirements and challenges," *IEEE communications surveys & tutorials*, vol. 15, no. 1, pp. 5–20, 2012.

[12] T. Basso, J. Hambrick, and D. DeBlasio, "Update and review of ieee p2030 smart grid interoperability and ieee 1547 interconnection standards," in *2012 IEEE PES Innovative Smart Grid Technologies (ISGT)*. IEEE, 2012, pp. 1–7.

[13] Y. Parag and B. K. Sovacool, "Electricity market design for the prosumer era," *Nature energy*, vol. 1, no. 4, pp. 1–6, 2016.

[14] I. Shandurkova, B. A. Bremdal, R. Bacher, S. Ottesen, and A. Nilsen, "A prosumer oriented energy market," *Developments and future outlooks for Smart Grid oriented energy markets, IMprosume Publication, Nce Smart Energy Markets, Halden*, 2012.

[15] V. C. Gungor, D. Sahin, T. Kocak, S. Ergut, C. Buccella, C. Cecati, and G. P. Hancke, "Smart grid technologies: Communication technologies and standards," *IEEE transactions on Industrial informatics*, vol. 7, no. 4, pp. 529–539, 2011.

[16] P. P. Verma, D. Srinivasan, K. Swarup, and R. Mehta, "A review of uncertainty handling techniques in smart grid," *International Journal of Uncertainty, Fuzziness and Knowledge-Based Systems*, vol. 26, no. 03, pp. 345–378, 2018.

[17] A. R. Jordehi, "How to deal with uncertainties in electric power systems? a review," *Renewable and sustainable energy reviews*, vol. 96, pp. 145–155, 2018.

[18] C. W. Gellings, "The concept of demand-side management for electric utilities," *Proceedings of the IEEE*, vol. 73, no. 10, pp. 1468–1470, 1985.

[19] G. Strbac, "Demand side management: Benefits and challenges," *Energy policy*, vol. 36, no. 12, pp. 4419–4426, 2008.

[20] J. U. Nef, "An early energy crisis and its consequences," *Scientific American*, vol. 237, no. 5, pp. 140–151, 1977.

[21] J. Richardson and R. Nordhaus, "The national energy act of 1978," *Natural Resources & Environment*, vol. 10, no. 1, pp. 62–88, 1995.

[22] A. Richman, "The polls: Public attitudes toward the energy crisis," *The Public Opinion Quarterly*, vol. 43, no. 4, pp. 576–585, 1979.

[23] S. Mak and D. Radford, "Communication system requirements for implementation of a large scale demand side management and distribution automation," *IEEE transactions on power delivery*, vol. 11, no. 2, pp. 683–689, 1996.

[24] M. Auffhammer, C. Blumstein, and M. Fowlie, "Demand-side management and energy efficiency revisited," *The Energy Journal*, vol. 29, no. 3, 2008.

[25] M. H. Albadi and E. F. El-Saadany, "Demand response in electricity markets: An overview," in *2007 IEEE power engineering society general meeting.* IEEE, 2007, pp. 1–5.

[26] C. W. Gellings and J. H. Chamberlin, "Demand-side management: concepts and methods," 1987.

[27] J. A. Short, D. G. Infield, and L. L. Freris, "Stabilization of grid frequency through dynamic demand control," *IEEE Transactions on power systems*, vol. 22, no. 3, pp. 1284–1293, 2007.

[28] G. Boyle, *Renewable energy*, 2004.

[29] J. A. Turner, "A realizable renewable energy future," *Science*, vol. 285, no. 5428, pp. 687–689, 1999.

[30] "Uk solar capacity: Is the future of solar cloudy?" GreenMatch, Tech. Rep., Jul. 2020.

[31] "Challenge for many eu countries to reach their 2020 renewable targets," PVEurope, Tech. Rep., Sep. 2019.

[32] C. R. Jones, B. J. Orr, and J. R. Eiser, "When is enough, enough? identifying predictors of capacity estimates for onshore wind-power development in a region of the uk," *Energy Policy*, vol. 39, no. 8, pp. 4563–4577, 2011.

[33] D. Toke, "The uk offshore wind power programme: A sea-change in uk energy policy?" *Energy Policy*, vol. 39, no. 2, pp. 526–534, 2011.

[34] J. A. McDowall, "Status and outlook of the energy storage market," in *2007 IEEE Power Engineering Society General Meeting.* IEEE, 2007, pp. 1–3.

[35] A. Nasiri, "Integrating energy storage with renewable energy systems," in *2008 34th Annual Conference of IEEE Industrial Electronics.* IEEE, 2008, pp. 17–18.

[36] Y. Wang, Q. Chen, T. Hong, and C. Kang, "Review of smart meter data analytics: Applications, methodologies, and challenges," *IEEE Transactions on Smart Grid*, vol. 10, no. 3, pp. 3125–3148, 2019.

[37] M. Kerai, "Smart meter statistics in great britain," Department for Business, Energy and Industrial Strategy, Tech. Rep., Mar. 2020. [Online]. Available: https://assets.publishing.service.gov.uk/government/uploads/system/uploads/attachment_data/file/887809/Q1_2020_Smart_Meters_Statistics_Report_FINAL.pdf

[38] D.-M. Han and J.-H. Lim, "Smart home energy management system using ieee 802.15. 4 and zigbee," *IEEE Transactions on Consumer Electronics*, vol. 56, no. 3, pp. 1403–1410, 2010.

[39] H. Ibrahim, A. Ilinca, and J. Perron, "Energy storage systems—characteristics and comparisons," *Renewable and sustainable energy reviews*, vol. 12, no. 5, pp. 1221–1250, 2008.

[40] J. Larminie and J. Lowry, *Electric vehicle technology explained.* John Wiley & Sons, 2012.

[41] R. Zafar, A. Mahmood, S. Razzaq, W. Ali, U. Naeem, and K. Shehzad, "Prosumer based energy management and sharing in smart grid," *Renewable and Sustainable Energy Reviews*, vol. 82, pp. 1675–1684, 2018.

[42] A. Toffler, "The third wave: The classic study of tomorrow," *New York: Bantam*, 1984.

[43] J. Hamari, M. Sjöklint, and A. Ukkonen, "The sharing economy: Why people participate in collaborative consumption," *Journal of the association for information science and technology*, vol. 67, no. 9, pp. 2047–2059, 2016.

[44] N. Liu, X. Yu, C. Wang, C. Li, L. Ma, and J. Lei, "Energy-sharing model with price-based demand response for microgrids of peer-to-peer prosumers," *IEEE Transactions on Power Systems*, vol. 32, no. 5, pp. 3569–3583, 2017.

[45] A. Lüth, J. M. Zepter, P. C. del Granado, and R. Egging, "Local electricity market designs for peer-to-peer trading: The role of battery flexibility," *Applied energy*, vol. 229, pp. 1233–1243, 2018.

[46] E. Al Kawasmi, E. Arnautovic, and D. Svetinovic, "Bitcoin-based decentralized carbon emissions trading infrastructure model," *Systems Engineering*, vol. 18, no. 2, pp. 115–130, 2015.

[47] S.-W. Park, K.-S. Cho, and S.-Y. Son, "Voltage management method of distribution system in p2p energy transaction environment," *IFAC-PapersOnLine*, vol. 52, no. 4, pp. 324 – 329, 2019, iFAC Workshop on Control of Smart Grid and Renewable Energy Systems CSGRES 2019. [Online]. Available: http://www.sciencedirect.com/science/article/pii/S2405896319305671

[48] T. Morstyn, A. Teytelboym, and M. D. Mcculloch, "Bilateral contract networks for peer-to-peer energy trading," *IEEE Transactions on Smart Grid*, vol. 10, no. 2, pp. 2026–2035, 2019.

[49] L. Thomas, Y. Zhou, C. Long, J. Wu, and N. Jenkins, "A general form of smart contract for decentralized energy systems management," *Nature Energy*, vol. 4, no. 2, pp. 140–149, 2019.

[50] https://www.ofgem.gov.uk/data-portal, Mar. 2020.

[51] https://www.powerledger.io/.

[52] D. Minoli, K. Sohraby, and B. Occhiogrosso, "Iot considerations, requirements, and architectures for smart buildings—energy optimization and next-generation building management systems," *IEEE Internet of Things Journal*, vol. 4, no. 1, pp. 269–283, 2017.

[53] P. Asmus, "Microgrids, virtual power plants and our distributed energy future," *The Electricity Journal*, vol. 23, no. 10, pp. 72–82, 2010.

[54] L. Gkatzikis, I. Koutsopoulos, and T. Salonidis, "The role of aggregators in smart grid demand response markets," *IEEE Journal on Selected Areas in Communications*, vol. 31, no. 7, pp. 1247–1257, 2013.

[55] S. Nojavan, K. Zare, and B. Mohammadi-Ivatloo, "Optimal stochastic energy management of retailer based on selling price determination under smart grid environment in the presence of demand response program," *Applied energy*, vol. 187, pp. 449–464, 2017.

[56] D. Li, W. Chiu, H. Sun, and H. V. Poor, "Multiobjective optimization for demand side management program in smart grid," *IEEE Transactions on Industrial Informatics*, vol. 14, no. 4, pp. 1482–1490, April 2018.

[57] https://www.stem.com/.

[58] https://www.energymeteo.com/.

[59] A. Di Giorgio and F. Liberati, "Near real time load shifting control for residential electricity prosumers under designed and market indexed pricing models," *Applied Energy*, vol. 128, pp. 119–132, 2014.

[60] https://global.abb/group/en.

[61] https://lo3energy.com/.

[62] M. Fowlie, M. Reguant, and S. P. Ryan, "Market-based emissions regulation and industry dynamics," *Journal of Political Economy*, vol. 124, no. 1, pp. 249–302, 2016.

[63] C. Ramstein, G. Dominioni, S. Ettehad, L. Lam, M. Quant, J. Zhang, L. Mark, S. Nierop, T. Berg, P. Leuschner *et al.*, *State and trends of carbon pricing 2019*. The World Bank, 2019.

[64] G. E. Metcalf and D. Weisbach, "The design of a carbon tax," *Harv. Envtl. L. Rev.*, vol. 33, p. 499, 2009.

[65] W. D. Nordhaus, "Revisiting the social cost of carbon," *Proceedings of the National Academy of Sciences*, vol. 114, no. 7, pp. 1518–1523, 2017.

[66] A. M. Driga and A. S. Drigas, "Climate change 101: How everyday activities contribute to the ever-growing issue," *International Journal of Recent Contributions from Engineering, Science & IT (iJES)*, vol. 7, no. 1, pp. 22–31, 2019.

[67] R. N. Stavins, "Experience with market-based environmental policy instruments," in *Handbook of environmental economics*. Elsevier, 2003, vol. 1, pp. 355–435.

[68] D. Newbery, D. Reiner, and R. Ritz, "When is a carbon price floor desirable?" 2018.

[69] M. H. Babiker, "Climate change policy, market structure, and carbon leakage," *Journal of international Economics*, vol. 65, no. 2, pp. 421–445, 2005.

[70] B. Doda, "How to price carbon in good times... and bad!" *Wiley Interdisciplinary Reviews: Climate Change*, vol. 7, no. 1, pp. 135–144, 2016.

[71] D. Hirst, "Carbon price floor (CPF) and the price support mechanism," House of Commons Library, Tech. Rep., Jan. 2018.

[72] L. H. Goulder and A. R. Schein, "Carbon taxes versus cap and trade: a critical review," *Climate Change Economics*, vol. 4, no. 03, p. 1350010, 2013.

[73] D. M. Newbery, D. M. Reiner, and R. A. Ritz, "The political economy of a carbon price floor for power generation," *The Energy Journal*, vol. 40, no. 1, 2019.

[74] M. Homam, "Economic efficiency of carbon tax versus carbon cap-and-trade," Homam Consulting and Business Solutions Inc., Tech. Rep., 2015.

[75] C. Kang, T. Zhou, Q. Chen, Q. Xu, Q. Xia, and Z. Ji, "Carbon emission flow in networks," *Scientific reports*, vol. 2, p. 479, 2012.

[76] "Environmental reporting guidelines: including streamlined energy and carbon reporting and greenhouse gas reporting," Department for Environment, Food & Rural Affairs, Tech. Rep., Mar. 2019.

[77] R. C. Thomson, G. P. Harrison, and J. P. Chick, "Marginal greenhouse gas emissions displacement of wind power in great britain," *Energy Policy*, vol. 101, pp. 201–210, 2017.

[78] K. Siler-Evans, I. L. Azevedo, and M. G. Morgan, "Marginal emissions factors for the us electricity system," *Environmental science & technology*, vol. 46, no. 9, pp. 4742–4748, 2012.

[79] A. D. Hawkes, "Estimating marginal CO_2 emissions rates for national electricity systems," *Energy Policy*, vol. 38, no. 10, pp. 5977–5987, 2010.

[80] J. Kneifel, "Life-cycle carbon and cost analysis of energy efficiency measures in new commercial buildings," *Energy and Buildings*, vol. 42, no. 3, pp. 333–340, 2010.

[81] "Environmental claims: Marketing of electricity from renewable sources-output and emissions claims," Committees of Advertising Practice, Tech. Rep., 2014.

[82] M. Ståhls, L. Saikku, and T. Mattila, "Impacts of international trade on carbon flows of forest industry in finland," *Journal of Cleaner Production*, vol. 19, no. 16, pp. 1842–1848, 2011.

[83] B. Li, Y. Song, and Z. Hu, "Carbon flow tracing method for assessment of demand side carbon emissions obligation," *IEEE Transactions on Sustainable Energy*, vol. 4, no. 4, pp. 1100–1107, 2013.

[84] C. Kang, T. Zhou, Q. Chen, J. Wang, Y. Sun, Q. Xia, and H. Yan, "Carbon emission flow from generation to demand: A network-based model," *IEEE Transactions on Smart Grid*, vol. 6, no. 5, pp. 2386–2394, Sep. 2015.

[85] M. Rui, L. Kai, L. Xuan, and Q. Zeyu, "An economic and low-carbon day-ahead pareto-optimal scheduling for wind farm integrated power systems with demand response," *Journal of Modern Power Systems and Clean Energy*, vol. 3, no. 3, pp. 393–401, 2015.

[86] G. B. Dantzig, *Linear programming and extensions.* Princeton university press, 1998, vol. 48.

[87] A. Schrijver, *Theory of linear and integer programming.* John Wiley & Sons, 1998.

[88] H. P. Williams, *Logic and Integer Programming.* Springer, 2009.

[89] M. S. Bazaraa, H. D. Sherali, and C. M. Shetty, *Nonlinear programming: theory and algorithms.* John Wiley & Sons, 2013.

[90] S. Javaid, M. Kaneko, and Y. Tan, "A linear programming model for power flow control problem considering controllable and fluctuating power devices," in *2019 IEEE 8th Global Conference on Consumer Electronics (GCCE)*, 2019, pp. 96–99.

[91] R. Fernández-Blanco, J. M. Arroyo, N. Alguacil, and X. Guan, "Incorporating price-responsive demand in energy scheduling based on consumer payment minimization," *IEEE Transactions on Smart Grid*, vol. 7, no. 2, pp. 817–826, 2016.

[92] S. Khushalani, J. M. Solanki, and N. N. Schulz, "Optimized restoration of unbalanced distribution systems," *IEEE Transactions on Power Systems*, vol. 22, no. 2, pp. 624–630, 2007.

[93] Y. Shi *et al.*, "Particle swarm optimization: developments, applications and resources," in *Proceedings of the 2001 congress on evolutionary computation (IEEE Cat. No. 01TH8546)*, vol. 1. IEEE, 2001, pp. 81–86.

[94] K. Deb, A. Pratap, S. Agarwal, and T. Meyarivan, "A fast and elitist multiobjective genetic algorithm: Nsga-ii," *IEEE transactions on evolutionary computation*, vol. 6, no. 2, pp. 182–197, 2002.

[95] D. Dasgupta, *Artificial immune systems and their applications*. Springer Science & Business Media, 2012.

[96] F. Meng and X. Zeng, "A profit maximization approach to demand response management with customers behavior learning in smart grid," *IEEE Transactions on Smart Grid*, vol. 7, no. 3, pp. 1516–1529, 2016.

[97] D. J. Olsen, Y. Dvorkin, R. Fernández-Blanco, and M. A. Ortega-Vazquez, "Optimal carbon taxes for emissions targets in the electricity sector," *IEEE Transactions on Power Systems*, vol. 33, no. 6, pp. 5892–5901, 2018.

[98] H. Chang, W. Chiu, H. Sun, and C. Chen, "User-centric multiobjective approach to privacy preservation and energy cost minimization in smart home," *IEEE Systems Journal*, vol. 13, no. 1, pp. 1030–1041, 2019.

[99] C. Zhang, J. Li, Y. Angela Zhang, and Z. Xu, "Data-driven sizing planning of renewable distributed generation in distribution networks with optimality guarantee," *IEEE Transactions on Sustainable Energy*, vol. 11, no. 3, pp. 2003–2014, 2020.

[100] H. R. Varian, *Intermediate Microeconomics: A Modern Approach: Ninth International Student Edition*. WW Norton & Company, 2014.

[101] H. Von Stackelberg, *Market structure and equilibrium*. Springer Science & Business Media, 2010.

[102] A. Belgana, B. P. Rimal, and M. Maier, "Open energy market strategies in microgrids: A stackelberg game approach based on a hybrid multiobjective evolutionary algorithm," *IEEE Transactions on Smart Grid*, vol. 6, no. 3, pp. 1243–1252, 2014.

[103] F.-L. Meng and X.-J. Zeng, "A stackelberg game-theoretic approach to optimal real-time pricing for the smart grid," *Soft Computing.*, vol. 17, no. 12, pp. 2365–2380, 2013.

[104] A. Ghosh, V. Aggarwal, and H. Wan, "Exchange of renewable energy among prosumers using blockchain with dynamic pricing," 2018.

[105] H. Wang, T. Huang, X. Liao, H. Abu-Rub, and G. Chen, "Reinforcement learning in energy trading game among smart microgrids," *IEEE Transactions on Industrial Electronics*, vol. 63, no. 8, pp. 5109–5119, 2016.

[106] R. Mohammadi, H. R. Mashhadi, and M. Shahidehpour, "Enhancement of distribution system reliability: A framework based on cournot game model," *IEEE Transactions on Smart Grid*, vol. 11, no. 3, pp. 2172–2181, 2020.

[107] J. Vuelvas and F. Ruiz, "A novel incentive-based demand response model for cournot competition in electricity markets," *Energy Systems*, vol. 10, no. 1, pp. 95–112, 2019.

[108] M. I. Jordan and D. E. Rumelhart, "Forward models: Supervised learning with a distal teacher," *Cognitive science*, vol. 16, no. 3, pp. 307–354, 1992.

[109] H. B. Barlow, "Unsupervised learning," *Neural computation*, vol. 1, no. 3, pp. 295–311, 1989.

[110] R. S. Sutton and A. G. Barto, *Reinforcement learning: An introduction*. MIT press, 2018.

[111] M. Gasse, D. Chételat, N. Ferroni, L. Charlin, and A. Lodi, "Exact combinatorial optimization with graph convolutional neural networks," in *Advances in Neural Information Processing Systems*, 2019, pp. 15 580–15 592.

[112] Z. Wen, D. O'Neill, and H. Maei, "Optimal demand response using device-based reinforcement learning," *IEEE Transactions on Smart Grid*, vol. 6, no. 5, pp. 2312–2324, 2015.

[113] F. Ruelens, B. J. Claessens, S. Vandael, S. Iacovella, P. Vingerhoets, and R. Belmans, "Demand response of a heterogeneous cluster of electric water heaters using batch reinforcement learning," in *2014 Power Systems Computation Conference*, 2014, pp. 1–7.

[114] D. Zhang, S. Li, M. Sun, and Z. O'Neill, "An optimal and learning-based demand response and home energy management system," *IEEE Transactions on Smart Grid*, vol. 7, no. 4, pp. 1790–1801, 2016.

[115] N. Kalchbrenner, E. Grefenstette, and P. Blunsom, "A convolutional neural network for modelling sentences," *arXiv preprint arXiv:1404.2188*, 2014.

[116] M. Valueva, N. Nagornov, P. Lyakhov, G. Valuev, and N. Chervyakov, "Application of the residue number system to reduce hardware costs of the convolutional neural network implementation," *Mathematics and Computers in Simulation*, 2020.

[117] D. Owerko, F. Gama, and A. Ribeiro, "Optimal power flow using graph neural networks," in *ICASSP 2020-2020 IEEE International Conference on Acoustics, Speech and Signal Processing (ICASSP)*. IEEE, 2020, pp. 5930–5934.

[118] Y. Du, F. Li, J. Li, and T. Zheng, "Achieving 100x acceleration for n-1 contingency screening with uncertain scenarios using deep convolutional neural network," *IEEE Transactions on Power Systems*, vol. 34, no. 4, pp. 3303–3305, 2019.

[119] B. J. Claessens, P. Vrancx, and F. Ruelens, "Convolutional neural networks for automatic state-time feature extraction in reinforcement learning applied to residential load control," *IEEE Transactions on Smart Grid*, vol. 9, no. 4, pp. 3259–3269, 2018.

[120] A. Gupta, G. Gurrala, and P. S. Sastry, "An online power system stability monitoring system using convolutional neural networks," *IEEE Transactions on Power Systems*, vol. 34, no. 2, pp. 864–872, 2019.

[121] H. Choi, S. Ryu, and H. Kim, "Short-term load forecasting based on ResNet and LSTM," in *2018 IEEE International Conference on Communications, Control, and Computing Technologies for Smart Grids (SmartGridComm)*. IEEE, 2018, pp. 1–6.

[122] H. Liao, J. V. Milanović, M. Rodrigues, and A. Shenfield, "Voltage sag estimation in sparsely monitored power systems based on deep learning and system area mapping," *IEEE Transactions on Power Delivery*, vol. 33, no. 6, pp. 3162–3172, 2018.

[123] J. M. Morales, R. Minguez, and A. J. Conejo, "A methodology to generate statistically dependent wind speed scenarios," *Applied Energy*, vol. 87, no. 3, pp. 843–855, 2010.

[124] K. N. Hasan, R. Preece, and J. V. Milanović, "Existing approaches and trends in uncertainty modelling and probabilistic stability analysis of power systems with renewable generation," *Renewable and Sustainable Energy Reviews*, vol. 101, pp. 168–180, 2019.

[125] M. J. Santos, P. Ferreira, and M. Araújo, "A methodology to incorporate risk and uncertainty in electricity power planning," *Energy*, vol. 115, pp. 1400–1411, 2016.

[126] M. Hemmati, B. Mohammadi-Ivatloo, and A. Soroudi, "Uncertainty management in power system operation decision making," *arXiv preprint arXiv:1911.10358*, 2019.

[127] R. Preece and J. V. Milanović, "Efficient estimation of the probability of small-disturbance instability of large uncertain power systems," *IEEE Transactions on Power Systems*, vol. 31, no. 2, pp. 1063–1072, 2015.

[128] M. Liang, W. Li, J. Yu, and L. Shi, "Kernel-based electric vehicle charging load modeling with improved latin hypercube sampling," in *2015 IEEE Power Energy Society General Meeting*, 2015, pp. 1–5.

[129] Y. Chen, Y. Wang, D. Kirschen, and B. Zhang, "Model-free renewable scenario generation using generative adversarial networks," *IEEE Transactions on Power Systems*, vol. 33, no. 3, pp. 3265–3275, 2018.

[130] H. Xiao, W. Pei, Z. Dong, L. Kong, and D. Wang, "Application and comparison of metaheuristic and new metamodel based global optimization methods to the optimal operation of active distribution networks," *Energies*, vol. 11, no. 1, p. 85, 2018.

[131] G. Mavromatidis, K. Orehounig, and J. Carmeliet, "Design of distributed energy systems under uncertainty: A two-stage stochastic programming approach," *Applied energy*, vol. 222, pp. 932–950, 2018.

[132] C. Huang, D. Yue, J. Xie, Y. Li, and K. Wang, "Economic dispatch of power systems with virtual power plant based interval optimization method," *CSEE Journal of Power and Energy Systems*, vol. 2, no. 1, pp. 74–80, 2016.

[133] C. Zhang, J. Wu, Y. Zhou, M. Cheng, and C. Long, "Peer-to-peer energy trading in a microgrid," *Applied Energy*, vol. 220, pp. 1–12, 2018.

[134] K. Kok and S. Widergren, "A society of devices: Integrating intelligent distributed resources with transactive energy," *IEEE Power and Energy Magazine*, vol. 14, no. 3, pp. 34–45, 2016.

[135] R. Luthander, J. Widén, D. Nilsson, and J. Palm, "Photovoltaic self-consumption in buildings: A review," *Applied energy*, vol. 142, pp. 80–94, 2015.

[136] S. Hielscher, "Community energy in the uk. a review of the research literature," 2011.

[137] C. Zhang, J. Wu, C. Long, and M. Cheng, "Review of existing peer-to-peer energy trading projects," *Energy Procedia*, vol. 105, pp. 2563–2568, 2017.

[138] C. Long, J. Wu, Y. Zhou, and N. Jenkins, "Peer-to-peer energy sharing through a two-stage aggregated battery control in a community microgrid," *Applied energy*, vol. 226, pp. 261–276, 2018.

[139] T. Morstyn, N. Farrell, S. J. Darby, and M. D. McCulloch, "Using peer-to-peer energy-trading platforms to incentivize prosumers to form federated power plants," *Nature Energy*, vol. 3, no. 2, pp. 94–101, 2018.

[140] E. Mengelkamp, B. Notheisen, C. Beer, D. Dauer, and C. Weinhardt, "A blockchain-based smart grid: towards sustainable local energy markets," *Computer Science-Research and Development*, vol. 33, no. 1-2, pp. 207–214, 2018.

[141] D. Kraus, T. Obrist, and O. Hari, *Blockchains, Smart Contracts, Decentralised Autonomous Organisations and the Law*. Edward Elgar Publishing, 2019.

[142] K. Christidis and M. Devetsikiotis, "Blockchains and smart contracts for the internet of things," *Ieee Access*, vol. 4, pp. 2292–2303, 2016.

[143] V. Buterin *et al.*, "A next-generation smart contract and decentralized application platform," *white paper*, vol. 3, no. 37, 2014.

[144] S. Hochreiter and J. Schmidhuber, "Long short-term memory," *Neural computation*, vol. 9, pp. 1735–80, 12 1997.

[145] S. D. Levi and A. B. Lipton, "An introduction to smart contracts and their potential and inherent limitations," in *Harvard Law School Forum on Corporate Governance & Financial Regulation*, 2018.

[146] G. O. Karame, E. Androulaki, and S. Capkun, "Double-spending fast payments in bitcoin," in *Proceedings of the 2012 ACM conference on Computer and communications security*, 2012, pp. 906–917.

[147] J. A. Fairfield, "Smart contracts, bitcoin bots, and consumer protection," *Wash. & Lee L. Rev. Online*, vol. 71, p. 35, 2014.

[148] S. S. Al-Riyami and K. G. Paterson, "Certificateless public key cryptography," in *International conference on the theory and application of cryptology and information security*. Springer, 2003, pp. 452–473.

[149] C. Greer, D. A. Wollman, D. E. Prochaska, P. A. Boynton, J. A. Mazer, C. T. Nguyen, G. J. FitzPatrick, T. L. Nelson, G. H. Koepke, A. R. Hefner Jr *et al.*, "Nist framework and roadmap for smart grid interoperability standards, release 3.0," Tech. Rep., 2014.

[150] S. Rouhani and R. Deters, "Performance analysis of ethereum transactions in private blockchain," in *2017 8th IEEE International Conference on Software Engineering and Service Science (ICSESS)*, 2017, pp. 70–74.

[151] D. Zhou, N. Ruan, and W. Jia, "A robust throughput scheme for bitcoin network without block reward," in *2019 IEEE 21st International Conference on High Performance Computing and Communications; IEEE 17th International Conference on Smart City; IEEE 5th International Conference on Data Science and Systems (HPCC/SmartCity/DSS)*, 2019, pp. 706–713.

[152] T. McConaghy, "Blockchain, throughput, and big data," *Bitcoin Startups Berlin, Oct*, vol. 28, 2014.

[153] M. Spain, S. Foley, and V. Gramoli, "The impact of ethereum throughput and fees on transaction latency during icos," in *International Conference on Blockchain Economics, Security and Protocols (Tokenomics 2019)*. Schloss Dagstuhl-Leibniz-Zentrum für Informatik, 2020.

[154] D. Shah and K. Zhang, "Bayesian regression and Bitcoin," in *2014 52nd annual Allerton conference on communication, control, and computing (Allerton)*. IEEE, 2014, pp. 409–414.

[155] K. Wüst and A. Gervais, "Do you need a blockchain?" in *2018 Crypto Valley Conference on Blockchain Technology (CVCBT)*. IEEE, 2018, pp. 45–54.

[156] M. L. Di Silvestre, P. Gallo, M. G. Ippolito, E. R. Sanseverino, and G. Zizzo, "A technical approach to the energy blockchain in microgrids," *IEEE Transactions on Industrial Informatics*, vol. 14, no. 11, pp. 4792–4803, 2018.

[157] Y. Li, W. Yang, P. He, C. Chen, and X. Wang, "Design and management of a distributed hybrid energy system through smart contract and blockchain," *Applied Energy*, vol. 248, pp. 390–405, 2019.

[158] M. Mihaylov, S. Jurado, N. Avellana, K. Van Moffaert, I. M. de Abril, and A. Nowé, "Nrgcoin: Virtual currency for trading of renewable energy in smart grids," in *11th International Conference on the European Energy Market (EEM14)*, 2014, pp. 1–6.

[159] S. Saxena, H. E. Farag, H. Turesson, and H. Kim, "Blockchain based transactive energy systems for voltage regulation in active distribution networks," *IET Smart Grid*, 2020.

[160] S. Myung and J.-H. Lee, "Ethereum smart contract-based automated power trading algorithm in a microgrid environment," *The Journal of Supercomputing*, pp. 1–11, 2018.

[161] K. N. Khaqqi, J. J. Sikorski, K. Hadinoto, and M. Kraft, "Incorporating seller/buyer reputation-based system in blockchain-enabled emission trading application," *Applied Energy*, vol. 209, pp. 8–19, 2018.

[162] Y. Pan, X. Zhang, Y. Wang, J. Yan, S. Zhou, G. Li, and J. Bao, "Application of blockchain in carbon trading," *Energy Procedia*, vol. 158, pp. 4286–4291, 2019.

[163] A. Richardson and J. Xu, "Carbon trading with blockchain," 2020.

[164] Q. Tang and L. M. Tang, "Toward a distributed carbon ledger for carbon emissions trading and accounting for corporate carbon management," *Journal of Emerging Technologies in Accounting*, vol. 16, no. 1, pp. 37–46, 2019.

[165] "Electricity ten year statement," National Grid, Tech. Rep., Nov. 2018.

[166] "The GB electricity wholesale market," The Office of Gas and Electricity Markets (Ofgem), Tech. Rep.

[167] "The GB electricity retail market," The Office of Gas and Electricity Markets (Ofgem), Tech. Rep.

[168] J. Bialek, "Tracing the flow of electricity," *IEE Proceedings - Generation, Transmission and Distribution*, vol. 143, no. 4, pp. 313–320, 1996.

[169] P. Heptonstall, "A review of electricity unit cost estimates," *UK Energy Research Centre Working Paper*, 2007.

[170] "Electricity generation costs," Department for Business, Energy and Industrial Strategy, Tech. Rep., Nov. 2016.

[171] B. Murray and N. Rivers, "British Columbia's revenue-neutral carbon tax: A review of the latest "grand experiment" in environmental policy," *Energy Policy*, vol. 86, pp. 674–683, 2015.

[172] H. W. Dommel and W. F. Tinney, "Optimal power flow solutions," *IEEE Transactions on Power Apparatus and Systems*, vol. PAS-87, no. 10, pp. 1866–1876, Oct 1968.

[173] G.-C. Luh, C.-H. Chueh, and W.-W. Liu, "Moia: multi-objective immune algorithm," *Engineering Optimization*, vol. 35, no. 2, pp. 143–164, 2003.

[174] C. A. C. Coello, G. B. Lamont, D. A. Van Veldhuizen *et al.*, *Evolutionary algorithms for solving multi-objective problems*. Springer, 2007, vol. 5.

[175] R. Shang, L. Jiao, F. Liu, and W. Ma, "A novel immune clonal algorithm for mo problems," *IEEE Transactions on Evolutionary Computation*, vol. 16, no. 1, pp. 35–50, 2012.

[176] K. Bell *et al.*, "Test system requirements for modelling future power systems," in *IEEE PES General Meeting*. IEEE, 2010, pp. 1–8.

[177] https://assets.publishing.service.gov.uk/government/uploads/system/uploads/attachment_data/file/826561/DUKES_5.11.xls.

[178] C. Fezeu, K. Bell, J. Ding, P. Panciatici, and M. Debry, "Simplified representation of a large transmission network for use in long-term expansion planning," in *2014 Power Systems Computation Conference*, 2014, pp. 1–7.

[179] https://www.gridwatch.templar.co.uk/download.php, Mar. 2020.

[180] https://www.group.rwe, Mar. 2020.

[181] "Digest of UK energy statistics (DUKES)," Department for Business, Energy, and Industrial Strategy, Tech. Rep., Apr. 2020.

[182] "Government emission conversion factors for greenhouse gas company reporting," Department for Business, Energy and Industrial Strategy, Tech. Rep., Apr. 2020.

[183] W. Chiu, H. Sun, and H. Vincent Poor, "A multiobjective approach to multimicrogrid system design," *IEEE Transactions on Smart Grid*, vol. 6, no. 5, pp. 2263–2272, 2015.

[184] R. T. Marler and J. S. Arora, "Survey of multi-objective optimization methods for engineering," *Structural and multidisciplinary optimization*, vol. 26, no. 6, pp. 369–395, 2004.

[185] C. Fischer and A. K. Fox, "Comparing policies to combat emissions leakage: Border carbon adjustments versus rebates," *Journal of Environmental Economics and Management*, vol. 64, no. 2, pp. 199–216, 2012.

[186] C. Shorten and T. M. Khoshgoftaar, "A survey on image data augmentation for deep learning," *Journal of Big Data*, vol. 6, no. 1, p. 60, 2019.

[187] B. W. Silverman, "Density estimation for statistics and data analysis," 2018.

[188] M. Stein, "Large sample properties of simulations using latin hypercube sampling," *Technometrics*, vol. 29, no. 2, pp. 143–151, 1987.

[189] C. Z. Mooney, *Monte Carlo simulation*. Sage publications, 1997, vol. 116.

[190] V. A. Epanechnikov, "Non-parametric estimation of a multivariate probability density," *Theory of Probability & Its Applications*, vol. 14, no. 1, pp. 153–158, 1969.

[191] A. Castillo and D. F. Gayme, "Grid-scale energy storage applications in renewable energy integration: A survey," *Energy Conversion and Management*, vol. 87, pp. 885–894, 2014.

[192] O. Schmidt, S. Melchior, A. Hawkes, and I. Staffell, "Projecting the future levelized cost of electricity storage technologies," *Joule*, vol. 3, no. 1, pp. 81 – 100, 2019. [Online]. Available: http://www.sciencedirect.com/science/article/pii/S254243511830583X

[193] K. Simonyan and A. Zisserman, "Two-stream convolutional networks for action recognition in videos," in *Advances in neural information processing systems*, 2014, pp. 568–576.

[194] B. Xu, N. Wang, T. Chen, and M. Li, "Empirical evaluation of rectified activations in convolutional network," *arXiv preprint arXiv:1505.00853*, 2015.

[195] D. Yu, H. Wang, P. Chen, and Z. Wei, "Mixed pooling for convolutional neural networks," in *International conference on rough sets and knowledge technology*. Springer, 2014, pp. 364–375.

[196] J. Nagi, F. Ducatelle, G. A. Di Caro, D. Cireşan, U. Meier, A. Giusti, F. Nagi, J. Schmidhuber, and L. M. Gambardella, "Max-pooling convolutional neural networks for vision-based hand gesture recognition," in *2011 IEEE International Conference on Signal and Image Processing Applications (ICSIPA)*. IEEE, 2011, pp. 342–347.

[197] L. Lazard, "Lazard's levelized cost of storage analysis, version 1.0," 2015.

[198] https://www.epexspot.com/.

[199] A. Jain, K. Nandakumar, and A. Ross, "Score normalization in multimodal biometric systems," *Pattern recognition*, vol. 38, no. 12, pp. 2270–2285, 2005.

[200] D. P. Kingma and J. Ba, "Adam: A method for stochastic optimization," *arXiv preprint arXiv:1412.6980*, 2014.

[201] P. Bühlmann and S. Van De Geer, *Statistics for high-dimensional data: methods, theory and applications*. Springer Science & Business Media, 2011.

[202] G. E. Hinton, A. Krizhevsky, I. Sutskever, and N. Srivastva, "System and method for addressing overfitting in a neural network," Aug. 2 2016, uS Patent 9,406,017.

[203] E. L. Lehmann and G. Casella, *Theory of point estimation*. Springer Science & Business Media, 2006.

[204] T. Mikolov, M. Karafiát, L. Burget, J. Černockỳ, and S. Khudanpur, "Recurrent neural network based language model," in *Eleventh annual conference of the international speech communication association*, 2010.

[205] S. Mohammadi, S. Soleymani, and B. Mozafari, "Scenario-based stochastic operation management of microgrid including wind, photovoltaic, micro-turbine, fuel cell and energy storage devices," *International Journal of Electrical Power & Energy Systems*, vol. 54, pp. 525–535, 2014.

[206] M. Swan, *Blockchain: Blueprint for a new economy*. " O'Reilly Media, Inc.", 2015.

[207] E. Porras, J. M. Martín, S. Belmonte, Y. Zhou, M. Cheng, J. Wu, and J. Gómez, "Peer to peer smart energy distribution networks," ENDESA, Tech. Rep., 2015.

[208] G. Wood, "Ethereum: A secure decentralised generalised transaction ledger," *Ethereum project yellow paper*, vol. 151, pp. 1–32, 2014.

[209] A. Pouttu, J. Haapola, P. Ahokangas, Y. Xu, M. Kopsakangas-Savolainen, E. Porras, J. Matamoros, C. Kalalas, J. Alonso-Zarate, F. D. Gallego *et al.*, "P2P model for distributed energy trading, grid control and ict for local smart grids," in *2017 European Conference on Networks and Communications (EuCNC)*. IEEE, 2017, pp. 1–6.

[210] M. Jakobsson and A. Juels, "Proofs of work and bread pudding protocols," in *Secure information networks*. Springer, 1999, pp. 258–272.

[211] S. D. Commission *et al.*, "Lost in transmission?: the role of ofgem in a changing climate," 2007.

[212] M. Wohrer and U. Zdun, "Smart contracts: security patterns in the ethereum ecosystem and solidity," in *2018 International Workshop on Blockchain Oriented Software Engineering (IWBOSE)*. IEEE, 2018, pp. 2–8.

[213] T. Smith, "Carbon price floor: reform and other technical amendments," HM Revenue and Customer, Tech. Rep., 2014.